/
Article / Book Information

( )	
Title(English)	Low-Cycle Fatigue Performance Evaluation of Beam-to-Column Connection in High-Rise Steel Moment Resisting Frames
( )	
Author(English)	Dongseok Lee
( )	: ( ), : , : 10983 , :2018 9 20 , : , : , , , ,
Citation(English)	Degree:Doctor (Engineering), Conferring organization: Tokyo Institute of Technology, Report number: 10983 , Conferred date:2018/9/20, Degree Type:Course doctor, Examiner:,,,,
( )	
Type(English)	Doctoral Thesis

The Dissertation Committee for **Dong-Seok LEE** Certifies that this is the approved

version of the following dissertation:

Low-Cycle Fatigue Performance Evaluation of

Beam-to-Column Connection

in High-Rise Steel Moment Resisting Frames

Dissertation Committee Members :

<u>Supervisor</u>
Prof. Satoshi Yamada

<u>Member</u>
Prof. Shojiro Motoyui

<u>Member</u>
Prof. Susumu Kono

<u>Member</u>
Assoc. Prof. Daiki Sato

<u>Member</u>
Assoc. Prof. Shoichi Kishiki

Low-Cycle Fatigue Performance Evaluation of

Beam-to-Column Connection

in High-Rise Steel Moment Resisting Frames

by

Lee Dong-Seok

Dissertation

Presented to Interdisciplinary Graduate School of Science and Engineering of
Tokyo Institute of Technology
in Partial Fulfillment of the Requirements for the Degree of Philosophy

DOCTOR (Engineering)

Tokyo Institute of Technology
September, 2018

ABSTRACT

In recent years, low cycle fatigue (LCF) behavior of beam-to-column connection during the massive earthquake, which have long-duration and long-period ground motion are causing great concern. So, the safety and cumulative damage of beam-to-column connections subjected large number of cycles deformation is highlighted as a problem. However, existing knowledge and data with which to evaluate the cumulative damage and LCF performance of bema-to-column connection that experienced cyclic deformation under many cycles are insufficient. Most of investigation on the behavior of beam-to-column connection is either from testing under load of large deformation, or from analytical studies. In addition, deformation capacity of beam-to-column connection depends on the variables such as material's properties, moment gradient of beam, beam-end geometry and loading history, and the effect on these variables are not quantitatively evaluated.

This dissertation aims to propose LCF performance evaluation method of beam-to-column connection in high-rise steel moment resisting frames. An experimental and analytical investigation is presented focusing on the Japanese connection details. First, the welded flange-bolted web (WFBW) connection, which is commonly used in high-rise steel moment resisting frames considering slip behavior is elaborated through cyclic loading tests with different bolt configuration. The slip behavior of bolted web connection was different under minor inelastic deformation according to the bolt configuration, and LCF performance of WFBW connection depends on the slip behavior. Slip behavior is evaluated from the slip moment defined form the test, and it was found that the minimum value between the slip-critical strength and the yield bending strength of the shear plate can be evaluated as an index of slip behavior. Furthermore, it is also confirmed that if the strength of bolted web connection of the WBFW connection is equal to yield strength of the welded web connection, the LCF capacity is the same. After a methodology for LCF performance assessment of beam-to-column connection is proposed considering beam-end geometry based on the database of cyclic loading test results. The database includes two types of beam-end connection details: bolted and welded web connections. In case of these connection type, the moment transfer efficiency at the web connection could be decreased due to slip behavior at the bolted web connection, out-of-plane deformation of column flange as well as loss of the web section by weld access hole. In order to consider these decreasing the moment transfer efficiency at the web connection according to the beam-end geometry, the coefficient, J_b, which is strength

ratio of beam member to beam-end connection is proposed. The proposed coefficients were examined and verified using the different beam-end geometry details of the database. If the coefficient, J_b, is determined almost the same, the fatigue curves are identical regardless of the mechanism of moment transfer even moment transfer mechanism is different which is bolted connection and welded connection. Furthermore, a coefficient, J_b, is reflected in the fatigue curve based on the relationship between the number of cycles to failure and the constant beam rotation amplitude obtained from cyclic loading tests. Here, the relationship between the number of cycles to failure and the constant beam rotation amplitude can be evaluated regardless of the yield strength of the beam steel. In other words, the LCF evaluation Eq. is proposed reflecting coefficient, J_b, in the relationship between the number of cycles to failure and the constant beam rotation amplitude, it mean proposed evaluation eq. considering yield strength of steel grade and beam-end geometry. Analytical approaches are also introduced to clarify the scope of the proposed methodology. The range of the beam rotation amplitude for LCF performance assessment is specified and calibrated considering the material's characteristics and shear span ratio. In the analytical approach, a hysteresis model considering Bauschinger effect was proposed to consider the material characteristics under cyclic loading, and analysis model considering slip behavior was introduced and verification based on the experimental results. In the analysis, it was confirmed that the effect of different steel material and shear span ratio can be equally evaluated up to the 0.02rad of beam rotation amplitude. In design criteria, the beam-to-column connection in high-rise SMRFs is limited up to 1/100 inter-storey drift under Level 2. It means, in high-rise SMRFs, the 0.02rad beam rotation amplitude is sufficiently large amplitude, and the proposed methodology is sufficiently covered the LCF evaluation range. As the results, the proposed approach is applicable to evaluating the comprehensive fatigue performance of beam-to-column connections, considering the material characteristics, moment gradient of beam and beam-end geometry.

ACKNOWLEDGEMENTS

CONTENTS

CHAPTER 1

INTRODUCTION

1.1 Background

Steel moment-resisting frames (MRFs) are commonly utilized as the lateral load resisting system in areas of high seismicity. In Steel MRFs systems, the strong-column/weak-beam design concept is commonly employed to achieve a stable frame behavior during strong earthquake ground shaking. For the stable and reliable seismic design of MRFs, the structural members and their joints should be designed to dissipate seismic energy properly through plastic deformation without collapse (**Fig. 1.1**). Especially, beam-to-column connection should be designed to ensure sufficient rotation capacity of a plastic hinge in the beam member adjacent to the connection. To evaluate the seismic performance of the steel MRFs, it is
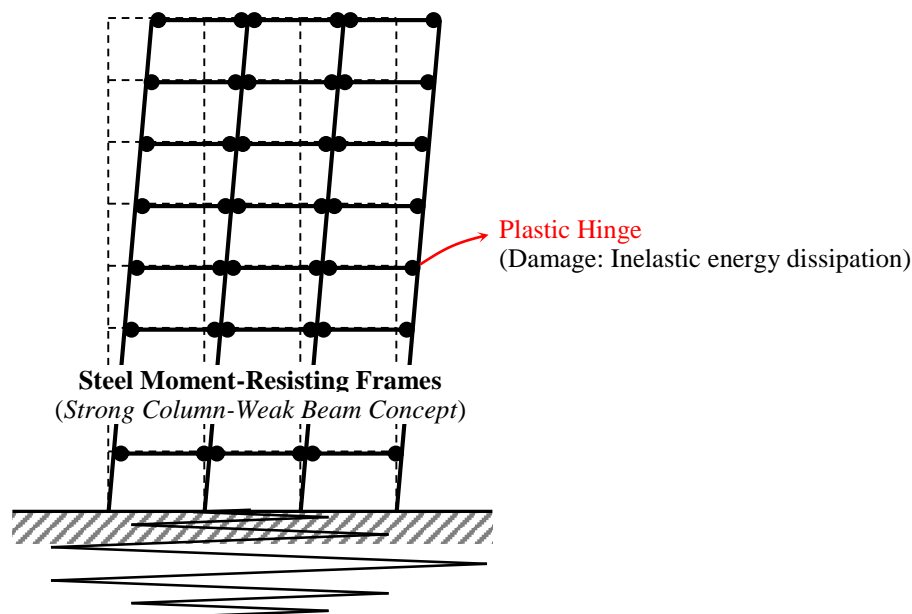
Fig. 1.1 Global failure mechanism with ductile beam sway

important to accurately identify the plastic deformation capacity of the beam-to-column connection.

(a)   **(b)**
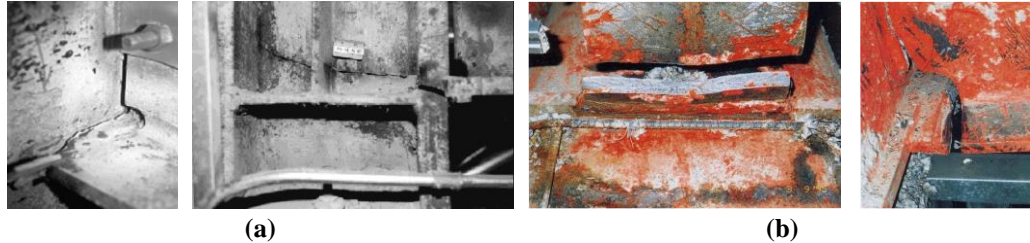
Fig. 1.2 Brittle fracture observed in the beam-to-column connection after **(a)** 1994 Northridge earthquake and **(b)** 1995 Kobe earthquake

Following the 1994 Northridge earthquake and the 1995 Kobe earthquake, unexpected brittle fractures were observed in the beam-to-column connections (EERI 1994; Youssef et al. 1995; Nakashima et al. 1998) as shown in **Fig. 1.2**. Experimental and analytical investigations were conducted to verify the causes of these observed failures (Kaufmann et al. 1997; Kuwamura1998; FEMA 355d 2000). The fracture was caused by the low material toughness, severe geometric discontinuities and poor filed welding, etc. (Nakagomi et al. 1997; SAC2000; 2000; Harada et al.2000) The improved connection details, named 'post-Northridge' and 'post-Kobe', were presented in FEMA-350 (FEMA 2000), and Architectural Institute of Japan (AIJ 1996). With the improvements in both the connection details and welding procedures, it became possible to avoid brittle fractures (FEMA 2000; AIJ 2012). The updated seismic design codes and recommendations, such as AISC 358 (AISC 2010) and the Japanese seismic design code (AIJ 2012), provide the detailed design requirements related to the stiffness, strength and ductility of the beam member adjacent to the beam-to-column connections.

1.2 Statement of Problem

In experimental investigations of the improved characteristics, the degrading performance of the connection was observed because of cracks, which might lead to the initiation of low cycle fatigue (LCF) failure at the edges of the weld access hole or the heat affected zones under inelastic cyclic loading (Stojadinović et al. 2000; Ricles et al. 2002). The accumulated fatigue damage of the connections is the greatest concern in steel MRFs. Furthermore,

massive earthquakes tend to have long-duration and long-period ground motion characteristics.

In the 2011 Great East Japan earthquake, many high-rise buildings in Tokyo, Nagoya and Osaka (the epicenter was 770 km northeast of Osaka) experienced long duration vibrations (Okawa et al. 2011; Kasai et al. 2013); thus, the beam-to-column connections were subjected to cyclic deformation under many cycles (**Fig. 1.3**). Although no visible structural damage resulted, insufficient knowledge and data exist with which to evaluate the safety margin of beam-to-column connections that experienced cyclic deformation under many cycles. In addition, long-duration ground motion (more than 200 s in duration), which is estimated to occur in Japan in the future (HERP 2012), could cause a large amount of cyclic deformation that has not been experienced in beam-to-column connections to date.
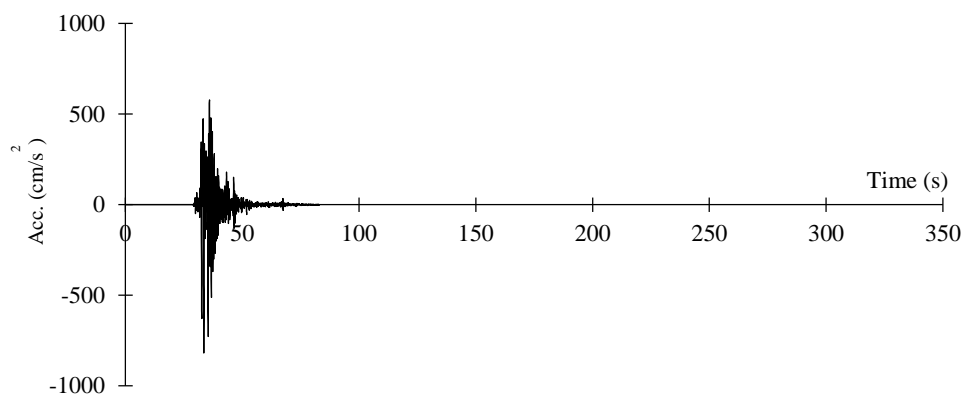
(a) Kobe earthquake 1995
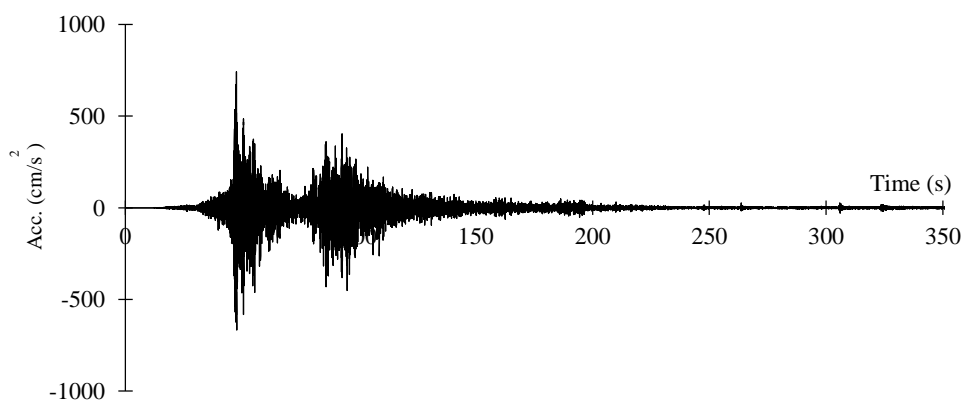
(b) Tohoku earthquake 2011

Fig. 1.3 Earthquake acceleration time history.

In Japan, seismic response analysis (time history response analysis) is carried out on high-rise buildings to determine whether the design criteria are satisfied as summarized in

| **(a)** JISF loading protocol | **(b)** SAC loading protocol |
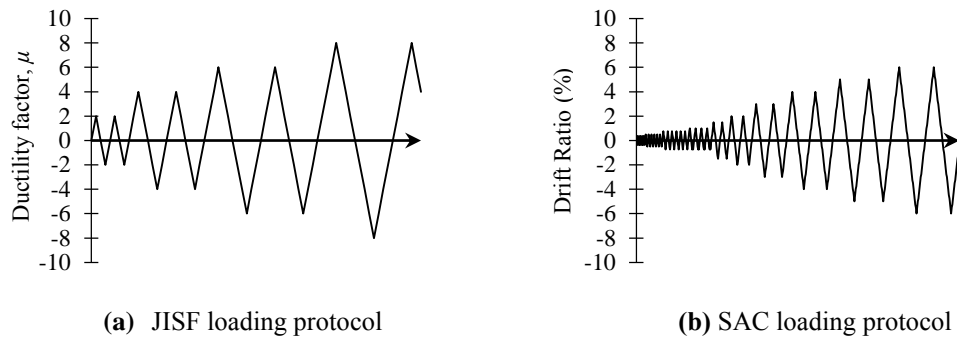
Fig. 1.4 Recommended loading protocol

Table 1.1 In case of structural member and joint, response ductility is specified to be 4.0 or less for Level 2 ground motion. However, the deformation capacity of beam-to-column connections were experimentally evaluated under incremental strain loading amplitude as shown in **Fig. 1.4** so far, and it does not in conformance with the design criteria described above. Furthermore, the data and knowledge for assessing cumulative damage when a subjected to cyclic deformation under many cycles are not enough.

Table 1.1 Criteria related to damage limit of high-rise buildings in design

Structure	Level 1	Level 2
Maximum inter-storey drift	≤1/200	≤1/100
Response ductility of structural member and joint	-	≤4.0*

* Except vibration control members

Considerable experimental researches were conducted to clarify fatigue curve of beam-to-column connection based on the Manson-Coffin relationship (Manson 1954; Coffin 1954) which relates fatigue life (number of cycles to failure) with constant amplitude cyclic loading. This relationship can be extended to variable amplitude cyclic loading by using Palmgren-Miner rule (Palmgren 1924; Miner 1945) cumulative damage rule. However, deformation capacity of beam-to-column connection depends on the material's characteristics, moment gradient of beam and beam-end geometry, it is very hard to predict the fatigue life by accurate calculation.

1.3 Previous Research on LCF Performance

The efforts to more accurately predict damage of structure member and joint due to earthquake have been proposed with various approaches. Bertero and Popov (1965) carried

out cycle loading tests were carried out on the structural steel cantilever beams. the decrease in the LCF performance occurred in the beams as the controlling strain was increased, and an analogous relationship was observed between number of cycles to failure with local buckling of the flange and controlling strain. It is pointed out that the preventing the local buckling of the elements is considerably important in the LCF performance of structural steel members. Krawinkler and Zohrei (1986) presented experimental data from LCF test of beam-to-column connection considering failure mode of local buckling and fracture at weldments. A crack growth rate model was also proposed based on the plastic strain range. Furthermore, testing protocols for determining the seismic capacity of structural elements to account for the cumulative damage expected during earthquakes were recommended. Further, fatigue life predictions were proposed based on the Manson-Coffin strain-life equation (**Fig. 1.5 (a)**), and hysteretic energy-life and energy-rotation relations were also developed with semi-rigid connection by Mander et al. (1994). The S-N curves proposed to predict the LCF behavior of structural members and connections, and it has been shown that Miner's rule can be used together with the S-N curves (**Fig. 1.5 (b)**) and with a cycle counting method to define a unified collapse criterion which is valid for LCF (Ballio et al. 1997). The above experimental results indicate that Manson-Coffin rule and Miner's rule can be employed in LCF performance of beam-to-column connection, and LCF performance depends on the details and loading amplitude. However, the details and parameters considered in test and the correlation with each parameters was not clearly defined.

(a) Fatigue Life vs. Plastic Rotation of semi-rigid connection. (Mander et al. 1994)   (b) Constant and variable amplitude test data fitted by the same S-N line. (Ballio et al. 1997)
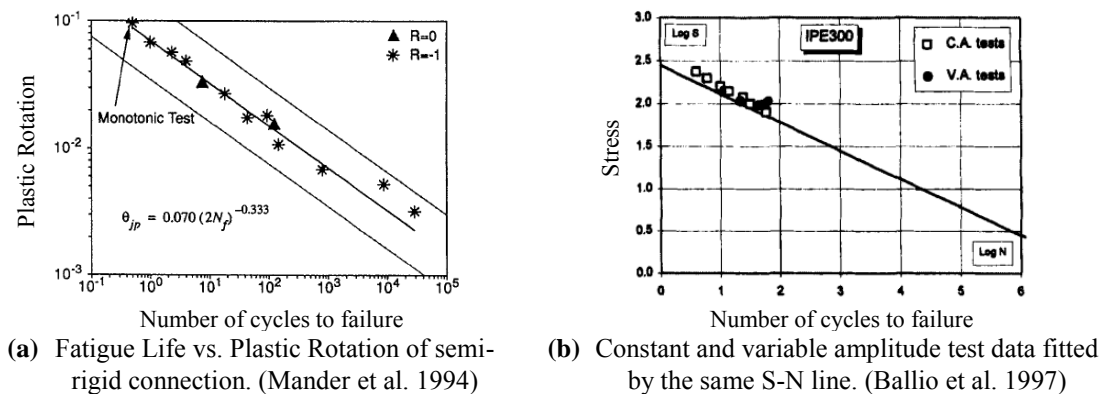
Fig. 1.5 LCF performance evaluation based on the Manson Coffin concept

After 1994 Northridge earthquake and the 1995 Kobe earthquake, much investigation to evaluate ductile crack growth have been conducted related to LCF performance. First, Kuwamura et al. (1997) reported that connection fractures were caused by fatigue cracks generated after undergoing a noticeable amount of plastic strain, and the initiation of the ductile crack is governed by average strain in the notched section, peak stress triaxiality underneath the notched surface and uniform strain capacity of materials. The cyclic void growth model (CVGM) is proposed and demonstrated by Kanvinde et al. (2006, 2007 and 2008) to evaluate ductile fracture initiation in structural steels due to LCF. In addition, the proposed CVGM was developed as a differentiated void growth model considering cycle loads. Iyama and Ricles (2009) also presented methodology for predicting the fatigue life of welded beam-to-column connection test specimens subjected to inelastic loading. The proposed methodology using accumulated crack length is based on concepts of LCF and micromechanics. In addition to the model proposed for ductile crack of welded connection, many experimental investigations have been conducted focusing on the Japanese beam-to-column connection details for LCF performance evaluation. Based on the hysteresis model of steel materials, Yamada et al (2010 and 2014) performed numerical analysis for LCF evaluation of beam-to-column connection. Also, in Japan, a large-scale shaking table test at the E-Defense National Research Institute to evaluate the seismic capacity of high-rise builds subjected to long-period ground motions is conducted (Chung, Lignos and Nagasima et al. 2010, 2011a, 2011b and 2012).The test indicated that the adopted long-period ground motion generated larger cumulative deformations at the beam-to-column connection that those expected in Japanese seismic design, and it is pointed out that improved beam-to-column connection subjected to a large number of inelastic cycles due to LCF could also be occur failure. A numerical model for evaluating such cumulative damage was also proposed and verified. Suita and Tanaka et al. (2011, 2012a, 2012b, 2014, 2015a, 2015b) conducted full-scale cyclic loading test under constant deformation amplitude to evaluate deformation capacity of beam-to-column connection. The main parameters considered are beam-end geometry such as thickness of column flange, weld access hole configuration and web connection type, floor slab and loading histories. Deformation capacity of beam-to-column connection is evaluated focusing crack propagation strength of connection (**Fig. 1.6 (a)**). Hasegawa et al. (2014) carried out earthquake response analysis of high-rise buildings and cyclic loading test on the structural member and joint under

a large number of inelastic amplitude for the establishing the safety verification method for high-rise steel moment resisting frames against long-period earthquake ground motions. The fatigue curve was clarified based on the cyclic loading test of structural member and joint, and were verified by a three-layer moment-resisting frames tests. Also, the evaluation method of seismic safety for high-rise building was proposed based on the fatigue curve obtained from test (**Fig. 1.6 (b)**).

(a) Formulation of velocity of crack propagation (Suita et al. 2011)

(b) Fatigue curve considering weld access hole and Haunchi (Hasegawa et al. 2014)
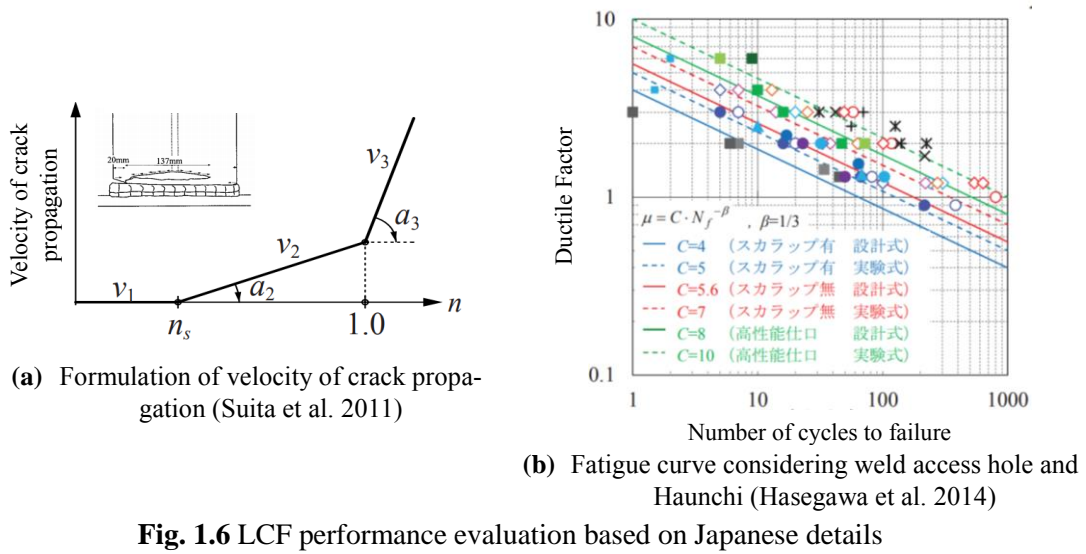
Fig. 1.6 LCF performance evaluation based on Japanese details

Many studies have been carried out to verify LCF behavior of beam-to-column connection so far, but only for the correspondence of the LCF performance for each parameter. A comprehensive evaluation equation considering all parameters affecting the LCF performance has not been proposed yet.

Especially, WFBW connection is extensively used in high-rise steel MRFs in Japan. This connection type was reported to exhibit lower ductility capacity than those with welded web connections because of the slip that occurred in the bolted web connection during cyclic loading (Chung et al. 2011). However, the WFBW connection differ in the stress transfer mechanism between the flange and the web connection, and it is difficult to evaluate the behavior under cyclic loading at the web connection because each bolt shears shear and bending force of beam. According to a recent investigation, seismic performance of the reduced beam section (RBS) with a bolted web connection (RBS-B) was investigated. (Lee et al. 2005). Subsequently, an improved RBS-B connection considering the redistribution of web bending stresses to the flange (Lee and Kim 2007) and the combination of validated heat-treated beam

sections (Morrison et al. 2016) was proposed and exhibited an excellent connection rotation capacity. However, these investigations evaluated the moment transfer efficiency of bolted web connections and cyclic performance under incremental loading amplitude (Tanaka et al. 1996; Emi et al. 2004). The evaluation of the effect of the moment transfer efficiency of bolted web connections on the cyclic performance under a large number of minor inelastic cycles remains still unclear.

1.4 Objectives and Scope of Research

The overall purpose of the dissertation is to establish a methodology for evaluating the comprehensive LCF performance of beam-to-column connection as well as cumulative damage and safety verification in time history response analysis design of high-rise steel MRFs. The beam-to-column connection types discussed in the dissertation are commonly used in Japanese steel MRFs and categorized as on-site-welding types: namely, the welded flange-bolted web (WFBW) and shop-welding types (Welded) connection. This dissertation has been mainly focused on the WFBW connection, which is extensively used in high-rise steel MRFs in Japan (**Fig. 1.7**). An experimental and analytical investigation of the above mentioned parameters is made (The data discussed in this paper considers only the deterioration mode due to the propagation of cracks and fractures at weldments and beam flanges. The deterioration mode induced by local buckling are not considered):

- In the experimental investigation, the effect of decreasing the moment transfer efficiency at
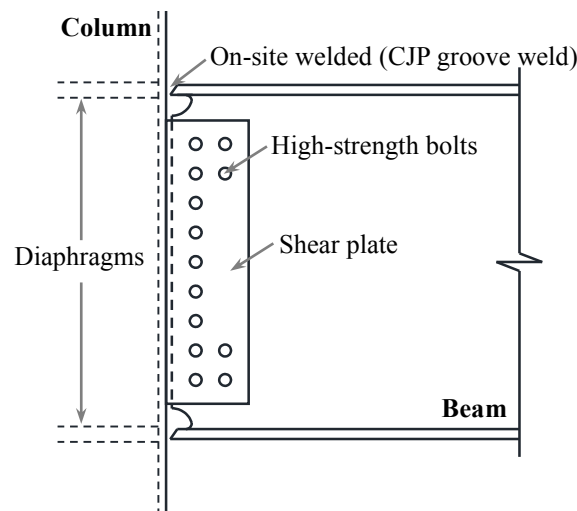
Fig. 1.7 Welded Flange-Bolted Web Connection (WFBW)

the beam-end connection due to the slip behavior of the bolts, the out-of-plane deformation of the column flange and the loss of web section due to the weld access hole on LCF performance are investigated. Furthermore, LCF performance equation is proposed considering beam-end geometry based on the experimental data. Here, the relationship between the moment transfer efficiency and cyclic deformation of WFBW connection was compared with welded web connection and investigated continuity in transferring bending moment in web connection.

- Analytical approaches are also introduced to clarify the scope of the proposed methodology based on the experimental data. The range of the beam rotation amplitude for LCF performance assessment is specified and calibrated considering the material's characteristics and shear span ratio.

1.5 Structure of Dissertation

This dissertation consists of 5 chapters, and describes an experimental and analytical investigation for comprehensive fatigue performance of beam-to-column connection.

Chpater 2 discusses experimental investigation of the effect of slip behavior of bolted wed connection on LCF performance of WFBW connection when subjected to a large number of minor inelastic amplitude.

Chpater 3 proposed a methodology for LCF performance assessment of beam-to-column connection based on the experimental data of **Chapter 2** and databased constructed.

Chpater 4 introduced analytical approaches to investigate LCF performance of beam-to-column connection. LCF performance assessment equation proposed in **Chapter 3** based on the experimental data, is specified and calibrated the scope of evaluation considering material's characteristic and geometry.

Chpater 5 summarized the research work reported in this thesis. Directions for further study are also recommended.

References

AISC, A. (2005). AISC 358-05. *Prequalified connections for special and intermediate steel moment frames for seismic applications. Chicago (IL): American Institute of Steel Construction*.

Architectural Institute of Japan (1996). Japanese Architectural Standard Specification JASS 6 Structural Steelwork Specification for Building Construction.

Architectural Institute of Japan. (2012). Recommendations for design of connections in steel structures. (in Japanese)

Ballio, G., Calado, L., & Castiglioni, C. A. (1997). Low cycle fatigue behavior of structural steel members and connections. *Fatigue & Fracture of Engineering Materials & Structures*, *20*(8), 1129-1146.

Bertero, V. V., & Popov, E. P. (1965). Effect of large alternating strains of steel beams. *Journal of the Structural Division*, *91*(1), 1-12.

Building Research Institute: National research and development. (2014). Study on Seismic Performance for Super-High-Rise Steel Buildings against Long-Period Earthquake Ground Motions, No.160. (in Japanese).

Chung, Y. L., Nagae, T., Hitaka, T., & Nakashima, M. (2010). Seismic resistance capacity of high-rise buildings subjected to long-period ground motions: E-Defense shaking table test. *Journal of Structural Engineering*, *136*(6), 637-644.

Chung, Y. L., Nagae, T., Matsumiya, T., & Nakashima, M. (2011b). Seismic resistance capacity of beam–column connections in high‐rise buildings: E‐Defense shaking table test. *Earthquake Engineering & Structural Dynamics*, *40*(6), 605-622.

Chung, Y. L., Nagae, T., Matsumiya, T., & Nakashima, M. (2012). Seismic capacity of retrofitted beam–column connections in high‐rise steel frames when subjected to long‐period ground motions. *Earthquake Engineering & Structural Dynamics*, *41*(4), 735-753.

Coffin Jr, L. F. (1954). A study of the effects of cyclic thermal stresses on a ductile metal. *trans. ASME*, *76*, 931-950.

Hall, J. F., Holmes, W. T., & Somers, P. (1994). Northridge earthquake, January 17, 1994. *Preliminary reconnaissance report*.

Harada Y., Morita K., Yamaguchi D. & Ishii T. (2000). Experimental study on brittle fracture in beam-to-column connection – Influence of connection detail and material properties-. J. Struct. Const. Eng., AIJ, 535, 141-148. (in Japanese)

Headquarter for Earthquake Research Promotion (HERP). (2012). Prediction Map for Long-Period Earthquake Ground : Motion for Nankai Earthquakes - Trial Version (In Japanese), available at http://www.jishin.go.jp/main/chousa/12_choshuki/choshuki2012.pdf (last accessed 13 Jan 2012). (in Japanese)

Iyama, J., & Ricles, J. M. (2009). Prediction of fatigue life of welded beam-to-column connections under earthquake loading. *Journal of structural engineering*, *135*(12), 1472-1480.

Kanvinde, A. M., & Deierlein, G. G. (2006). The void growth model and the stress modified critical strain model to predict ductile fracture in structural steels. *Journal of Structural Engineering*, *132*(12), 1907-1918.

Kanvinde, A. M., & Deierlein, G. G. (2007). Cyclic void growth model to assess ductile fracture initiation in structural steels due to ultra low cycle fatigue. *Journal of engineering mechanics*, *133*(6), 701-712.

Kanvinde, A. M., & Deierlein, G. G. (2008). Validation of cyclic void growth model for fracture initiation in blunt notch and dogbone steel specimens. *Journal of structural engineering*, *134*(9), 1528-1537.

Kasai, K., Mita, A., Kitamura, H., Matsuda, K., Morgan, T. A., & Taylor, A. W. (2013). Performance of seismic protection technologies during the 2011 Tohoku-Oki earthquake. *Earthquake Spectra*, *29*(s1), S265-S293.

Kaufmann, E. J., Kaufmann, E. J., Di Julio, R. M., & Gross, J. L. (1997). *Failure analysis of welded steel moment frames damaged in the Northridge earthquake*. US Department of Commerce, National Institute of Standards and Technology.

Kishiki, S., Sato, R., Yamada, S. & Hasegawa, T. (2016). Evaluation method of cyclic deformation capacity for beam-end connections using various steel grades. J. Struct. Const. Eng., AIJ, 81(723), 917-927. (in Japanese)

Krawinkler, H., Cofie, N. G., Hadidi-Tamjed, H., Lashkari-Irvani, B., & Zohrei, M. (1983). *Recommendation for experimental studies on the seismic behavior of steel components and materials* (p. 61). John A. Blume Earthquake Engineering Center, Stanford University.

Kuwamura, H. (1998). Fracture of steel during an earthquake—state-of-the-art in Japan. *Engineering Structures*, *20*(4-6), 310-322.

Kuwamura, H., & Yamamoto, K. (1997). Ductile crack as trigger of brittle fracture in steel. *Journal of Structural Engineering*, *123*(6), 729-735.

Lignos, D. G., Chung, Y., Nagae, T., & Nakashima, M. (2011a). Numerical and experimental

evaluation of seismic capacity of high-rise steel buildings subjected to long duration earthquakes. *Computers & Structures*, *89*(11-12), 959-967.

Mander, J. B., Chen, S. S., & Pekcan, G. (1994). Low-cycle fatigue behavior of semi-rigid top-and-seat angle connections. *AISC Engineering Journal*, *31*(3), 111-122.

Manson, S. S. (1954). Behavior of materials under conditions of thermal stress.

Miner, M. A. (1945). Cumulative fatigue damage. *Journal of applied mechanics*, *12*(3), A159-A164.

Nakagomi T., Fujita T., Minami K., Lee K. & Murai. (1997). Study on beam-end details for the method of non-scallop on beam-to-column welded joints. J. Struct. Const. Eng., AIJ, 498, 145-151. (in Japanese)

Nakashima, M., Inoue, K., & Tada, M. (1998). Classification of damage to steel buildings observed in the 1995 Hyogoken-Nanbu earthquake. *Engineering Structures*, *20*(4-6), 271-281.

Okawa, I., Kashima, T., Koyama, S., Iiba, M., & Çelebi, M. (2011). Summary of recorded building responses during the 2011 off the Pacific Coast of Tohoku earthquake with some implications to design motions. In *Proceedings of the International Symposium on Engineering Lessons Learned from the Giant Earthquake—One year the*.

Palmgren, A. (1924). Die Lebensdauer von Kugellagern. Z. VDI 68. *S339–S341*.

Ricles, J. M., Fisher, J. W., Lu, L. W., & Kaufmann, E. J. (2002). Development of improved welded moment connections for earthquake-resistant design. *Journal of Constructional Steel Research*, *58*(5-8), 565-604.

Roeder, C. W. (2000). State of the art report on connection performance. *FEMA 355d. Washington DC: Federal Emergency Management Agency*.

Stojadinović, B., Goel, S. C., Lee, K. H., Margarian, A. G., & Choi, J. H. (2000). Parametric tests on unreinforced steel moment connections. *Journal of Structural Engineering*, *126*(1), 40-49.

Suita, K., Tanaka, T., Manabe, Y. & Takatsuka, K. (2012b). Effect of variable amplitude loading protocol on deformation capacity: Deformation capacity of welded beam-to-column connection subjected to repeated plastic strain Part 3. J. Struct. Const. Eng., AIJ, 77(682), 1951-1958. (in Japanese)

Suita, K., Tanaka, T., Sato, A., Manabe, Y., Tsukada, T. & Su, Z. (2011). Effect of ultimate flexural strength of beam end connection on deformation capacity: Deformation capacity of welded beam-to-column connection subjected to repeated plastic strain Part 1. J. Struct. Const. Eng.,

AIJ, 76(664), 1135-1142. (in Japanese)

Takatsuka, K., Manabe, Y., Suita, K., Tanaka, T., Tsukada, T. & Su, Z. (2012a). Effect of weld access hole on deformation capacity: Deformation capacity of welded beam-to-column connection subjected to repeated plastic strain Part 2. J. Struct. Const. Eng., AIJ, 77(673), 453-459. (in Japanese)

Takatsuka, K., Suita, K., Tanaka, T. & Umeda, T. (2014). Effect of beam section size and connection detail on deformation capacity: Deformation capacity of welded beam-to-column connection subjected to repeated plastic strain Part 4. J. Struct. Const. Eng., AIJ, 77(696), 315-321. (in Japanese)

Tanaka, T., Suita, K., Asakura, N., Tsukada, T., Uozumi, N. & Takatsuka, K. (2015a). Influence of floor slab on deformation capacity: Deformation capacity of welded beam-to-column connection subjected to repeated plastic strain Part 5. J. Struct. Const. Eng., AIJ, 80(707), 127-136. (in Japanese)

Umeda, T., Takatsuka, K., Suita, K. & Tanaka, T. (2015b). Deformation capacity of flange-welded web-bolted moment connection: Deformation capacity of welded beam-to-column connection subjected to repeated plastic strain Part 6. J. Struct. Const. Eng., AIJ, 80(718), 1971-1979. (in Japanese)

Venture, S. J., & Guidelines Development Committee. (2000). *Recommended seismic design criteria for new steel moment-frame buildings*. Federal Emergency Management Agency.

Yamada, S., Jiao, Y., & Kishiki, S. (2010). Plastic deformation capacity of structural steel under various axial strain histories. J. Struct. Const. Eng., AIJ, 75(656), 1909-1916. (in Japanese)

Yamada, S., Jiao, Y., Narigara, H., Yasuda, S. & Hasegawa, T. (2014). Plastic deformation capacity of steel beam-to-column connection under long-duration earthquake. International Journal of High-Rise Buildings, 3(3), 231-241.

Youssef, N. F., Bonowitz, D., & Gross, J. L. (1995). *A survey of steel moment-resisting frame buildings affected by the 1994 Northridge earthquake*. US National Institute of Standards and Technology.

CHAPTER 2

CYCLIC LOADING TEST OF WELDED FLANGE-BOLTED WEB CONNECTION CONSIDERING BOLT CONFIGRUATION

2.1 Introduction

In Japan, the welded flange-bolted web (WFBW) connection is extensively employed in mid- and high-rise steel MRFs because of its advantages in construction ability and transportation. This connection type was reported to exhibit lower ductility capacity than those with welded web connections because of the slip that occurred in the bolted web connection during cyclic loading (Chung et al. 2011). According to a recent investigation, seismic performance of the reduced beam section (RBS) with a bolted web connection (RBS-B) was investigated. (Lee et al. 2005). Subsequently, an improved RBS-B connection considering the redistribution of web bending stresses to the flange (Lee and Kim 2007) and the combination of validated heat-treated beam sections (Morrison et al. 2016) was proposed and exhibited an excellent connection rotation capacity. However, these investigations evaluated the moment transfer efficiency of bolted web connections and cyclic performance under incremental loading amplitude (Tanaka et al. 1996; Emi et al. 2004). The evaluation of the effect of the moment transfer efficiency of bolted web connections on the cyclic performance under a large number of minor inelastic cycles remains unclear.

Regarding the cyclic performance of the beam-to-column connection under a constant amplitude, Krawinkler and Zohrei (1983) proposed a crack growth rate model based on the Manson-Coffin relationship (Manson 1954 and Coffin 1954). After that, an experimental and analytical study on the LCF performance of beam-to-column connection was made (Ballio et al. 1997. Kanvinde et al. (2006, 2007, 2008). The investigation on the WFBW connection is as follows. Hasegawa et al (2014) and Suita and Tanaka et al. (2014) carried out cyclic loading

test under constant deformation amplitude on the WFBW connection to investigate effect of bean-end geometry on cyclic deformation. Based on the test results, it is confirmed that WFBW connection, the moment transmission efficiency is lowered due to sliding of the bolted connection, and the cyclic deformation is lower than weld connection. However, they conducted test using one connection details, bolts configuration at the bolted connection were not considered. The quantitative evaluation criteria, which can be based on the predicted fatigue curves according to the connection details, are not adequate to clarify the LCF behavior of beam-to-column connections subjected a large number of minor inelastic cycles. The LCF behavior of bolted web connections in WFBW connections is difficult to evaluate because of the interdependent moment transfer mechanism that arises from individual bolts against beam shear and web moment components. The project discussed in this study, the cyclic loading tests of the WFBW beam-to-column connection commonly used in Japan were conducted to investigate the plastic deformation demand associated with LCF failure due to ductile fracture. To evaluate the effect of the slip behavior of bolted web connections on the LCF behavior, various bolt configurations of bolted web connections were designed, and a comparative investigation with welded web connections was conducted.

2.2 General Description of Welded Flange-Bolted Web Connection

The typical WFBW connection designed in conformance with the Japanese Standard Design Recommendation (AIJ 2012) is shown in **Fig. 2.1(a)**. The beam flanges are welded to the column by complete joint penetration (CJP) groove welds and the beam web is bolted to a single shear plate, welded to the column in the shop.

(a) Local Sharing in a bolted web connection by bearing

(b) Weld access hole
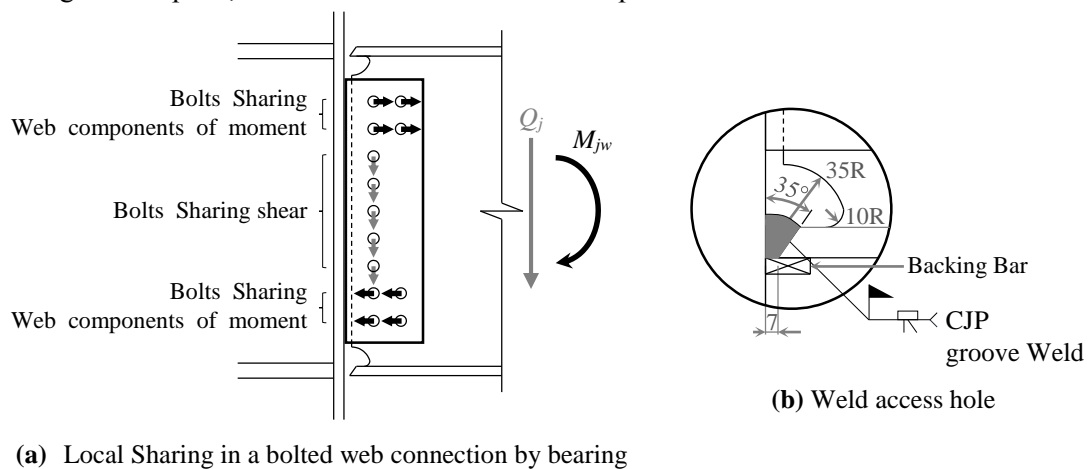
Fig. 2.1 Typical Welded Flange-Bolted Web (WFBW) Connection in Japan

In Japan, the WFBW connection is considered, as shown in **Fig. 2.1(a)**, to account for the moment distribution to the bolts in the web connection, to ensure that sufficient plastic deformation can be exhibited at the beam end. In the Allowable Stress Design (ASD), the bolted web connections can be designed as a slip-critical connection to prevent bolt slip during moderate earthquakes. Therefore, all bolts were tightened in holes, which are normally 2 mm larger than the nominal bolt diameter, d, (in the case of d < 27 mm), before introducing flange welds. The faying surfaces were treated to satisfy a 0.45 standard slip coefficient per the Japanese design criterion. The bolts also must be checked for shear and bearing strength in plastic design considerations for severe earthquakes. As shown in **Fig. 2.1(a)**, the bolts are designed assuming that the bolts at the neutral axis resist the beam shear force, Q, and the other bolts resist the beam web components of the moment, M_w, equally by bearing. As a result, the bolted connection moment by bearing was designed to satisfy the connection coefficient, which ensures a sufficient bending strength. The site-welded connection details of beam flange to column flange groove welds that are commonly used in Japan (Okada et al. 2012) are shown in **Fig. 2.1(b)**. The weld access hole consists of two arcs, with 35R and 10R to minimize the stress/strain concentration, and a backing bar (FB-9×5).

2.3 Test Program

2.3.1 Specimens

Cantilever specimens are used. The specimens are shown in **Fig. 2.2(a)**. The beam selected is the RH-600 (depth) × 200 (width) × 11 (web thickness) × 17 (flange thickness) (unit is mm and the nominal value is given) of SN490B (yield stress, F_y, is 325 N/mm² and nominal tensile stress, F_u, is 490 N/mm²). The beam flanges are welded by complete joint penetration (CJP) groove welds to an end-plate (TMCP325: Thermo-Mechanical Control Process, yield stress, F_y, is 325 N/mm² and nominal tensile stress, F_u, is 490 N/mm²) of 50 mm thickness, meanwhile the web is bolted to a single shear tab which is welded to the end-plate using high-tension bolts (S10T M20: Tension Control Bolts). All beams were 2.05 m in length, measured from the point of the applied load to the end plate.

Details of beam-flange groove welds are shown in **Fig. 2.2(b)** (AIJ 2003). The beam CJP groove welds for all the specimens were performed by the semi-automatic arc welding process using a YGW-18 corresponding to ER70S-G of the AWS (American Welding Society); and in the welding work, all the passes were controlled under the heat input of 40 kJ/cm and
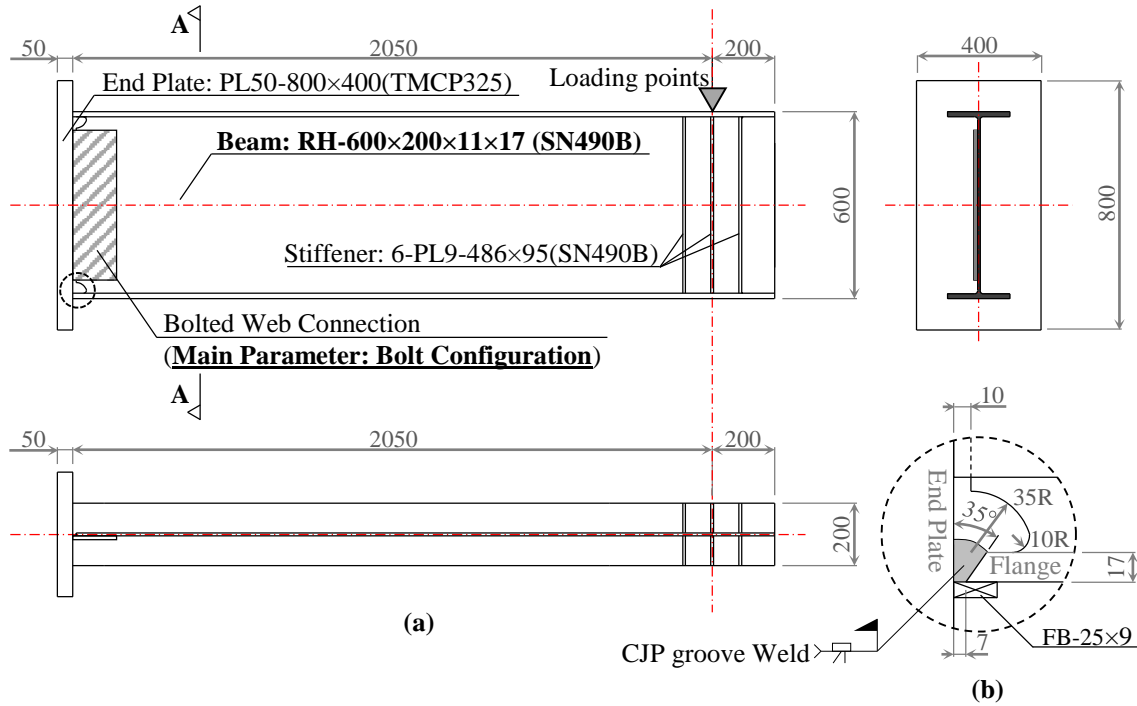
Fig. 2.2 WFBW Beam-End Connection: **(a)** specimen and **(b)** details of beam-flange groove welds

inter-pass temperatures of 350°C in accordance with JASS6 (AIJ 2012). In the case of the WFBW connection field welds, the backing bars are placed on the outer surface of the bottom flanges because of the construction conditions and not removed later. Therefore, a root pass that is liable to cause weld defects is located on the outer surface of the beam flanges, which receives a relatively large bending stress. This condition may be considered to have a detrimental effect on the flange fracture. In these tests, both side flanges of the WFBW connection are the same as the bottom flange (see **Fig. 2.1(a)**) to reflect these conditions.

The details of beam-end connection are shown in **Fig. 2.3**. Five different bolt configurations of the bolted web connections were designed to investigate the slip behavior. As shown in **Fig. 2.3**, the bolt configuration FR is a typical WFBW connection in Japan, and bolt configurations F2 is designed to investigate the effect of the moment transfer efficiency by supplemental bolts in the vicinity of the neutral axis. In case of bolt configurations F2S is designed to investigate the effect of the interval of bolt pitch on cyclic deformation. In addition, bolt configurations F3 and F4, which have a number of supplemental web bolts, are designed to investigate the upper limit in slip behavior. The tension control bolts (TCBs) used in the

bolted web connection are grade S10T, which are grade 10.9 bolts with the minimum ultimate tensile stress 1000 N/mm^2 and the minimum yield stress (0.2% proof stress) of 900 N/mm^2. The friction surfaces were applied using the shot-blast treatment. Welded web connections which is beam-end details SW were also included as a test specimen for comparison. In case of the welded web connection, the geometry of beam-end is same as WFBW connection except of beam web connection type and welding direction of beam flange, and stiffeners were installed to prevent local buckling of the flanges and web.
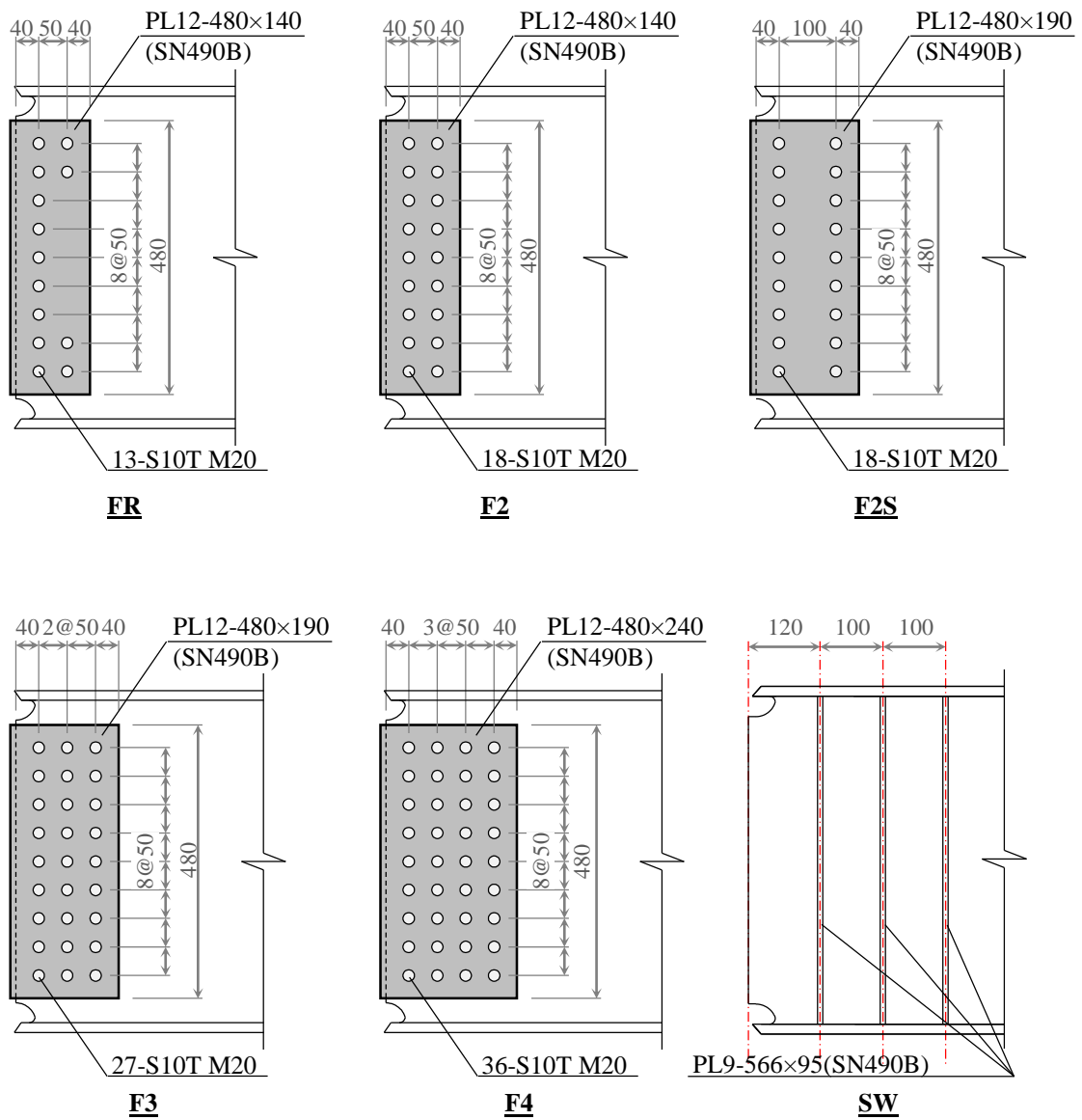
Fig. 2.3 Details of beam-end connection

2.3.2 Test Set-up and Loading History

The tests were conducted by laterally applying cyclic loads to the beam tip through an oil jack, as shown in **Fig. 2.4(a)**. The beam lateral supports were provided to prevent out-of-plane instability and beam twisting. Displacement transducers, as shown in **Fig. 2.4(a)**, were used on the specimens during the test to measure the beam behavior. The imposed load, $_bQ$, was measured by a load cell in pin 2 of the oil jack. d_{V1} is the vertical displacement that was measured at 1000 mm from rotation pin 1 of the oil jack. d_0 is the horizontal displacement at the end of the beam. d_2 to d_3 and d_4 to d_5 are the horizontal displacement and vertical displacement of the end-plate, respectively. The beam moment, $_bM$, and the beam rotation angle, $_b\theta$, were calculated using equations (2.1) to (2.5).

$$_bM =\ _bQ \cdot L_n \tag{2.1}$$

$$L_n = L \cdot Sin\left(\theta_0 + \theta_j\right) \tag{2.2}$$

$$_b\theta = \delta_b / L_b - \varphi \tag{2.3}$$

$$\delta_b = d_0 - \left(d_{H2} + d_{H3}\right)/2 \tag{2.4}$$

$$\varphi = \left(d_{V4} - d_{V5}\right)/h_b \tag{2.5}$$

where L_n is the distance from the center of the beam-to-column connection to the shaft center of the oil jack, L is the distance from the center of the beam-to-column connection to the center of rotation pin 1 of the oil jack, θ_0 is the rotation angle between L and the horizontal line, θ_j is the angle of inclination calculated from the vertical displacement of the oil jack, d_{V1} and d_0 are the horizontal displacement of the load acting point, L_b is the distance of the beam, φ is the rotation angle of the end plate, and h_b is the distance between the center of the top flange and the bottom flange

All the specimens were subjected to a constant beam rotation amplitude, $\Delta_b\theta_{const.}$ through the oil jack at the tip of the cantilever. $\Delta_b\theta_{const.}$ were used to control the loading histories. The subjected $\Delta_b\theta_{const.}$ are summarized in **Table 2.1**. As summarized in Table 2.1, $\Delta_b\theta_{const.}$ are set between about 0.010 rad and 0.040 rad to examine the LCF performance of the beam-to-column connections at relatively low plastic amplitudes. In case of WFBW connection, all bolt configurations are subjected 0.015rad, and some bolt configuration FR and F3 are subjected 0.020rad, while Welded connections are subjected 0.015rad, 0.020rad, 0.025rad and 0.030rad.
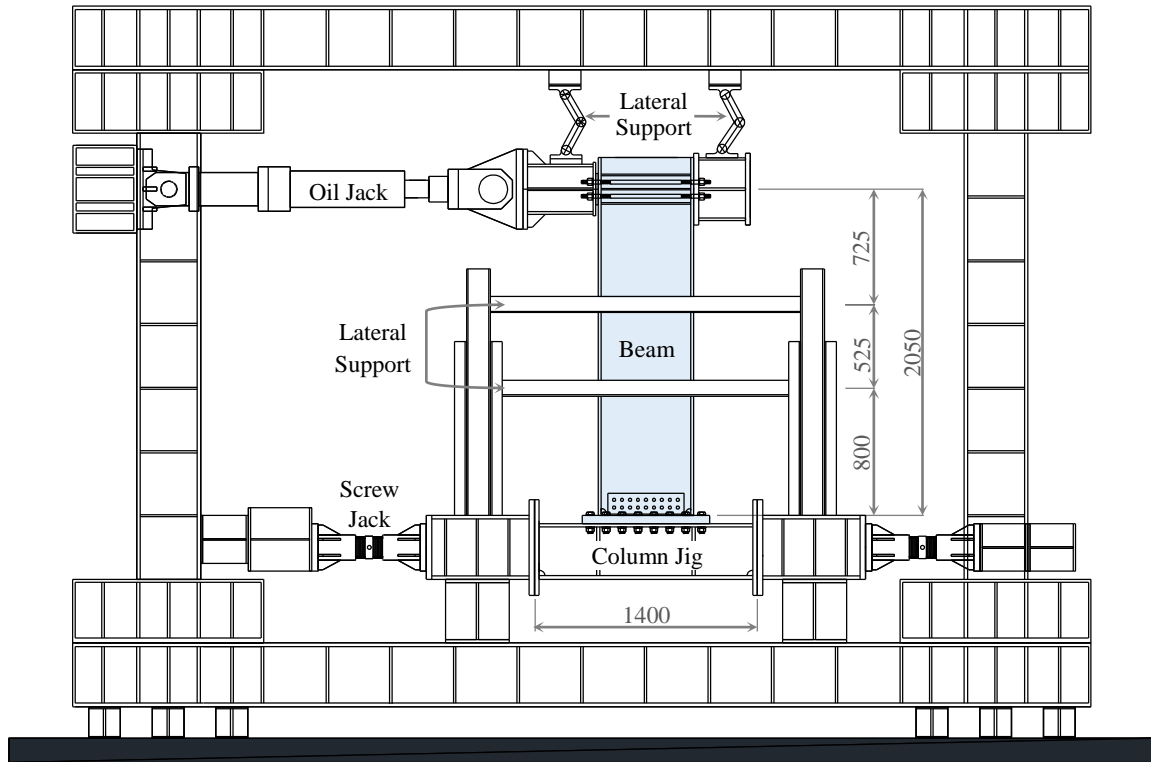
(a) Schematic of the Test setup
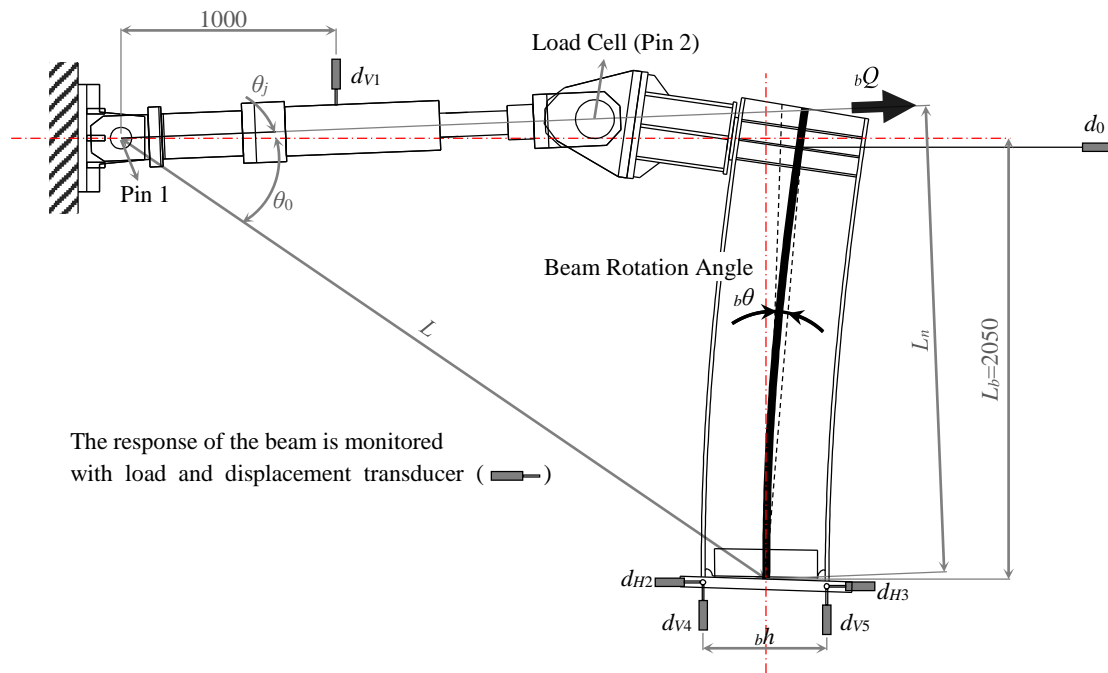
(b) Location of the displacement transducers for measuring beam behavior

Fig. 2.4 Experimental setup

Table 2.1 Loading Histories

Beam-End Connection Type		Loading Histories (Constant Beam Rotation Amplitude, $\Delta_b\theta_{const.}$)
Bolted	FR	0.015rad / 0.020rad
	F2	0.015rad
	F2S	0.015rad
	F3	0.015rad / 0.020rad
	F4	0.015rad
Welded	SW	0.0150rad
		0.020rad
		0.025rad
		0.0300rad

2.3.3 Material's Properties and Slip Coefficients.

Tensile coupon tests were conducted on specimens according to JIS (*Japanese Industrial Standards*) No.1A to examine the mechanical properties of steel materials. The test results are shown in **Fig. 2.5** and summarized in **Table 2.2**.

Table 2.2 Material Properties

Member	Coupon	Thickness mm	Yield Stress N/mm^2	Tensile Stress N/mm^2	Yield Ratio %	Elongation %
WFBW Con-nection	Flange	17.00*	347	514	68	28
	Web	11.00*	391	528	74	26
	Shear Plate		373**	519**	72**	29**
Welded Con-nection	Flange	16.73*	349	520	67	29
	Web	10.54*	373	522	71	26

*Actual Thickness

**Inspection certificate by mill test report

- Tensile Test specimens
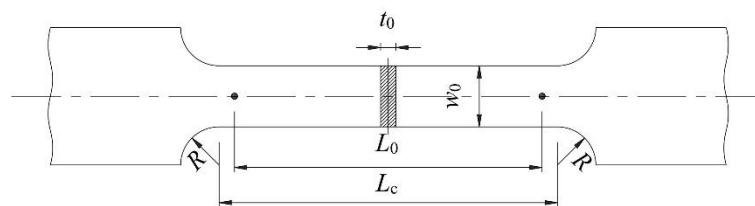
JIS No.1A
Width w_0 : 40 mm
Parallel length L_c : ≥220 mm
Gauge length L_0 : 200 mm
Transition radius R : ≥25 mm
Thickness t_0 : Original thickness
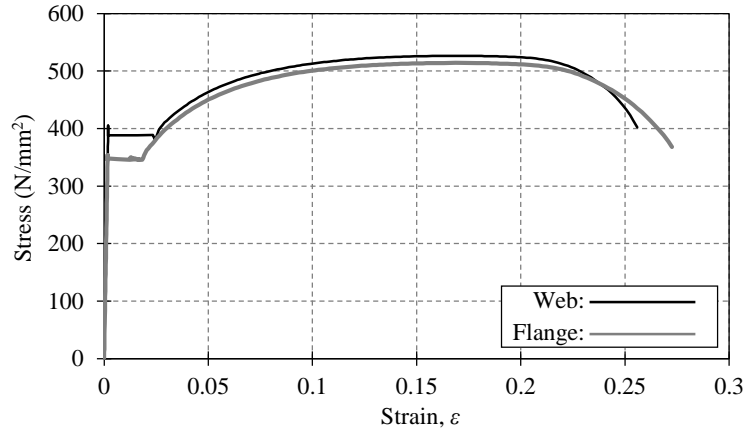
(a) Stress-Strain Curve of WFBW Connection
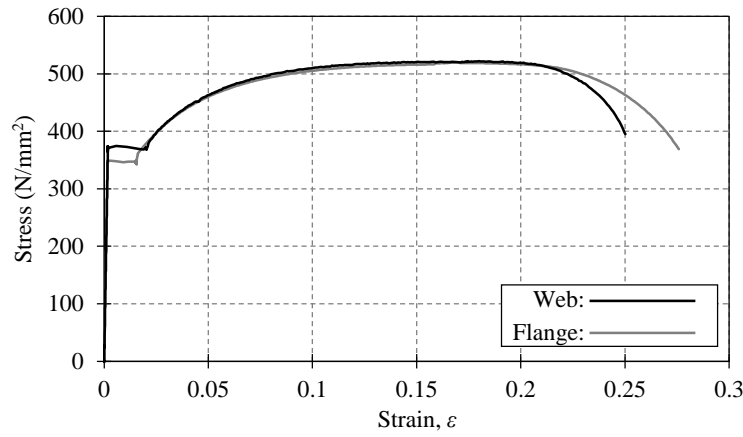
(b) Stress-Strain Curve of Welded Connection

Fig. 2.5 Stress-Strain Curve

Furthermore, since the slip coefficient can be erratic depending on the faying surface treatments and connection condition, slip resistance tests were conducted to obtain the actual slip coefficients. Test specimens are shown in **Fig. 2.6(a)**. The materials of the base plate and splice plate were a shear plate coupon (12 mm) and a web coupon (11 mm), respectively. High Tension Bolts (H.T. Bolts) of grade F10T with nearly identical properties as S10T were used. In the test, all the bolts were clamped by standard tension at N_0=117kN. The fastener tension was measured from strain gauges, as shown in **Fig. 2.6(b)**, and the load-strain relationship used here was calibrated in a pre-test. The bolt axial force can be obtained as follows:

$$N = A \cdot E \cdot \varepsilon_\gamma \qquad (3)$$

where, N is bolt axial force (kN), A is bearing surface area (mm2), E is young's modulus and ε_γ is strain of bearing surface.
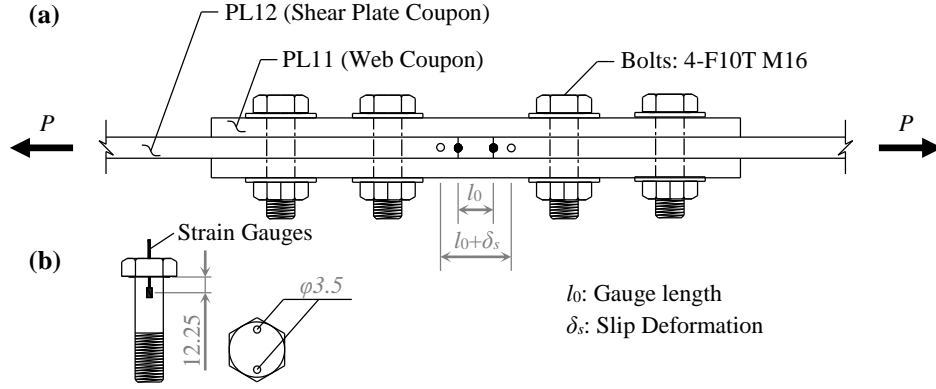
Fig. 2.6 (a) Schematic of a double lap connection with two single holes for the slip re-sistance test and **(b)** bolt axial strain

Slip resistance tests were conducted for three specimens. The load versus slip deformation relationships and test results are summarized in **Fig. 2.7** and **Table 2.3**, respectively. In the calculation slip coefficient, the bolt tensions used were the preloading forces of bolts meas-ured by strain gauges summarized in **Table 2.3**. Slip coefficients, μ, were calculated using equation (4).

$$\mu = \frac{P_{slip}}{N_i \cdot n \cdot m} \tag{4}$$

where, N_i is preload of a bolt (kN), P_{slip} is slip load (kN), n is number of bolt and m is s Number of friction faces. The slip occurrence was defined by the relative slip displacement when it reached 0.2 mm. The average slip coefficient of 0.57 obtained from the test was used for the calculation of the slip-critical strength of the bolted webs for specimens.
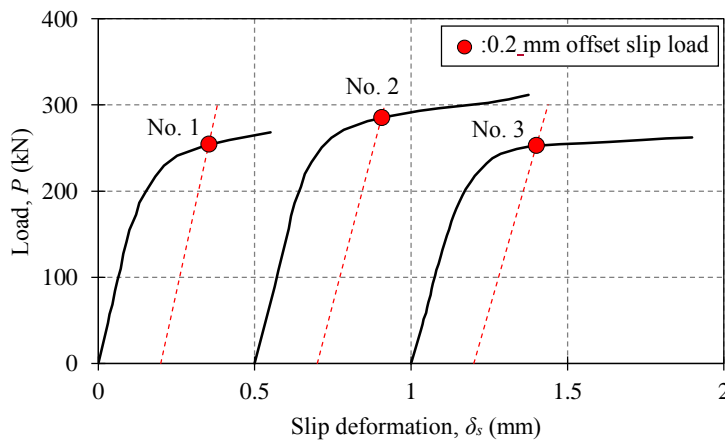
Fig. 2.7 Load versus slip deformation relationship

Table 2.3 Slip resistance test results

Slip Resistance Test Specimen	Preloading Force of a Bolt kN	Slip Load kN	Slip Coefficient
No.1	114	254	0.56
No.2	116	285	0.61
No.3	114	253	0.55
Average Slip Coefficient, $\mu_{avg.}$, is 0.57.			

2.4 Test Result

2.4.1 Failure Modes

The failure modes are shown in **Fig. 2.8**. All the specimens discussed in this test showed similar failure modes. The crack generally initiated at the weld access hole (see **Fig. 2.8(a)**) or the weld toe (see **Fig. 2.8(b)**) for all the specimens. Next, the crack propagated across the width of the flange during the cycles and then failure occurred, as shown in **Fig. 2.8(c)**. All the specimens reached failure as fracture at or near the groove weld and beam flanges of one side. However, beam local buckling and fracturing of bolts was not observed.

(a) Crack at the weld access hole   (b) Crack at the weld toe   (c) Propagation of cracks

Fig. 2.8 Typical failure modes

2.4.2 Hysteretic Behavior

The hysteretic response plotted as the beam moment $_bM$ versus beam rotation $_b\theta$ is illustrated in **Fig. 2.9**. The dotted line represents the plastic moment $_bM_p$ calculated with its material properties. The maximum strength for all the specimens was achieved in the first few cycles and showed stable hysteretic loops until first crack initiation. The strength of the tested specimens decreased with crack propagation. In the last few cycles, the strength abruptly

dropped, and the specimens reached failure. During the cycles, slip in the bolted web connection was observed for all the specimens with no noticeable change in strength. The test results are summarized in **Table 2.4**. The beam plastic rotation amplitude $\Delta_b\theta_{pl.}$ calculated by using the calculated elastic stiffness of the beam, the constant beam rotation amplitude $\Delta_b\theta_{const.}$, the slip-critical strength of the bolted web $_{Bw}M_s$ and the yield bending strength of the shear plate $_sM_y$ are listed in the table. Details of the calculation method of the slip-critical strength of the bolted web $_{Bw}M_s$ are described in **APPENDIX A**. The number of cycles to failure N_f (LCF performance) is defined in this test as when the specimens underwent fracture at the beam flange or when the peak moment in each cycle dropped to 50% from the maximum moment.

Table 2.4 Slip resistance test results

Beam-End Connection		$\Delta_b\theta_{pl.}$	$\Delta_b\theta_{const.}$	$_{Bw}M_s$	$_sM_y$	$_bM_{max}$	$_bM_{max}/_bM_p$	N_f	Crack initiation_N_0
		rad	rad	kN·m	kN·m	kN·m			
WFBW Connection	FR	0.0049	0.0150	116	172	973	0.97	232	(a)_71
		0.0089	0.0200			1065	1.06	89	(a)&(b)_61
	F2	0.0086	0.0200	137		1093	1.08	99	(a)_55
	F2S	0.0083	0.0200	144		1126	1.12	108	(b)_71
	F3	0.0045	0.0150	214		1017	1.01	317	(b)_211
		0.0084	0.0200			1121	1.11	127	(b)_72
	F4	0.0083	0.0200	298		1134	1.13	128	(b)_77
Welded Connection	SW	0.0041	0.0150	-	162*	1009	1.02	295	(a)_100
		0.0083	0.0200	-		1100	1.11	137	(a)_52
		0.0119	0.0250	-		1237	1.25	74	(a)_20
		0.0168	0.0300	-		1300	1.31	44	(a)_11

* indicates web yield strength of welded web connection $_bM_w$

- N_0 is the cycle at which the crack is visible at the specimen surface. (see **Fig. 2.9 (a),(b) and (c)**)

<u>*Bolts configuration FR ($\Delta_b\theta$: 0.0150rad)*</u> – The maximum strength was achieved after 4 cycles (negative bending moment). For both flanges, the crack was initiated at the access hole after 71 cycles and 131 cycles were recorded for bottom flange and upper flange, respectively, as shown in **Fig. 2.8(a)**. The crack was initiated at the outer side of the upper flange at 112 cycles while 131 cycles were achieved before the crack was noticed in the bottom flange at the same location (see **Fig. 2.8(b)**).

Eventually, the crack was propagated during the cycles and the failure was occurred at 232 cycles under positive bending moment (see **Fig. 2.8(c)**).

Bolts configuration FR ($\Delta_b\theta$: 0.0200rad) – The maximum strength was achieved after 2 cycles (negative bending moment). The crack initiated at the access hole after 61 cycles were recorded for upper flange and at the outer side of the upper flange after 81 cycles. The crack was propagated during the cycles and the failure was occurred at the 89cycle for the upper flange, as shown in **Fig. 2.8(c)**.

Bolts configuration F2 ($\Delta_b\theta$: 0.0200rad) – The maximum strength was achieved after 2cycles (negative bending moment). For both flanges, the crack was initiated at the access hole after 55 cycles and 62cycles were recorded for upper flange and bottom flange, respectively. The crack was initiated at the outer side of the bottom flange and upper flange after 71cycles and 77cycles, respectively. Eventually, the failure was occurred at 99cycles for upper flange, as shown in **Fig. 2.8(c)**.

Bolts configuration F2S ($\Delta_b\theta$: 0.0200rad) – The maximum strength was achieved after 1 cycles (negative bending moment). The crack at the access hole and outer side of upper flange initiated after 71cycles and 81cycles, while bottom flange at the weld access hole and outer side, crack was initiated after 75cycles and 76cycles.Eventually, the crack was propagated for upper flange and the failure was occurred at 108cycles (see. **Fig. 2.8(c)**).

Bolts configuration F3 ($\Delta_b\theta$: 0.0150rad) – The maximum strength was achieved after 3 cycles (negative bending moment). The crack was initiated at the outer side of the upper flange at 211 cycles and at the access hole after 233 cycles, as shown in **Fig. 2.8(a)** and **(b)**. The crack also initiated at the access hole after 228 cycles at the bottom flange, as shown in **Fig. 2.8(a)**. the crack was propagated at the upper flange during the cycles and the failure was occurred at the 317cycles (see **Fig. 2.8(c)**).

Bolts configuration F3 ($\Delta_b\theta$: 0.0200rad) – The maximum strength was achieved after 2cycles (negative bending moment). The crack initiated outer side and access hole after 72cycles and 105cycles were recorded for bottom flange, respectively, while the crack was initiated at the access hole and outer side of upper flange after 74cycles and 104cycles, respectively. Eventually, the failure of bottom flange occurred at 127cycles (see **Fig. 2.8(c)**).

Bolts configuration F4 ($\Delta_b\theta$: 0.0200rad) – The maximum strength was achieved after 2cycles (negative bending moment). The crack initiated at the outer side and access hole for the bottom flange, after 77cycles and 80cycles, respectively, while the crack was initiated at the access hole and outer side for the upper flange, after 82cycles and 86cycles, respectively. The failure occurred at 128cycles for the bottom flange, as shown in **Fig. 2.8(c)**.
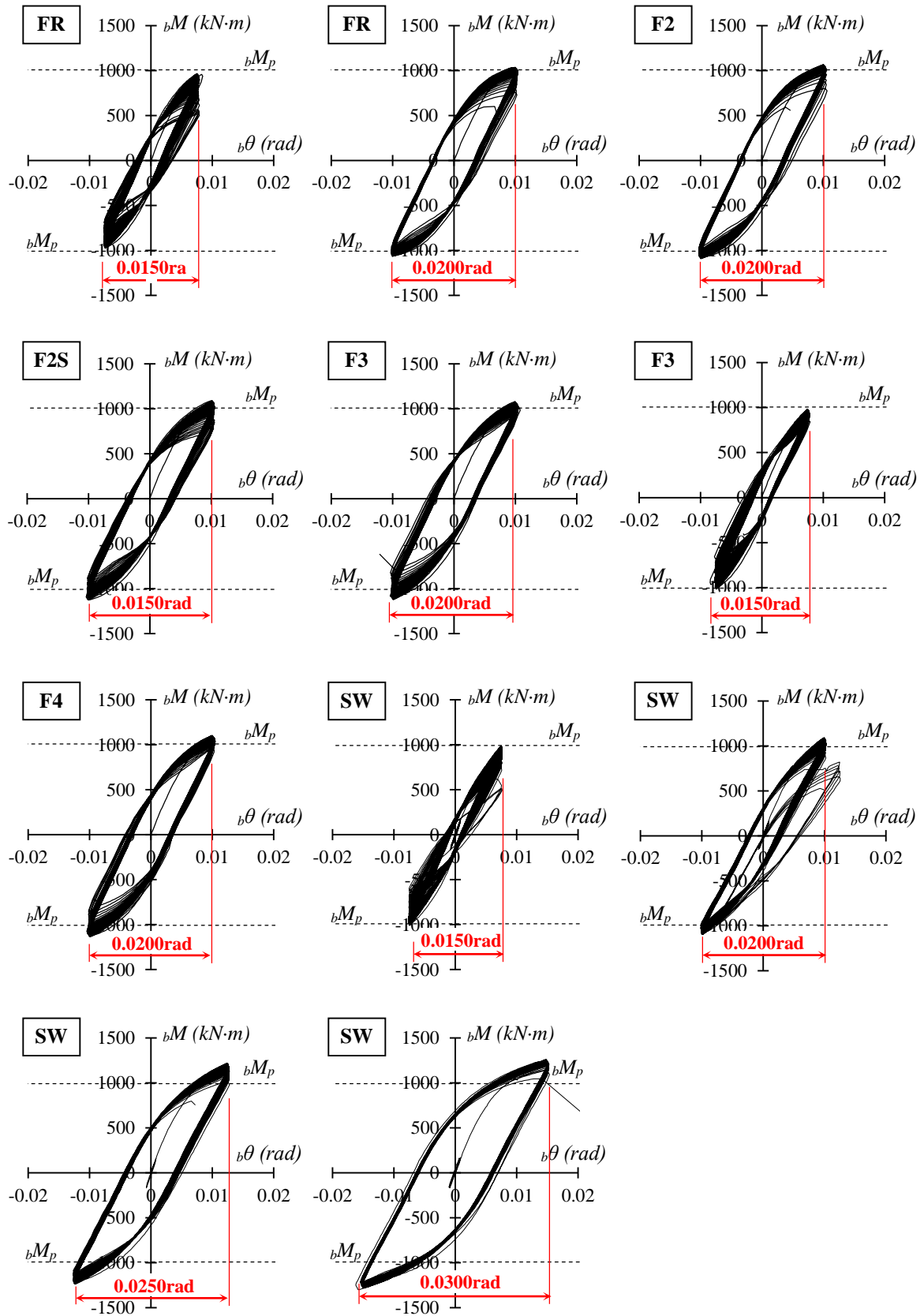
Fig. 2.9 Hysteretic response

2.4.3   Low-Cycle Fatigue Performance

The LCF performance plotted as the number of cycles to failure, N_f, versus constant beam rotation amplitude, $\Delta_b\theta_{const.}$, are shown in **Fig. 2.10**. The graph below compares LCF performance of welded connection and WFBW connection in different bolts configuration The gray line represents fatigue curve for welded connection. As shown in **Fig. 2.10**, welded connection exhibits excellent LCF performance comparing with WFBW connection. LCF performances for WBFW connection were different according to the bolt configuration under identical loading histories. Some WFBW connection exhibit nearly the same LCF performance as welded connection. It can be interpreted that the slip behavior in bolted web connections affect the moment transmission efficiency in the web connection, even under small beam plastic rotation amplitude before bending of the bolts.
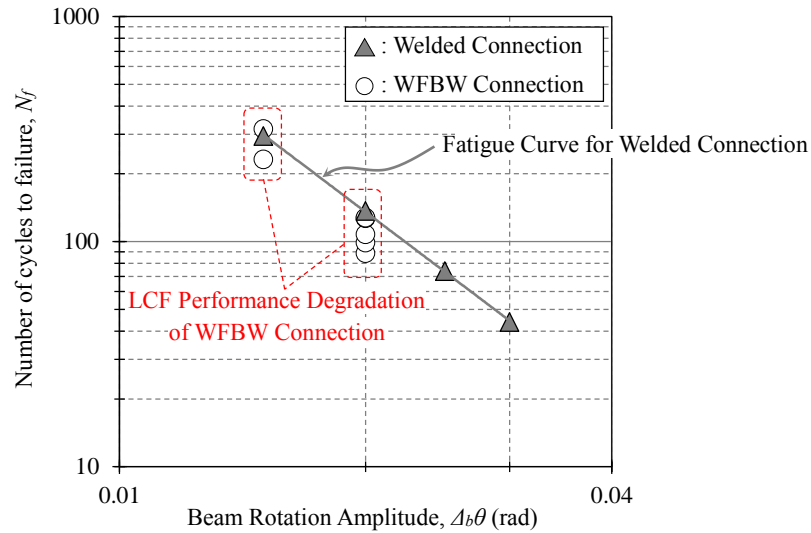
Fig. 2.10 LCF Performance WFBW Connection and Welded Connection

2.5   Discussions

2.5.1   Slip Behavior

During the cycles, slip behavior of bolted web connection is monitored with displacement measuring instruments as shown in **Fig. 2.11**. The relative slip displacement between shear plate and beam web is measured by using displacement transducer installed shear plate and beam web which is the same location (**Fig. 2.11(a)**). Slip rotation angle, θ_s, can be obtained as follows.
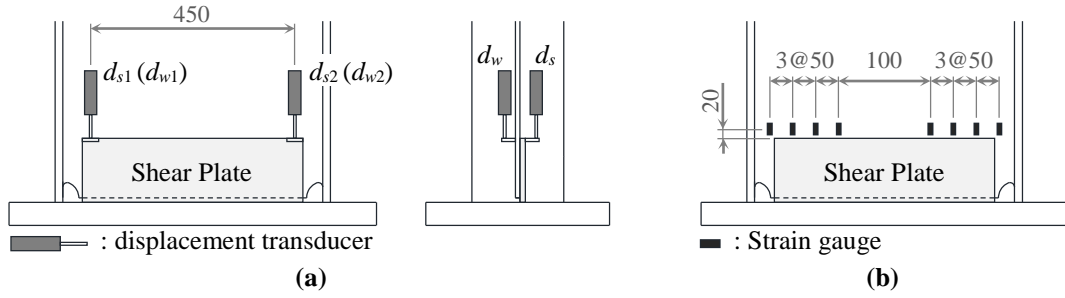
Fig. 2.11 Measurements slip behavior: **(a)** slip (relative displacement between shear plate and web) and **(b)** moment sharing in a bolted web connection

$$\theta_s = \frac{(\delta_{w1} - \delta_{s1}) - (\delta_{w2} - \delta_{s2})}{450} \qquad (5)$$

where, δ_s and δ_w are displacement on the tip of shear tab and same location of web, respectively. Local strain was measured with the strain gauge glued on the web as shown in **Fig. 2.11(b)** during the cycles. By using the local strain on the beam web, moment sharing in a bolted web connection, $_{Bw}M_e$, was calculated. In the calculation, strain distribution was obtained assuming straight distribution interval of local strain at each beam web section, and stress were obtained from the tensile test results for web coupon.

Slip behavior of bolt configuration FR, F2 and F2s plotted as the slip rotation angle, θ_s, versus moment sharing in a bolted web connection, $_{Bw}M_e$, are shown in **Fig. 2.12**.
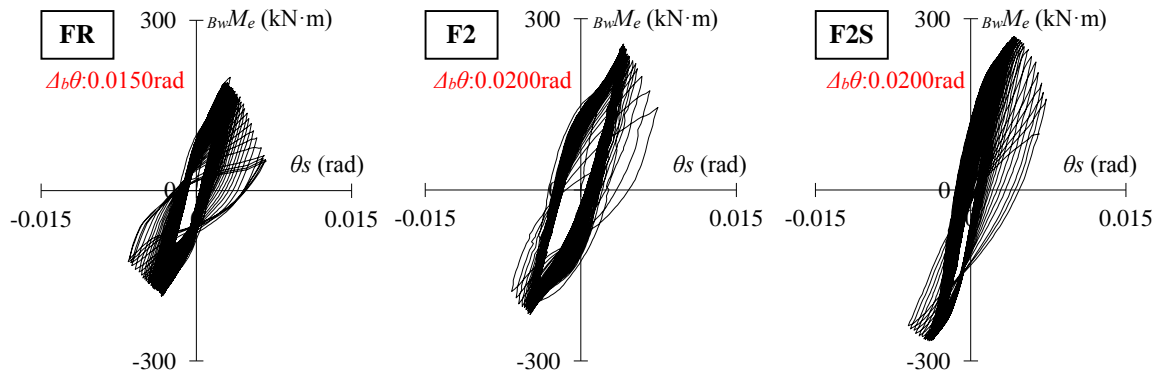
Fig. 2.12 Slip behavior

As shown in **Fig. 2.12**, slip occurred with slip rotation angle increased after a relative slip displacement between shear plate and beam web occurred at the low stress levels while resisting the web components of moment (Kato et al. 2003).

In this study, the load at which the slip rotation angle begins to increase is defined as the experimental slip strength, and this is used as an index representing the behavior of bolt web connection. With respect to the experimental slip strength, initial slip moment and primary slip moment are defined corresponding to the point when the slip behavior begins to appear to the load and when clear slip deformation was found, respectively, on the skeleton curve extracted from the relationship between $_{Bw}M_e$ and θ_s. Here, initial slip moment, $_{Bw}M_1$, was defined as load corresponding to the intersection of the tangent of the 1/3 initial stiffness line and initial stiffness in the skeleton curve extracted from the relationship between $_{Bw}M_e$ and θ_s as shown in **Fig. 2.13(a)**. Initial stiffness was defined from the unloading part of 1/3 to 2/3 load sections from peak load. The primary slip moment, $_{Bw}M_2$, was defined 0.01rad offset strength, which is slip rotation angle corresponding to the bolt slip displacement of 0.2mm at the outermost edge as shown in **Fig. 2.13(b)**.

(a) Initial Slip Moment (b) Primary Slip Moment
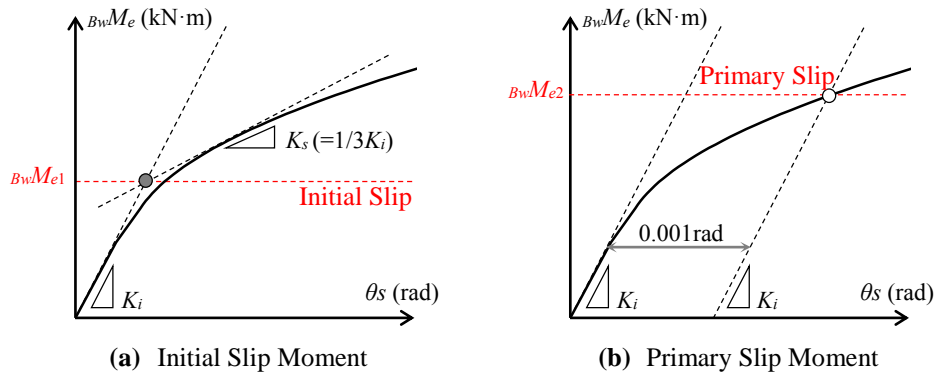
Fig. 2.13 Definition of slip moment through experimentally obtained slip behavior.

The experimental slip moment, which are $_{Bw}M_1$ and $_{Bw}M_2$ of each bolts configuration is shown in **Fig. 2.14** with the peak moment of the 1st cycle by the dashed line in the skeleton curve extracted from the relationship between $_{Bw}M_e$ and θ_s, and summarized in **Table 2.5**.

Table 2.5 Experimental slip moment

Bolts Configuration	Beam rotation Amplitude, $\Delta_b\theta$ rad	Initial Stlip Moment, $_{Bw}M_1$ kN·m	Primary Slip Moment, $_{Bw}M_2$ kN·m
FR	0.0150	92	128
	0.0200	117	166
F2	0.0200	117	165
F2S	0.0200	162	216
F3	0.0150	152	-
	0.0200	174	229
F4	0.0200	156	233
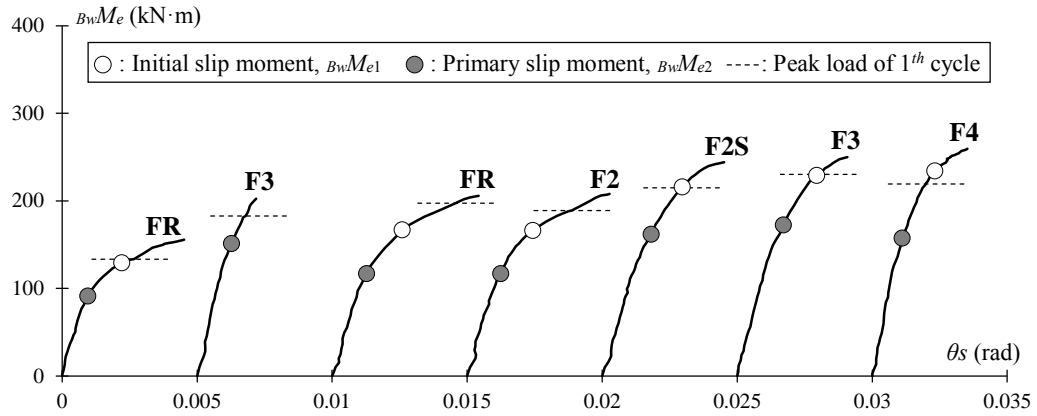
Fig. 2.14 Initial slip moment and primary slip moment

Experimental slip moments are different for FR and F3 of the same bolt configuration, but it can be seen that this is not the influence of the loading history but the variation between the specimens.

The comparison of calculated slip-critical strength, $_{Bw}M_S$, and experimental slip moment, $_{Bw}M_e$, are shown in **Fig. 2.15**. In the **Fig. 2.15**, the yield strength of shear plate (full cross-section, not considering the loss of shear plate section due to the bolts hole) calculated by using the nominal thickness and yield stress obtained from inspection certificate by mill test report is also shown.
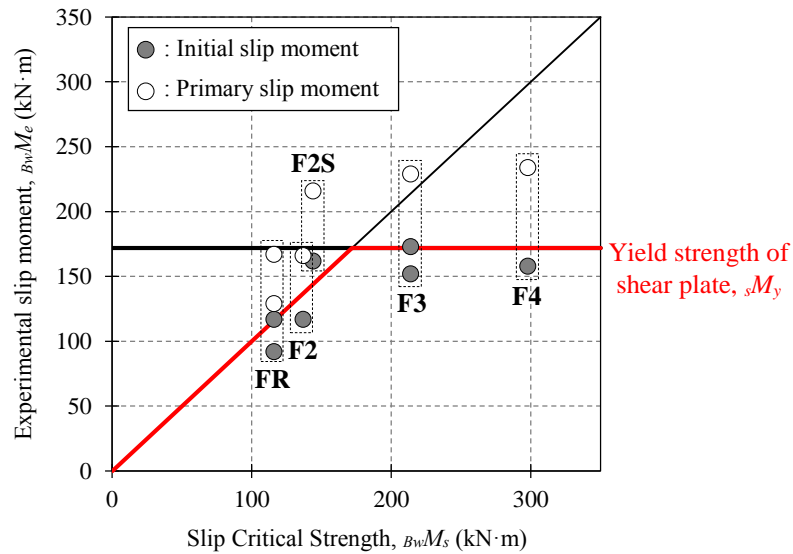
Fig. 2.15 Evaluation of experimental slip moment.

As shown in **Fig. 2.15**, the experimental initial slip moment, $_{Bw}M_1$, roughly correspond with slip-critical strength, $_{Bw}M_s$, below yield strength of shear plate, $_sM_y$, and $_sM_y$ corresponds to the upper limit of $_{Bw}M_1$. Because the thickness of shear plate and beam web were reduced on the tensile side by bending so that the axial force of the high-strength bolt decreased and slip occurred, the $_{Bw}M_1$ have shown such as the above correspondence. On the other hand, primary slip moment, $_{Bw}M_2$, is a higher value than $_{Bw}M_s$, and the upper limit is the load exceeding the $_sM_y$. According to the test results, it is confirmed that the lower value between $_{Bw}M_s$ and $_sM_y$ corresponds to $_{Bw}M_1$ when the out-of-plane deformation of the column flange is negligible. In the study, the LCF performance of the WFBW connection is evaluated by using the lower value of $_{Bw}M_s$ and $_sM_y$ as an index to evaluate the slip behavior of bolted web connection.

2.5.2   Low-Cycle Fatigue Performance Assessment Considering Slip Behavior

The relationship of the values $\min\{_{Bs}M_s, _sM_y\} / _sM_y$ versus the number of cycles to failure, N_f, relationship for the WFBW connection is illustrated in **Fig. 2.16**. In the case of the welded connections, the values of $\min\{_{Bs}M_s, _sM_y\} / _sM_y$ are estimated as 1.0. The led dashed-line circles represent the same loading history groups. Note that the yield strength of the shear plate for the WBFW connection ($_sM_y$ =172 kN.m) possesses an approximate equivalent web strength for the welded web connection ($_bM_w$=162 kN.m).
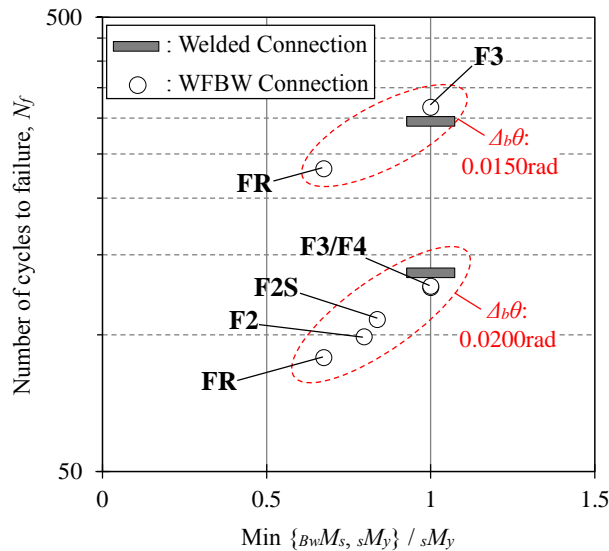
Fig. 2.16 LCF Performance with strength of bolted web connection

The min$\{_{Bs}M_s, _sM_y\}$ / $_sM_y$ for WBFW connection specimens is proportional to the number of cycles to failure, N_f. In the case of the web connection, the strength is determined by the yield strength of the shear plate for WBFW connections, and this calculation gives an approximate N_f with a welded web connection. In light of these test results, if the yield strength of the shear plate was designed to be smaller than the slip-critical strength for the WBFW connection, then the slip behavior would be negligible when evaluating the LCF performance.

2.6 Summary and Conclusion

This study investigated experimentally LCF performance of WFBW connection considering the behavior of bolted web connection according to the bolt configuration. The cycle loading test was carried out using five different bolts configuration at the bolted web connection under a large number of minor inelastic cycles.

The following conclusions are made:

- All the tests occurred ductile fracture via the growth of cracks at the weld access hole or weld toe of the beam flange; However, the LCF capacity varied according to the bolt configuration at the bolted web connection.

- Slip occurred with slip rotation angle increased after a relative slip displacement between shear plate and beam web occurred at the low stress levels while resisting the web components of moment because the thickness of shear plate and beam web were reduced on the tensile side by bending so that the axial force of the high-strength bolt decreased.

- The slip behavior of bolted web connection was different under minor inelastic deformation, the LCF performance enhanced the corresponding slip-critical strength; however, the specimens that possess a larger slip-critical strength than yield bending strength of the shear plate exhibit an increase in the number of cycles to failure.

- The strength of the web connection for the WFBW connections determined the minimum value between the slip-critical strength and the yield bending strength of the shear plate. If the strength of bolted web connection of the WBFW connection is equal to yield strength of the welded web connection, the LCF capacity is the same.

References

Architectural Institute of Japan, (2003). Guidebook on Design and Fabrication of High Strength Bolted Connections. (In Japanese)

Architectural Institute of Japan, (2012). Japanese Architectural Standard Specification JASS6〈2007〉: Structural Steelwork Specification for Building Construction. (in Japanese)

Architectural Institute of Japan, (2012). Recommendation for Design of Connections in Steel Structures. (in Japanese)

Ballio, G., Calado, L., & Castiglioni, C. A. (1997). Low cycle fatigue behavior of structural steel members and connections. *Fatigue & Fracture of Engineering Materials & Structures*, *20*(8), 1129-1146.

Building Research Institute: National research and development. (2014). Study on Seismic Performance for Super-High-Rise Steel Buildings against Long-Period Earthquake Ground Motions, No.160. (in Japanese).

Chung, Y. L., Nagae, T., Matsumiya, T., & Nakashima, M. (2011). Seismic resistance capacity of beam–column connections in high‐rise buildings: E‐Defense shaking table test. *Earthquake Engineering & Structural Dynamics*, *40*(6), 605-622.

Coffin Jr, L. F. (1954). A study of the effects of cyclic thermal stresses on a

Emi, T., Tabuchi, M., Tanaka, T., Mamba, H. & Nagatani, Y. (2004). Stress transfer of high strength bolt connection on beam to SHS column joint whose web bolted and flange welded. Steel Construction Engineering, 11(43), 25-40. (in Japanese)

Kanvinde, A. M., & Deierlein, G. G. (2006). The void growth model and the stress modified critical strain model to predict ductile fracture in structural steels. *Journal of Structural Engineering*, *132*(12), 1907-1918.

Kanvinde, A. M., & Deierlein, G. G. (2007). Cyclic void growth model to assess ductile fracture initiation in structural steels due to ultra low cycle fatigue. *Journal of engineering mechanics*, *133*(6), 701-712.

Kanvinde, A. M., & Deierlein, G. G. (2008). Validation of cyclic void growth model for fracture initiation in blunt notch and dogbone steel specimens. *Journal of structural engineering*, *134*(9), 1528-1537.

Kato, B., Kaneko, H. & Usami, T. (2003). Mechanical Performance of Web Bolted Joint Steel Beam. J. Struct. Constr. Eng., 10(40), 1-7. (in Japanese)

Krawinkler, H., & Zohrei, M. (1983). Cumulative damage in steel structures subjected to earthquake ground motions. *Computers & Structures*, *16*(1-4), 531-541.

Lee, C. H., & Kim, J. H. (2007). Seismic design of reduced beam section steel moment connections with bolted web attachment. *Journal of Constructional Steel Research*, *63*(4), 522-531.

Lee, C. H., Jeon, S. W., Kim, J. H., & Uang, C. M. (2005). Effects of panel zone strength and beam web connection method on seismic performance of reduced beam section steel moment connections. *Journal of Structural Engineering*, *131*(12), 1854-1865.

Manson, S. S. (1954). Behavior of materials under conditions of thermal stress.

Morrison, M. L., Schweizer, D. Q., & Hassan, T. (2016). Seismic enhancement of welded unreinforced flange-bolted web steel moment connections. *Journal of Structural Engineering*, *142*(11), 04016102.

Takatsuka, K., Suita, K., Tanaka, T. & Umeda, T. (2014). Effect of beam section size and connection detail on deformation capacity: Deformation capacity of welded beam-to-column connection subjected to repeated plastic strain Part 4. J. Struct. Const. Eng., AIJ, 77(696), 315-321. (in Japanese)

Tanaka, A., Masuda, H., Takagi, M. & Hisada, T. (1996). Experimental study on the static characteristics of the WBFW type beam-to-column connections. J, Struct, Const. Eng, AIJ, 61(484), 121-130. (in Japanese)

CHAPTER 3

LOW-CYCLE FATIGUE PERFORMANCE ASSESSMENT OF

BEAM-TO-COLUMN CONNECTION

3.1 Introduction

In steel moment-resisting frame (MRF) systems, the strong-column/weak-beam design concept is commonly employed to achieve a stable frame behavior during strong earthquake ground shaking. To evaluate the seismic performance of the steel MRFs, it is important to accurately identify the plastic deformation capacity of the beam-to-column connection. Recent design codes such as the American Institute of Steel Construction seismic provision (AISC 2005) and Japanese design recommendations (AIJ 2012) provide detailed design requirements to achieve sufficient plastic deformation of a beam against a relatively small number of inelastic response displacements of steel MRFs due to earthquake ground motion. However, massive earthquakes tend to have long-duration and long-period ground motion characteristics. The 2011 Tohoku earthquake produced long-duration and long-period ground motions in metropolitan areas such as Tokyo, Nagoya and Osaka, and high-rise buildings swayed severely (Takewaki et al. 2011). Thus, the beam-to-column connections were subjected to cyclic deformation under many cycles; however, recent design codes are determined from insufficient data and knowledge and cannot evaluate the safety margin of beam-to-column connections subjected to cyclic deformation under many cycles caused by massive earthquakes.

This paper aims to evaluate the low-cycle fatigue (LCF) performance, as determined by ductile fracture, of beam-to-column connections that are used commonly in Japanese steel MRFs. Typical beam-to-column connection types in Japan are categorized as on-site-welding types: namely, the welded flange-bolted web (WFBW) and shop-welding types. Welded
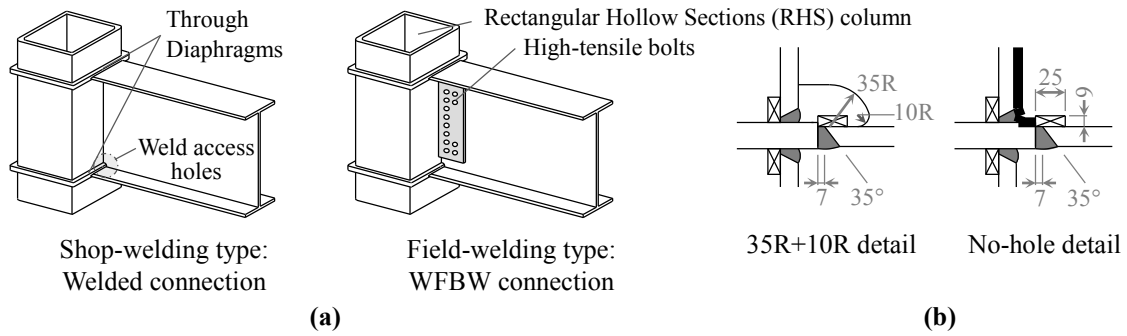
Fig. 3.1 Japanese connection details: (a) beam-to-RHS column connection and (b) current weld access hole details.

beam-to-column connection details with 35R+10R and no-hole weld access hole configurations are shown in **Fig. 3.1**. In the previous experimental study, the effect of the material characteristics and slip behavior of a WFBW connection were investigated by using three different steel grades (400 N/mm2, 490 N/mm2 and 590 N/mm2 class steel) and bolt configurations (Chapter 2 and Kishiki et al 2016). The test results show that the fatigue curves of the relationship between the number of cycles to failure and beam rotation amplitude are similar regardless of the different steel grades used due to the plastic range concentrated at the beam-end connection under minor inelastic cyclic deformation. The effect of the slip behavior on the LCF performance was shown to depend on the slip-critical strength and yield strength of the shear plate. The above tests were carried out with beam-end connection types. However, Japanese steel MRFs typically employ an H-beam-to-rectangular hollow section (RHS) column connection (see **Fig. 3.1(a)**). In the case of beam-to-RHS column, beam flanges are connected to the RHS column by through diaphragms, while beam web is connected to the RHS column flange without any reinforcement. Thus, the efficiency in transferring the moment of the beam web should be properly considered due to the local out-of-plane deformation of the column flange, as well as the loss of web sections when using the weld access hole configurations shown in **Fig. 3.1(b)**.

In this study, a comprehensive LCF performance assessment equation of beam-to-column connection is proposed considering the effects of steel grade and beam-end connection detail. The effect of the decreasing moment transfer efficiency of a beam web due to the slip behavior of the bolts, out-of-plane deformation of the column flange and loss of web section due to the weld access hole on LCF performance are evaluated by the coefficient, J_b. The LCF performance assessment equation for beam-to-column connections is proposed by assigning

the defined coefficient, J_b, to the relationship between the number of cycles to failure and beam rotation amplitude. To consider various beam-end connection details, a database is constructed. The database consists of test results from cyclic loading tests under minor inelastic deformation. Based on the test results collected in the database, an LCF performance assessment equation is proposed.

3.2 Database

3.2.1 List of Database

A list of beam-to-column connections in the database is summarized in **Table 3.1**. The database consists of the experimental data of minor inelastic deformation of beam-to-column connections subjected to constant-amplitude cyclic loading until fracturing (**Fig. 3.2**). The experimental data discussed in this paper considers only the deterioration mode due to the propagation of cracks and fractures at weldments and beam flanges. The deterioration mode induced by local buckling are not considered. The database consists of 9 series of WFBW connections (21 specimens) and 12 series of welded web connections (46 specimens) with different beam and column section dimensions, steel grades, shear span ratios and efficiencies in transferring moment at the beam web connection by using different beam-end connection types. The specimens in each series have the same steel grade, span and connection details but different loading amplitudes (constant beam rotation amplitude $\Delta_b\theta_{const.}$). The range of loading amplitude for each series is summarized in **Table 3.1**. The steel grades of the beams in the database are 400 N/mm^2, 490 N/mm^2 and 590 N/mm^2, and the material properties. Beam depth D and length $_bL$ range from 400 mm to 800 mm and 2017 mm to 4100 mm, respectively (shear span ratios $_bL/D$ range from 3.42 to 5.65). Two types of weld access hole configurations, 35R+10R and no-hole details (**Fig. 3.1(b)**) are discussed in this paper. In the case of the WFBW connection, the details of the bolt configurations are shown in **Fig. 3.3**.

Fig. 3.2 Cycle loading test of beam-to-column connection: (a) constant beam rotation amplitude (b) Beam rotation angle.

Table 3.1 Database of Japanese beam-to-column connection tested under constant amplitude cyclic loading.

Reference	Connection Type	Series	Section & Steel grade		Beam Span mm	Weld Access Hole Configuration	Contant Beam Rotation Ampltude rad	Number of Cycles to failure
Chapter 2	WFBW Connection	FR	End plate (TMCP325)	H-600×200×11×17 (SN490B)	2050	35R+10R	0.0150	232
							0.0200	317
		F2					0.0200	89
		F2S					0.0200	99
		F3					0.0150	108
							0.0200	127
		F4					0.0200	128
	Welded Connection	SW	End plate (TMCP325)	H-600×200×11×17 (SN490B)	2050	35R+10R	0.0150	295
							0.0200	137
							0.0250	74
							0.0300	44
Kishiki et al. (2016)	WFBW Connection	SN40	H-500×400×32×19 (SN400B)	H-600×200×11×17 (SN400B)	3000	35R+10R	0.0187	107
							0.0250	39
	WFBW Connection	SN49	H-500×400×32×19 (SN490B)	H-600×200×11×17 (SN490B)	3000	35R+10R	0.0200	94
							0.0230	64
							0.0306	18
	WFBW Connection	SA59	H-500×400×32×19 (SA440B)	H-600×200×12×19 (SA440B)	3000	35R+10R	0.0240	64
							0.0248	38
							0.0257	33
							0.0300	14
							0.0397	6

Reference	Connection Type	Series	Section & Steel grade		Beam Span mm	Weld Access Hole Configuration	Contant Beam Rotation Ampltude rad	Number of Cycles to failure
Umeda et al. (2015)	WFBW Connection	SCWB	□-350×350×22 (BCR295)	H-500×200×10×16 (SN490B)	2492	35R+10R	0.0117	531
							0.0175	119
							0.0292	23
							0.0438	7
	Welded Connection	SCS	□-350×350×22 (BCR295)	H-500×200×10×16 (SN490B)	2492	35R+10R	0.0172	265
							0.0172	256
							0.0288	30
							0.0432	9
Suita et al. (2011)	Welded Connection	NSS	□-350×350×22 (BCR295)	H-500×200×10×16 (SN490B)	2492	No-hole	0.0180	274
							0.0180	225
							0.0300	63
							0.0300	55
							0.0450	25
							0.0450	20
							0.0600	13
							0.0600	14
	Welded Connection	NSW	□-350×350×22×9 (SN490B)	H-500×200×10×16 (SN490B)	2492	No-hole	0.0170	220
							0.0170	280
							0.0284	38
							0.0284	28
							0.0426	15
							0.0426	17
							0.0568	7
							0.0568	6

Reference	Connection Type	Series	Section & Steel grade		Beam Span mm	Weld Access Hole Configuration	Contant Beam Rotation Ampltude rad	Number of Cycles to failure
Suita et al. (2009)	Welded Connection	SC	□-350×350×16 (BCR295)	H-400×200×8×13 (SN400B)	2017	35R+10R	0.0144	241
							0.0144	302
							0.0240	66
							0.0360	20
	Welded Connection	NS	□-350×350×16 (BCR295)	H-400×200×8×13 (SN400B)	2017	No-hole	0.0144	541
							0.0144	635
							0.0240	101
							0.0360	49
Uozumi et al. (2013)	Welded Connection	SCS-2.B	□-550×550×22 (BCP325)	H-500×200×10×16 (SN490B)	2825	35R+10R	0.0340	19
		SCW-2.0B	□-550×550×22×9 (SN490B)	H-500×200×10×16 (SN490B)			0.0340	12
Seki et al. (2013)	Welded Connection	N	□-500×500×25 (SN490C)	H-600×200×12×19 (SN490B)	3000	No-hole	0.0287	105
							0.0573	27
Takatsuka et al. (2014)	Welded Connection	NSL	□-550×550×22 (BCP325)	H-800×300×16×28 (SN490B)	3770	No-hole	0.0180	154
							0.0300	46
							0.0450	13
	Welded Connection	SCL	□-550×550×22 (BCP325)	H-800×300×16×28 (SN490B)	3770	35R+10R	0.0180	106
							0.0300	33
							0.0450	13
							0.0600	5
Uozumi et al. (2014)	Welded Connection	SCW	□-350×350×22×9 (SN490B)	H-500×200×10×16 (SN490B)	2325	35R+10R	0.0176	101
							0.0292	15
							0.0438	4

(a) Kishiki et al. 2016

Beam: H-600×200×11×17 (SN400B/SN490B)
PL11-480×140 (SN400B&SN490B)
8@50
13-F10T M20
Column: H-500×400×32×19 (SA440)
SN40 & SN49

Beam: H-600×200×12×19(SA440)
PL12-480×140(SA440B)
8@50
13-F14T M20
SA59

35R
10R
Flange
35°
17/19
FB-25×9
Details of beam-flange groove

(b) Umeda et al. 2015

Beam: H-500×200×10×16(SN490B)
PL12-260×90(SN490B)
4@60
4-S10T M22
Column: □-350×350×22(BCR295)
SCWB

SCS

FB-25×9
35R
10R
Flange
35°
16
Details of beam-flange groove

(c) Suita et al. 2011

Beam: H-500×200×10×16(SN490B)
Column: □-350×350×22(BCR295)
NSS

Column: □-350×350×22×9(SN490B)
NSW

FB-25×9
35R
10R
Flange
35°
16
Details of beam-flange groove

(d) Suita et al. 2009

Beam: H-400×200×8×13(SN400B)
Column: □-300×300×16(BCR295)

FB-25×9
35R
10R
Flange
35°

FB-25×9
Flange
35°
13
Details of beam-flange groove

SC

NS

(e) Uozumi et al. 2013

(f) Seki et al. 2013

(g) Takatsuka et al. 2014

(h) Uozumi et al. 2014

Fig. 3.3 Beam-end connection details

3.2.2 Scope of Evaluation

From the database, the number of cycles to failure $N_{f,exp.}$ with imposed beam rotation amplitude (constant amplitude) $\Delta_b\theta_{const.}$ are plotted in **Fig. 3.4**. The shaded section represents the range for evaluation discussed in this study (the range of beam rotation is approximately 0.01~0.06 rad). According to the cycle loading tests on WFBW connection (Kishiki et al. 2016), the LCF performance can be evaluated by the same fatigue curve in the relationship of $N_{f,exp.}$ and $\Delta_b\theta_{const.}$ regardless of the yield stress of steel (**Appendix B**). In order to evaluated effect of beam-end geometry on LCF performance, the details of beam-end connection type are grouped into WFBW and welded connection with 35R+10R weld access hole configuration, as well as welded connection with no-hole details in weld access hole configuration.

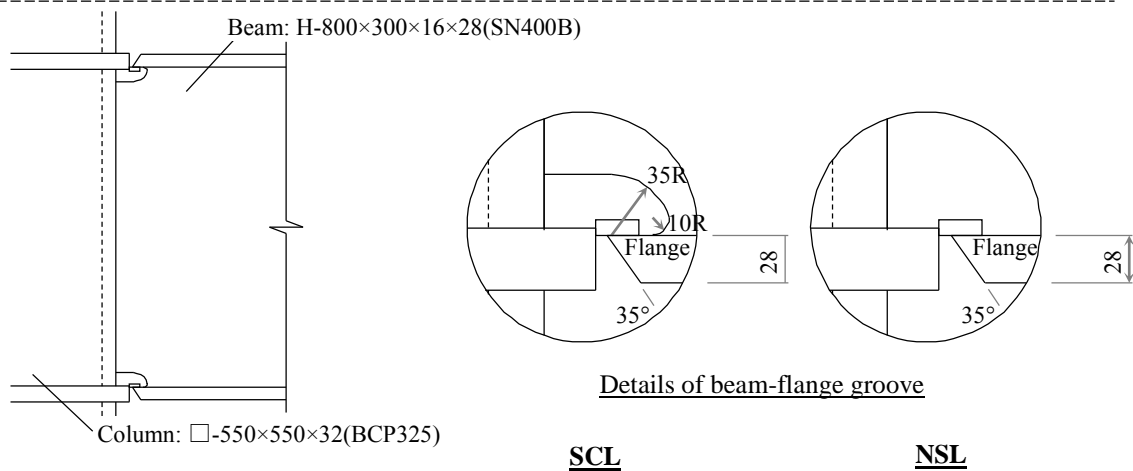On the whole, the $N_{f,exp.}$ of the WFBW connection is low compared to the welded web connection, and in the case of the welded web connection, according to the weld access hole configuration, the $N_{f,exp.}$ of specimens with no-hole details is higher than that of specimens with 35R+10R details, as shown in **Fig. 3.4**. This result is caused by the decrease in the moment transfer efficiency at the web connection due to the slip behavior of the bolted web and loss of web section due to the weld access hole. In this study, an LCF performance evaluation method for beam-to-column connections is proposed for specimens with current connection details. The effect of steel grade was evaluated with the fatigue curve from the $N_{f,exp.}$ and $\Delta_b\theta_{const.}$ relationship
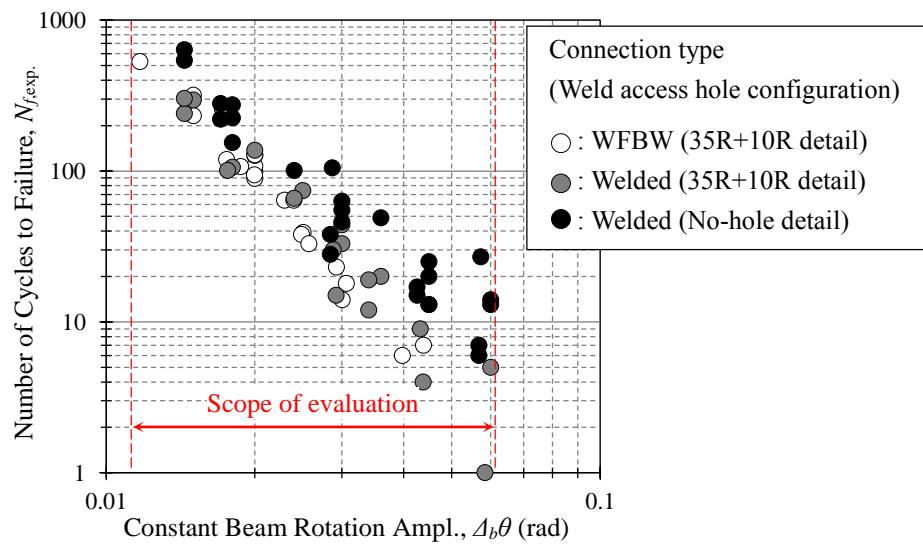
Fig. 3.4 N_f versus $\Delta_b\theta$

3.2.3 Assessment of Low-Cycle Fatigue Performance by using Hasegawa Eq. 2014

In the previous study (Hasegawa et al. 2014), the LCF evaluation equation of beam-to-column connection for the safety of the high-rise steel moment resisting frames was proposed based on the relationship between number of cycles, $N_{f,exp.}$ to failure and ductility factor, μ.

$$\mu = C \cdot N_{f,Narihara}^{-\beta} \tag{3.8}$$

where constant, C, is determined beam-end connection geometry and β is set to 1/3 with a constant gradient. Constant, C, is defined as follows based on the cyclic loading test results.

Table 3.2 Constant, C

	Weld Access Hole Configuration	
	35R+10R or 35R details	No-hole details
Experimentally obtained constant, C	5	7

The Eq. (3.8) considers two types of beam-end connection geometry with weld access hole configuration. The effects of steel grade were not considered. Using previous evaluation Eq. (3.8) for LCF performance, the test results of database are evaluated and shown in **Fig. 3.5**. As shown in **Fig. 3.5**, number of cycles to failure, $N_{f,exp.}$, are not correspond with the calculated number of cycles to failure, $N_{f,Narihara}$ and linear regression coefficient are 0.24 and 0.89, respectively.

(b) WFBW and welded connection with 35R+10R   **(a)** Welded connection with No-hole
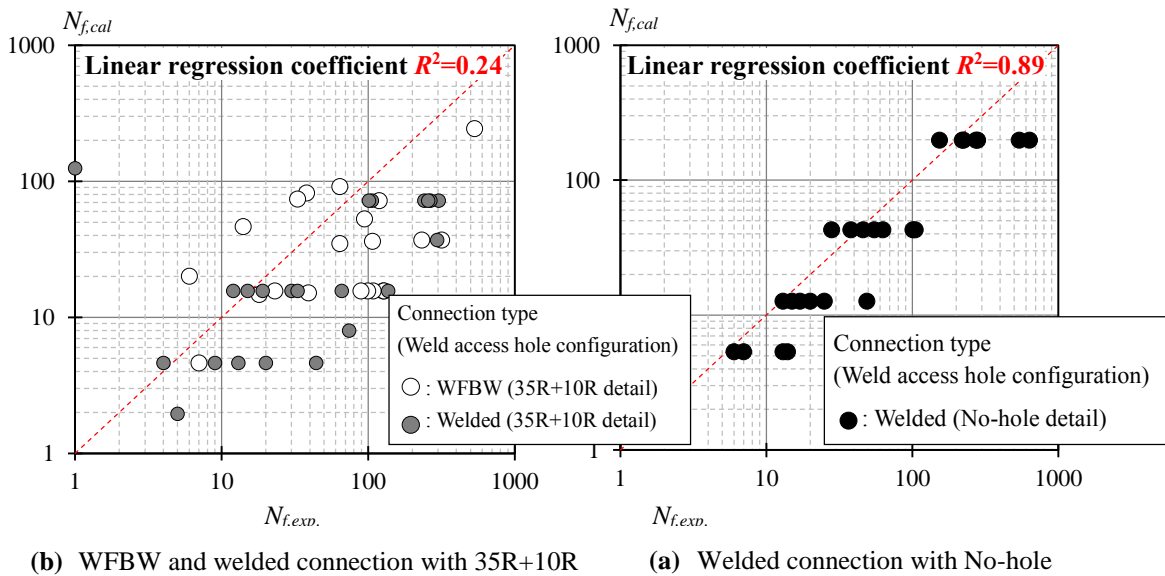
Fig. 3.5 $N_{f,cal.}$ versus $N_{f,exp.}$ (Narihara et al. 2013)

3.3 Evaluation of Moment Transfer Efficiency at the Beam-End Connection

3.3.1 Effective Strength at the Beam Web Connection

The moment transfer efficiency at the beam web connection depends on the beam web connection geometry, and it affect LCF performance of beam-to-column connection. In this **chapter 3**, two connection type which are WFBW and welded beam-to- column are considered, and the decrease of moment transfer efficiency at the beam web connection due to slip behavior of bolts (see **Fig. 3.6(a)**) and out-of-plane deformation of column flange as well as loss of web section by weld access hole is considered (see **Fig. 3.6(b)**).

Moment sharing at WFBW beam-end connection

Moment sharing at beam-end connection with thin column flange
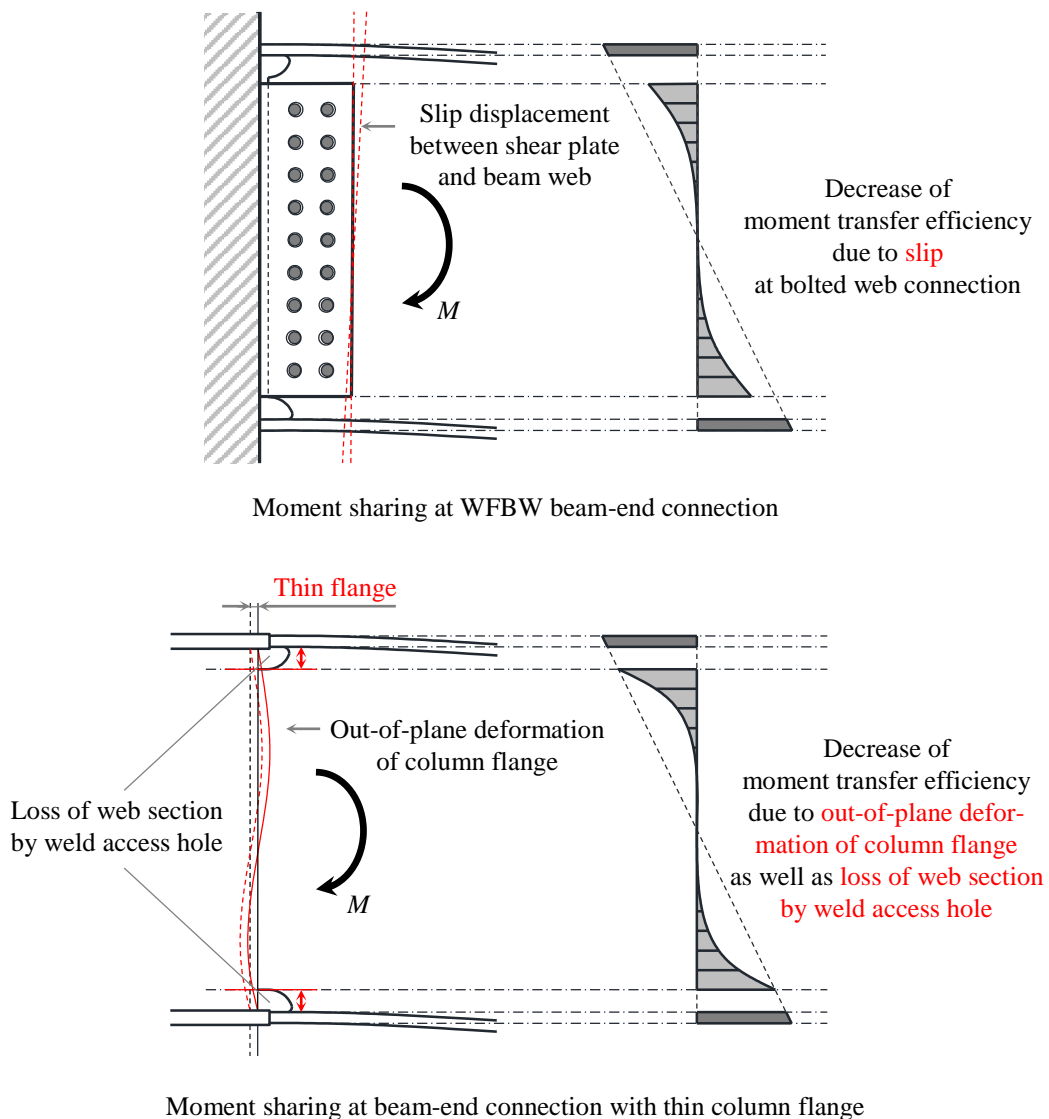
Fig. 3.6 Decrease of moment transfer efficiency at the beam web connection

The effect of slip behavior of WFBW connection on LCF performance is evaluated in **Chapter 2**. The results of **Chapter 2** are summarized as follows.

LCF performance of WFBW connection depends on the bolts slip behavior. The slip behavior of bolted web connection was evaluated the slip-critical strength, $_{Bw}M_s$, and yield bending strength of shear plate, $_sM_y$. The strength bolted web connection can be calculated as follows.

$$_{jBw}M = \min\left\{_{Bw}M_s, _sM_y\right\}$$ (3.1)

where $_sM_y$ calculated by using a cross section which is not considered partial loss due to the bolt holes. The calculation method of the $_{Bw}M_s$ is summarized in **Appendix A**. In addition, according to the experimental results, it is noted that the slip behavior of bolted web connection determined by yield strength of shear tab performed all most equal to welded web connection.

The efficiency in transferring moment of beam-end connection due to the out-of-plane deformation of column flange, as well as the loss of web section by the weld access hole is defined as effective yield strength, $_{jw}M_y$, based on the yield line theory by Suita (2000). The detailed calculation method is summarized in **Appendix C**. In addition, the yield strength of the beam web connection, $_{jw}M_y$, is calculated by Eq. (3.2) using the strength ratio coefficient m, as summarized in **Appendix C**.

$$_{jw}M_y = m \cdot _{bw}Z \cdot _{bw}\sigma_y$$ (3.2)

where, $_{bw}Z$ and $_{bw}\sigma_y$ are section modulus and yield stress of beam web, respectively. In the case of the WFBW connection, $_sM_y$ is replaced by the effective yield strength of shear plate, $_{js}M_y$, with the same method which is summarized in **Appendix C**. As a result, the strength at the web connection, $_{jw}M$, is determined from the smallest strength which can be described by Eq. (3.3).

$$_{jw}M = \min\left\{_{Bw}M_s, _{js}M_y, _{jw}M_y\right\}$$ (3.3)

3.3.2 Moment Ratio of Beam-End Connection to Beam Member – Coefficient, J_b

In the previous experimental study (Kishiki et al. 2016), it is reported that the relationship between $N_{f,exp.}$ and $\Delta_b\theta_{const.}$ can be evaluated by Eq. (3.4) regardless of the yield strength

of the beam steel.

$$N_{f,\text{exp.}} = \alpha \cdot \Delta_b \, \theta_{const.}^{-\beta} \qquad (3.4)$$

where α and β of Eq. (3.4) are parameters related to beam-end connection geometry. To evaluate constants α and β considering the beam-end geometry, coefficient, J_b, which indicates the moment transfer contribution of the beam web to the beam member, is defined by Eq. (3.5).

$$J_b = \frac{{}_{bf}M_y + \min\left\{{}_{Bw}M_s, \, {}_{js}M_y, \, {}_{jw}M_y\right\}}{{}_bM_y} \qquad (3.5)$$

where ${}_{bf}M_y$ and ${}_bM_y$ are yield strength of beam flange and beam full section, respectively. Coefficient, J_b, implies ratio of the effective yield strength at the web connection and yield strength of beam flange to the beam yield strength, which is calculated under cross section remain plane as shown in **Fig. 3.7**.
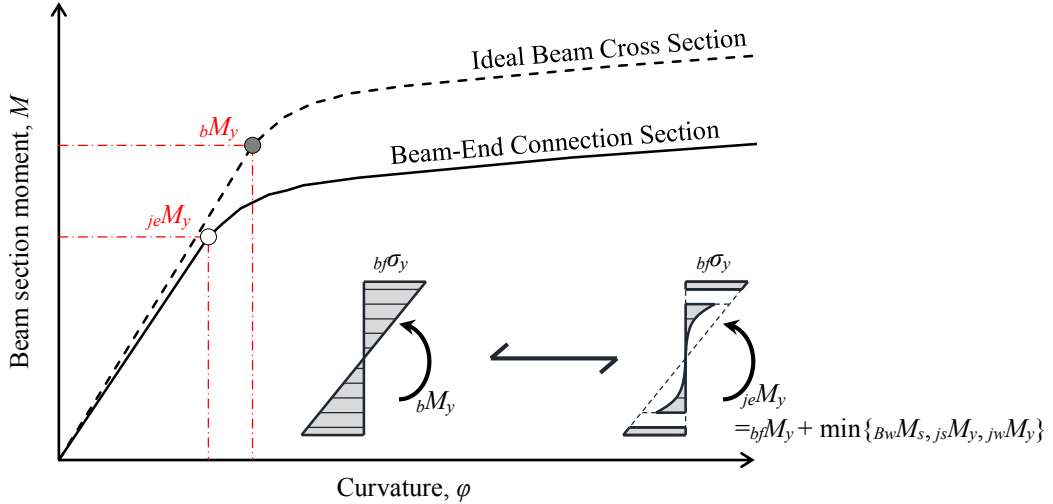
Fig. 3.7 Beam section moment, M, versus curvature, φ, at beam-end connection

3.3.3　Coefficient, J_b, of Beam-to-Column Connection

The strength required for calculation of coefficient, J_b, and the coefficient, J_b, are summarized in **Table 3.3** and **Fig. 3.8** The numbers in parentheses in **Fig. 3**.8 represent the number of specimens. In the calculation of yield strength required for coefficient, J_b, tensile test results were used. If the measured material properties are unknown from the paper, the average value of the measured yield stress specified in "Investigation of Mechanical Properties of Steel"

(Fujisawa et al. 2013) were used (e.g. SN490C steel grade: 372N/mm^2 and BCR295 steel grade: 392 N/mm^2). In case of calculation of the slip-critical strength of WFBW connection, slip coefficient 0.45, which is the minimum requirements in slip-critical bolted connection, were used except specimens from Yamada et al (2016). These specimens, slip coefficient of 0.57 which obtained from the slip coefficient test were used for calculation of slip-critical strength. The effective yield strength at the beam web connection in WFBW connection except part of specimens "F3 and F4" series were determined as slip-critical strength. In case of specimens F3 and F4, the strength at the bolted web connection was determined as yield strength of shear plate. The coefficient, J_b, discussed in this chapter are calculated ranging from 0.84 to 1.05. As shown in **Fig. 3.8**, the three groups, which are group A, B and C, were divided for evaluation of applicability coefficient, J_b. Group A is a group of coefficient, J_b, with 1.03 to 1.05, and is a group of specimens with higher strength at the beam end connection than the yield strength of beam member, which is ideal beam-end connection. Group B and C are assemblies of specimens to confirm that the coefficient, J_b, can evaluate by considering different moment transfer mechanism at the beam-end connection.
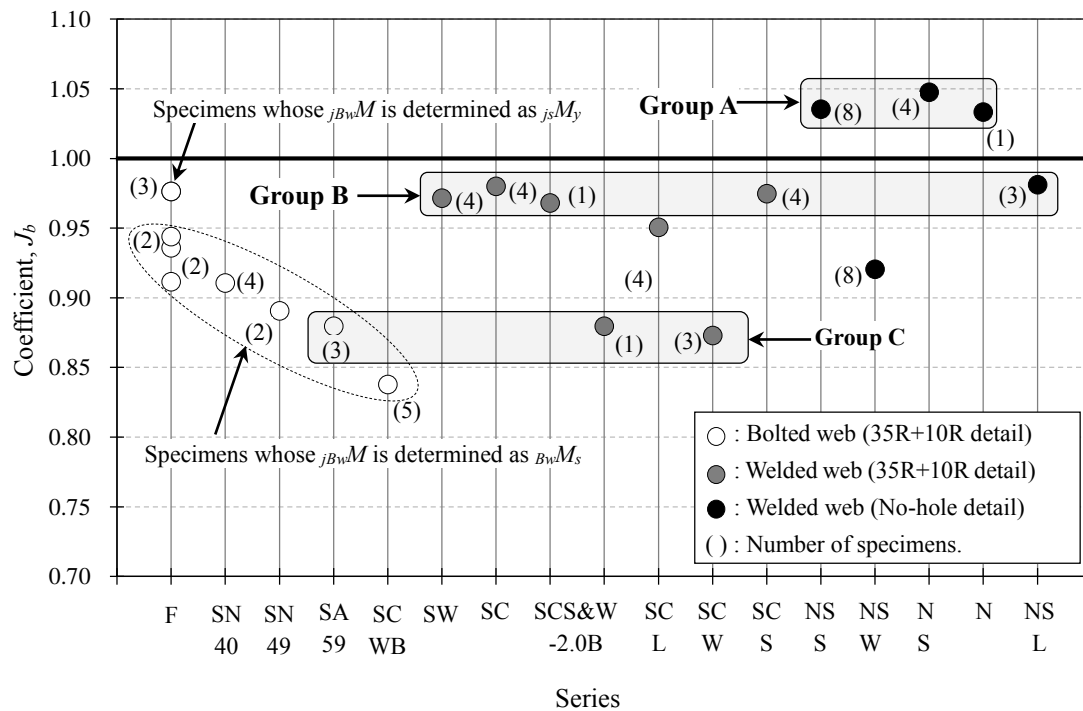

Fig. 3.8 Series of each specimens and coefficient, J_b.

Table 3.3 Strength required for calculation of coefficient, J_b, of each specimen.

References	Series	Yield Stress				Strength Ratio	Strength					Coefficient
		$_c\sigma_y$ N/mm²	$_{bf}\sigma_y$ N/mm²	$_{bw}\sigma_y$ N/mm²	$_s\sigma_y$ N/mm²	m	$_bM_y$ kN·m	$_{bf}M_y$ kN·m	$_{Bw}M_y$ kN·m	$_{js}M_y$ kN·m	$_{jw}M_y$ kN·m	J_b
Yamada et al. (2016)	FR								116			0.91
	F2								137			0.94
	F2S	-	347	391	373	-	861	669	144	373	-	0.94
	F3								214			0.98
	F4								298			0.98
	SW	-	349	373	-	-	849	662	-	-	162	0.97
Kishiki et al. (2016)	SN40		298	319	319	1.00	739	574	99	135		0.91
	SN49	-	347	408	408	1.00	861	669	98	172	-	0.89
	SA59		510	539	539	1.00	1392	1091	134	248		0.88
Umeda et al. (2015)	SCWB	393	352	386	366	1.00	648	528	15	45		0.84
	SCS	422	343	383	-	1.00	632	514	-	-	101	0.97
Suita et al. (2011)	NSS	378	352	392	-	1.00	648	528	-	-	143	1.04
	NSW	376				0.48					69	0.92
Suita et al. (2009)	SC	392[1]	277	340	-	1.00	318	270	-	-	42	0.98
	NS										63	1.05
Uozumi et al. (2013)	SCS-2.B	358	371	397	-	1.00	383	556	-	-	105	0.97
	SCW-2.0B					0.42					44	0.88
Seki et al. (2013)	N	372[1]	337	364	-	1.00	920	721	-	-	230	1.03
akatsuka et al. (2014)	NSS	366	344	384		0.75	2626	2154	-	-	423	0.98
	SCL	366	340	412	-	0.68	2595	2129	-	-	338	0.95
Uozumi et al. (2014)	SCW	392	368	395	-	0.38	678	552	-	-	40	0.87

[1]The average value of the measured yield stress specified in "Investigation of Mechanical Properties of Steel" were used

3.3.4 Assessment Coefficient, J_b

Group A

The coefficient, J_b, of ideal beam-end connection is the upper limit 1.00, however, the coefficients, J_b, of some specimens in welded web connection with no-access hole detail were calculated as 1.03 to 1.05 (Group A). These specimens are not influenced by the out-of-plane deformation of column flange because thickness of beam flange is thick (See **Table 3.3**). Also, the yield stress of the web was relatively higher than that of the beam flange, as a result the coefficient, J_b, was estimated to be 1.03 to 1.05. The closer the coefficient, J_b, is to 1.00, the more the ideal beam-end connection. The comparison of the LCF performance for specimens whose coefficient, J_b, is 0.97 to 0.98 and 1.03 to 1.05 is shown in **Fig. 3.9**. The black circles and gray diamond mark represent specimen of Group A with coefficient, J_b, of 1.03 to 1.05 and specimen of ideal connection which is 0.97 to 0.98 coefficient, J_b, respectively. The group A consists of the series "NS", "NSS" and "N" which are welded connection with no-hole detail in weld access hole configuration. And the group, which is coefficient, J_b, is 0.97 to 0.98, consists of the series "NSL", "SC", "F3", "F4", "SCS" and "SW" which are WFBW and welded connection with no-hole and 35R+10R details in weld access hole configuration. As shown in **Fig. 3.9**, it can be seen that the LCF performance of the specimen with coefficient, J_b, of 1.03 to 1.05 is higher than that of the specimen with 0.97 to 0.98 coefficient, J_b. It is confirmed that the fatigue life is increased corresponding moment transfer efficiency at the web connection even if the yield.
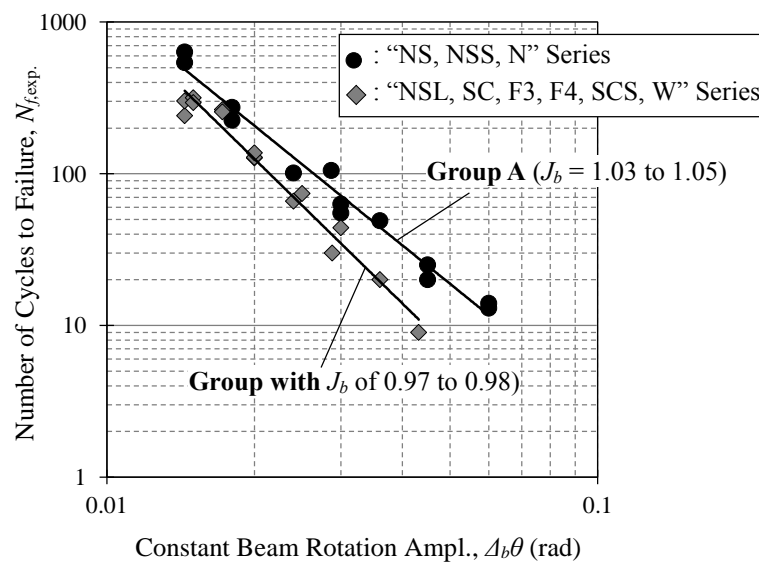

Fig. 3.9 LCF performance of group A

Group B & C

The coefficient, J_b, evaluates transferring moment contribution of web connection to beam with different mechanism such as slip behavior at bolted web and effective yield strength considering out-of-plane deformation of column flange as well as loss of the web section by weld access hole. It was investigated as to whether the moment transfer efficiency by different mechanisms can be evaluated as identical fatigue curve in the identical coefficient, J_b.
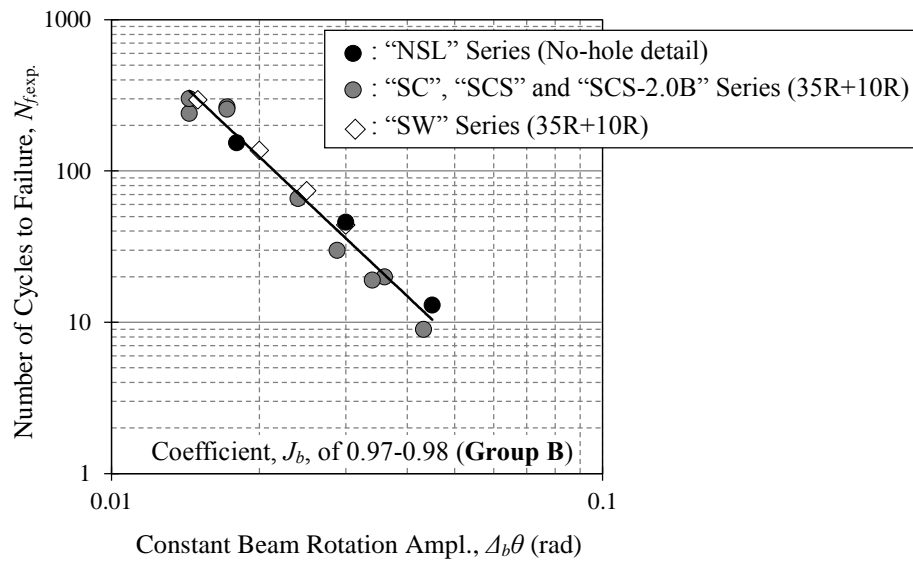
Fig. 3.10 Same coefficient, J_b, group with different weld access hole configuration

The relationship of $\Delta_b\theta_{const.}$ versus $N_{f,exp.}$ for specimens of Group B with 0.97-0.98 coefficient, J_b, is plotted in **Fig. 3.10**. The specimens "NSL" series were fabricated with no-hole details in weld access hole configuration and in the calculation of effective web yield strength, $_{jw}M$, out-of-plane deformation of column flange was only considered. The specimens "SC", "SCS", "SCS-2.0B" and "SW" series were fabricated with 35R+10R detail in weld access hole configuration, and in case of specimens "SC", "SCS" and "SCS-2.0B" series, in the calculation of $_{jw}M$, the loss of web section by weld access hole were considered. These specimens did not take into consideration the yield strength of the web connection due to the out-of-plane deformation of column flange, which is coefficient, m, of 1.00. Also, the specimens "SW" series were used 50mm of end plate instead of the column flange and the $_{jw}M$ was determined by the only the loss of the web section by weld access hole. When coefficient, J_b, are estimated to be the almost same, it can be evaluated almost same as one fatigue curve as

shown in **Fig. 3.10**, although the variables to be considered in the calculation of coefficient, *m,* are different. That is shown that not only effect of the out-of-plane deformation of column flange, but also specimens with no-hole details and 35R+10R detail in weld access hole configuration can be evaluated as same LCF performance under identical coefficient, J_b.
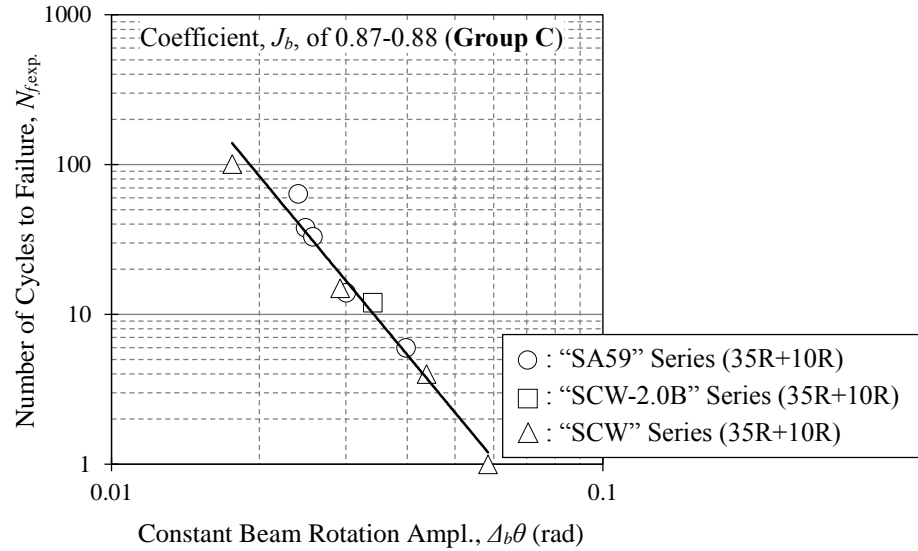
Fig. 3.11 Same coefficient, J_b, group with different beam web connection type

Fig. 3.11 shows "SCW-2.0B" and "SCW" series of welded web connection and "SA59" series of WFBW connection with the 0.87 to 0.88 coefficient, J_b. The contribution of moment at the beam web connection of the "SCW-2.0B" and "SCW " series were determined by the out-of-plane deformation of column flange and loss of the web section by weld access hole, while "SA59" series were determined by slip-critical strength. Although the moment transfer mechanism at the web connection of the two specimens which are "SA59" and "SCW-2.0B" and "SCW" series, is different, it can be seen that the similar LCF performance performed under almost same coefficient, J_b, as shown in **Fig. 3.11**. In conclusion, it is confirmed that the different mechanisms in moment transfer at the web connection, such as slip behavior, out-of-plane deformation of column flange and loss of the web section by weld access hole can be evaluated with coefficient, J_b. In other words, it was confirmed that the continuity of the WFBW connection and welded connection can be evaluated by coefficient, J_b. So, based on the coefficient, J_b, LCF performance evaluation Eq. is proposed considering beam-end geometry.

3.4 Low-Cycle Fatigue Performance Assessment

3.4.1 Coefficient, J_b, on Fatigue Curve of Beam-to-Column Connection

To propose the LCF performance assessment equation for beam-to-column connection considering beam-end connection details, coefficient, J_b, is substituted into Eq. (3.4). The constant a and β in Eq. (3.4) are defined to reflect coefficient, J_b, as follows.

The fatigue curves of each group A, B and C which has different coefficient, J_b, is plotted in **Fig. 3.12**. As shown in **Fig. 3.12**, the slope of each fatigue curve is different according to the coefficient, J_b, and it tends to become steep as the coefficient, J_b, becomes smaller. Furthermore, as the applied beam amplitude increase, the moment transfer efficiency of the web connection at the beam-end has a greater effect on the LCF performance.
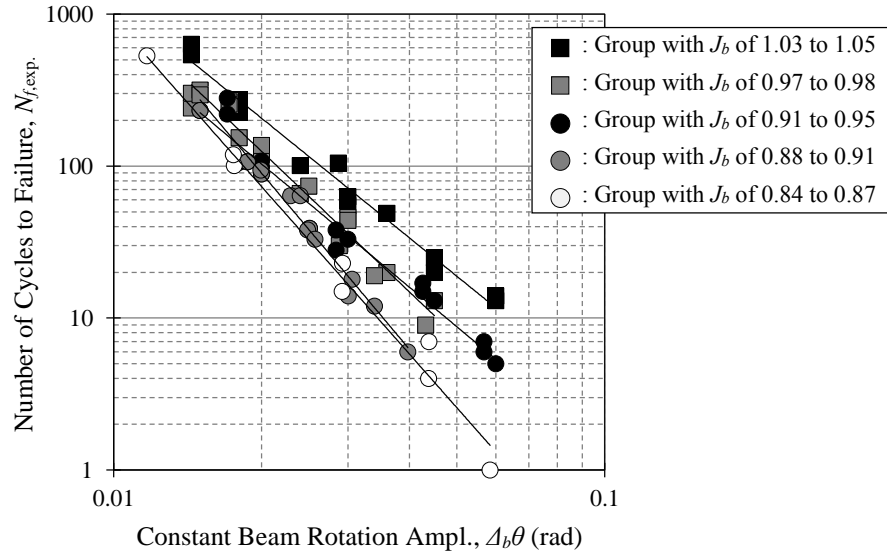
Fig. 3.12 Slope of fatigue curve according to the coefficient, J_b.

In order to investigate the relationship between β and coefficient, J_b, the groups of data with the almost same coefficient, J_b, were created. The regression Eq. for fatigue curves of each group are as follow.

$$J_{(1.03\sim1.05)} : N_{f,\text{exp.}} = 7.40 \times 10^{-3}\, \Delta b\theta_{const.}^{-2.62} \qquad (3.5.1)$$

$$J_{(0.97\sim0.98)} : N_{f,\text{exp.}} = 8.00 \times 10^{-4}\, \Delta b\theta_{const.}^{-3.07} \qquad (3.5.2)$$

$$J_{(0.92\sim0.95)} : N_{f,\text{exp.}} = 2.70 \times 10^{-3}\, \Delta b\theta_{const.}^{-2.70} \qquad (3.5.3)$$

$$J_{(0.88\text{-}0.91)} : N_{f,\exp.} = 3.00 \times 10^{-5} \Delta b \theta_{const.}^{-3.85} \qquad (3.5.4)$$

$$J_{(0.84\text{-}0.87)} : N_{f,\exp.} = 4.00 \times 10^{-5} \Delta b \theta_{const.}^{-3.67} \qquad (3.5.5)$$

where, the numbers in parentheses are the range of coefficient, J_b, of the data considered.
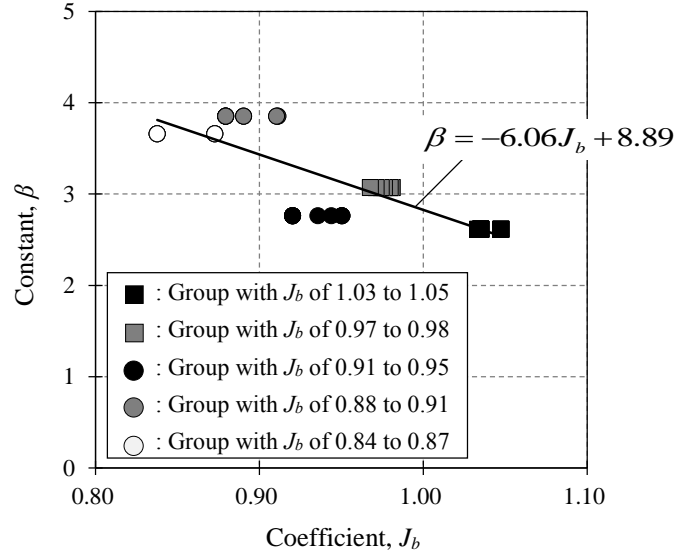
Fig. 3.13 Constant, β, versus coefficient, J_b.

The constant β which is obtained from regression Eq. (3.5.1) to (3.5.5) and coefficient, J_b, are plotted in **Fig. 3.13**. As shown in **Fig. 3.13**, constant, β, decreases with the increasing the coefficient, J_b. This relationship is estimated by Eq. (3.6).

$$\beta = -6.06J_b + 8.89 \qquad (3.6)$$

Substituting Eq. (3.6) into Eq. (3.4), Eq. (3.7) is obtained.

$$N_{f.cal.} = \alpha \cdot \Delta b \theta_{const.}^{-(-6.06J_b + 8.89)} \qquad (3.6)$$

where constant, a, is also determined according to the coefficient, J_b. In the same way, the relationship between the constant, a, which is obtained from regression Eq. (3.5.1) to (3.5.5) and coefficient, J_b, are plotted in **Fig. 3.14**. The regression Eq. (3.7) obtained from the relationship between the constant, a, and coefficient, J_b, is as follows.

$$\alpha = 2.60 \times 10^{-3} J_b^{27.23} \qquad (3.7)$$

Consequently, substitute the coefficient a of Eq. (3.7) to Eq. (3.6) to make

$$N_{f,cal.} = 2.60 \times 10^{-3} J_b^{27.23} \cdot \Delta_b \theta_{const.}^{-(6.06 J_b + 8.89)} \qquad (3.7)$$

where $N_{f,cal.}$ is calculated number of cycles to failure considering efficiency in transferring moment of beam web connection i.e. the bolts slip at bolted web connection, out-of-plane deformation of column flange, as well as loss of web section by weld access hole. A methodology for Low-Cycle Fatigue (LCF) performance assessment of beam-to-column connection is presented.
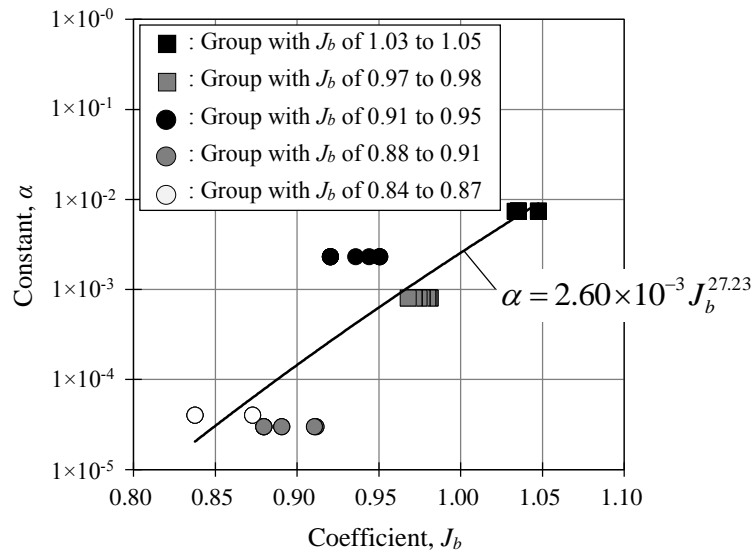
Fig. 3.14 Constant, α, versus coefficient, J_b.

3.4.2 Assessment of Proposed Low-Cycle Fatigue Performance Equation

A comparison between number of cycles to failure $N_{f,cal.}$ calculated by using Eq. (3.7) and cyclic loading tests results $N_{f.exp.}$ is shown in **Fig. 3.15**. As shown in **Fig. 3.15**, most of cyclic loading test results $N_{f.exp.}$ are correspond with the calculated number of cycles to failure $N_{f,cal.}$ and linear regression coefficient is 0.95. The proposed LCF performance prediction Eq. (3.7) in this paper can be evaluated not only for different steel grade but also for specimens with different contributions of moments at the beam web connection to the beam, which are slip behavior of bolts out-of-plane deformation of column flange as well as loss of web section by weld access hole. The proposed approach is applicable to evaluate comprehensive fatigue performance of beam-to-column connection considering moment transfer efficiency by web connection details and its steel grade. In addition, it was confirmed that LCF performance can be evaluated with higher accuracy than the evaluation Eq. proposed in the previous research (Hasegawa et al. 2014).
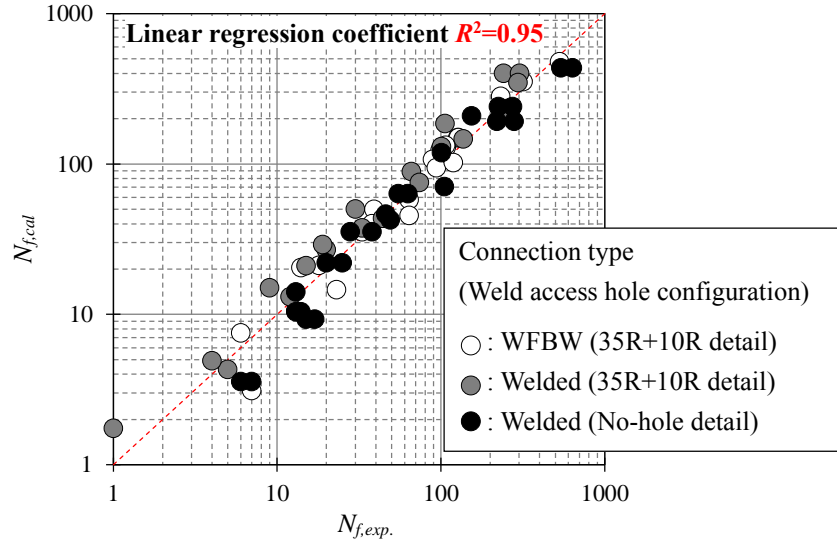
Fig. 3.15 $N_{f,cal.}$ versus $N_{f,exp.}$

3.4.3 Assessment of cumulative damage of variable & incremental amplitude loading based on the combination of Manson-Coffin relationship and Miner rule

LCF performance of beam-to-column connection is evaluated based on the Manson-Coffin relation which relates number of cycles to failure with beam rotation amplitude. The relationship was established for constant amplitude cyclic loading and could be extended to variable amplitude cyclic loading by using Miner's rule (Eq. 3.8).

$$\sum_{i=1}^{k} \frac{n_i}{N_i} = D \qquad (3.8)$$

where n_i is the number of cycles accumulated at the i level of beam rotation amplitude and D is damage index. If the damage index, D, is 1.0, it means beam flange at the beam-end is failure.
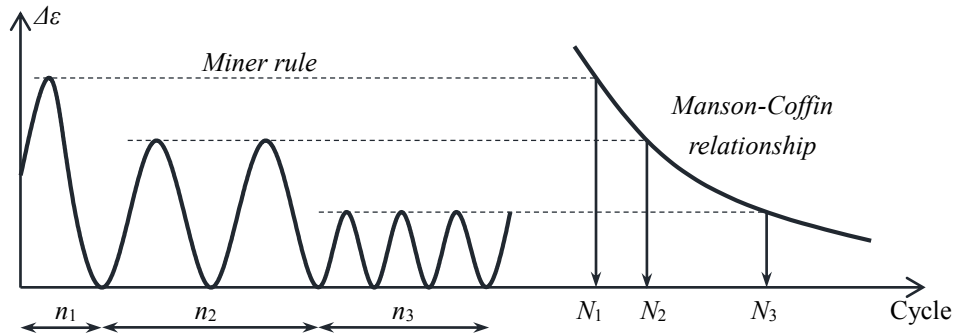
Fig. 3.16 Combination of Manson-Coffin relationship and Miner rule

In order to evaluate the cumulative damage of beam-to-column connection by using the combination of Manson-Coffin relationship and Miner rule, a database was constructed for the beam-to-column connection tested under variable and incremental loading amplitude. The data based is summarized in **Table 3.4** and **Table 3.5**. The database consists of the experimental data of beam-to-column connections subjected to variable amplitude cyclic loading and incremental amplitude cyclic loading until fracturing. Incremental loading amplitude is shown in **Fig. 3.17**. As shown in **Fig. 3.17**, incremental loading amplitude includes the displacement amplitude out of applicable range of the LCF performance evaluation Eq. (3.7), while displacement amplitude of variable loading amplitude within the evaluation range of LCF performance evaluation Eq. (3.7).

The database consists of 1 series of WFBW connection (2 specimens) and 3 series
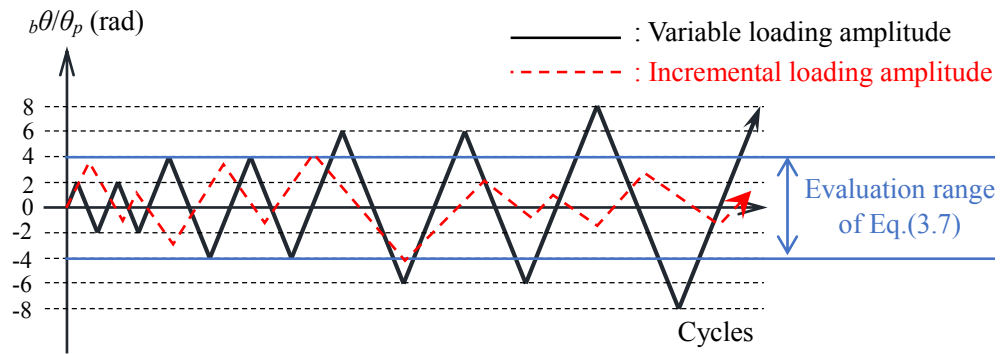
Fig. 3.17 Variable and Incremental loading amplitude

of welded web connection (19 specimens) with different beam and column section dimensions, shear span ratio and efficiencies in transfer-ring moment at the beam web connection by using different beam-end connection type as summarized in **Table 3.4** and **3.5**. The beam depth and span are ranging from 500mm to 600mm and 2050mm to 2492mm, respectively. Steel grade of all specimens in database is 490MPa. Bolts configuration of SCWB_Var is same with SCWB series as shown in **Fig. 3.4**. The strength required for calculation of coefficient, J_b, and coefficient, J_b, are summarized in **Table 3.6**. Coefficient, J_b, is ranging from 0.84 to 1.04. Damage index, D, is calculated based on the coefficient, J_b, and Eq. (3.7), and is summarized in **Table 3.7**.

Table 3.4 Database of Japanese beam-to-column connection tested under variable amplitude cyclic loading.

Reference	Connection Type	Series	Section & Steel grade		Beam Span	Weld Access Hole Configuration	Beam Rotation Amplitude
					mm		
Suita et al. (2012)	Welded Connection	NSS_Var	□-350×350×22 (BCR295)	H-500×200×10×16 (SN490C)	2492	No-hole	Variable(0.018rad×108c + 0.060rad)
							Variable(0.018rad×108c + 0.060rad)
							Variable(0.060rad×7c + 0.018rad)
							Variable(0.060rad×7c + 0.018rad)
							Variable(0.018rad×167c + 0.060rad)
							Variable(0.060rad×10c + 0.018rad)
							Variable(0.030rad×28c + 0.060rad)
							Variable(0.060rad×7c + 0.030rad)
							Variable(0.030rad×42c + 0.060rad)
							Variable(0.030rad×42c + 0.060rad)
							Variable(0.060rad×3c + 0.030rad)
							Variable(0.060rad×3c + 0.030rad)
Umeda et al. (2015)	Welded Connection	SCS_Var	□-350×350×22 (BCR295)	H-500×200×10×16 (SN490B)	2492	35R+10R	Variable(0.0173rad×52c + 0.0432rad)
							Variable(0.0432rad×5c + 0.0173rad)
	WFBW Connection	SCWB_Var	□-350×350×22 (BCR295)	H-500×200×10×16 (SN490B)	2492	35R+10R	Variable(0.0173rad×58c + 0.0432rad)
							Variable(0.0432rad×4c + 0.0173rad)

Table 3.5 Database of Japanese beam-to-column connection tested under incremental amplitude cyclic loading.

Reference	Connection Type	Series		Section & Steel grade		Beam Span	Weld Access Hole Configuration	Beam Rotation Amplitude
						mm		
Yamada et al. (2016)	Welded Connection	A	A-12	□-400×400×12 (BCR295)	H-600×200×11×17 (SN490B)	2050	35R+10R	Incremental (**Fig. 3.17**)
			A-19	□-400×400×19 (BCR295)	H-600×200×11×17 (SN490B)			
			A-F	PL50	H-600×200×11×17 (SN490B)			
		B	B-12	□-400×400×12 (BCR295)	H-600×200×11×17 (SN490B)	2050	No-hole	Incremental (**Fig. 3.17**)
			B-19	□-400×400×19 (BCR295)	H-600×200×11×17 (SN490B)			

Table 3.6 Strength required for calculation of coefficient, J_b, of each specimen.

References	Series	Yield Stress				Strength Ratio	Strength					Coefficient
		$c\sigma_y$	$bf\sigma_y$	$bw\sigma_y$	$s\sigma_y$	m	$_bM_y$	$_{bf}M_y$	$_{Bw}M_y$	$_{js}M_y$	$_{jw}M_y$	J_b
		N/mm²	N/mm²	N/mm²	N/mm²		kN·m	kN·m	kN·m	kN·m	kN·m	
Suita et al. (2012)	NSS_Var	378	352	392	-	1.00	648	528			143	1.04
Umeda et al. (2015)	SCS_Var	422	343	383	-	1.00	632	514	-	-	101	0.97
	SCWB_Var	422	343	383	368	1.00	632	514	15	48	-	0.84
Yamada et al. (2016)	A-12	366	326	381	-	0.49	809	628	-	84	-	0.88
	A-19	377	326	381	-	0.78	809	628	-	134	-	0.94
	A-F	-	326	381	-	1.00	809	628	-	172	-	0.99
	B-12	366	326	381	-	0.49	809	628	-	110	-	0.91
	B-19	377	326	381	-	0.78	809	628	-	175	-	0.99

Table 3.7 Total damage

Series	Beam Rotation Amplitude / Number of Cycles to failure						Total damage
	$\Delta_b\theta_1$	N_{f1}	D_1	$\Delta_b\theta_2$	N_{f2}	D_2	D
NSS_Var	0.0180	108	0.44	0.0600	5	0.48	0.92
	0.0180	108	0.44	0.0600	6	0.57	1.01
	0.0600	7	0.67	0.0180	173	0.71	1.37
	0.0600	7	0.67	0.0180	197	0.80	1.47
	0.0180	167	0.68	0.0600	1	0.10	0.78
	0.0600	10	0.95	0.0180	50	0.20	1.16
	0.0300	28	0.43	0.0600	6	0.57	1.01
	0.0600	7	0.67	0.0300	27	0.42	1.09
	0.0300	42	0.65	0.0600	4	0.38	1.03
	0.0300	42	0.65	0.0600	1	0.10	0.75
	0.0600	3	0.29	0.0300	61	0.95	1.23
	0.0600	3	0.29	0.0300	46	0.71	1.00
SCS_Var	0.0173	52	0.22	0.0432	7	0.46	0.68
	0.0432	5	0.33	0.0173	151	0.65	0.98
SCWB_Var	0.0173	58	0.53	0.0432	3	0.89	1.42
	0.0432	4	1.19	0.0173	77	0.70	1.89
A-12	0.0212rad×2c(D_1:0.03)+0.04241rad×2c(D_2: 0.32)						0.35
A-19	0.0212rad×2c(D_1:0.02)+0.04241rad×2c(D_2: 0.17)						0.19
A-F	0.0212rad×2c(D_1:0.01)+0.04241rad×2c(D_2: 0.11)+0.06361rad×1c(D2: 0.18)						0.30
B-12	0.0212rad×2c(D_1:0.02)+0.04241rad×2c(D_2: 0.23)+0.06361rad×1c(D2: 0.45)						0.70
B-19	0.0212rad×2c(D_1:0.01)+0.04241rad×2c(D_2: 0.11)+0.06361rad×1c(D2: 0.34)						0.46

The cumulative damage of each specimen are shown in **Fig. 3.18** with specimens subjected constant beam rotation amplitude. The specimens in **Fig. 3.18** is grouped according to the loading amplitude which are constant, variable and incremental. As shown in **Fig. 3.18**, The cumulative damage of specimens subjected variable amplitude at the relatively small deformation are evaluated similar to specimens subjected constant beam rotation amplitude. However, the damage index, D is low for specimens subjected incremental beam rotation amplitude. It can be considered that out of evaluation range. Generally, the boundary condition between the LCF and the ultra-LCF is classified by the fracture mechanism in the case of the material (W. Bleck et al. 2009), but the boundary condition of the column-to-beam connection is unclear so far. According to empirical rule, the LCF evaluation range is considered to be between about 0.01rad to 0.04rad (Ductility ratio is $1.0\theta_p \sim 4.0\theta_p$) in inelastic range.
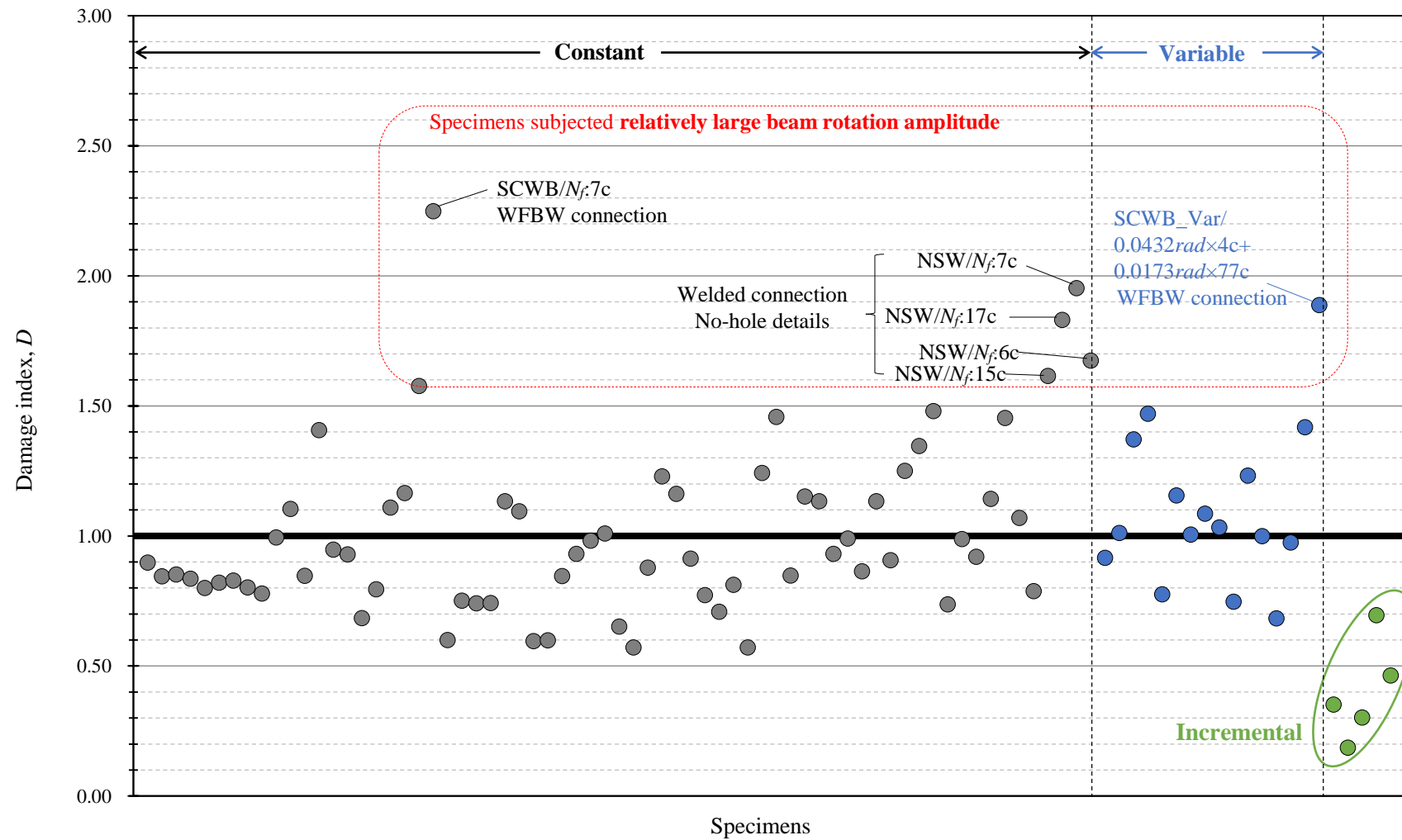
Fig. 3.18 Assessment of cumulative damage

3.5 Summary and Conclusion

A methodology for low-cycle fatigue (LCF) performance assessment of beam-to-column connections used commonly in Japanese steel moment-resisting frames is presented in this study. The proposed assessment methodology is based on a database of cyclic loading test results. The database includes two types of beam-end connection details: bolted and welded web connections.

The following conclusion are made:

- The moment transfer efficiency was evaluated according to the connection details by defining a coefficient, J_b, that considered the slip behavior of the bolts, out-of-plane deformation of the column flange and loss of the web section strength due to the weld access hole. It was confirmed that when the specimen coefficient, J_b, are almost the same, the fatigue curves are identical regardless of the mechanism of moment transfer.

- A coefficient, J_b, is reflected in the fatigue curve based on the relationship between the number of cycles to failure and the constant beam rotation amplitude obtained from cyclic loading tests. The proposed approach is applicable to evaluating the comprehensive fatigue performance of beam-to-column connections, considering the moment transfer efficiency of the web connection details and the steel grade.

- The proposed LCF performance evaluation Eq. based on the constant loading amplitude was extended to variable amplitude cyclic loading by the combination of Miner's rule, and the accumulative damage of beam-to-column connection subjected variable loading amplitude was evaluated. However, the LCF evaluation range is not clear, especially, the boundary condition between LCF and ultra LCF. According to the empirical rule, the LCF evaluation range can be defined between about 0.01rad to 0.04rad (Ductility ratio is $1.0\theta_p \sim 4.0\theta_p$) in inelastic range.

References

American Institute of Steel Construction. (2002). *Seismic provisions for structural steel buildings*. American Institute of Steel Construction.

Architectural Institute of Japan. (2012). Recommendations for design of connections in steel structures. (in Japanese)

Asakuara, N., Tanaka, T., Suita K., Tsukada, T. & Ueta, R. (2012). Deformation capacity evaluation of welded beam to column connection subjected to repeated plastic strain: Influence of composited slab Part9. Architectural Institute of Japan Kinki Branch, 449–452. (in Japanese)

Bleck, W., Dahl, W., Nonn, A., Amlung, L., Feldmann, M., Schäfer, D., & Eichler, B. (2009). Numerical and experimental analyses of damage behaviour of steel moment connection. Engineering Fracture Mechanics, 76(10), 1531-1547.

Building Research Institute: National research and development. (2014). Study on Seismic Performance for Super-High-Rise Steel Buildings against Long-Period Earthquake Ground Motions, No.160. (in Japanese)

Fujisawa, K., Ichinohe, Y., Sugimoto, M., & Sonoda, M. (2013). Statistical study on mechanical properties and chemical compositions of SN steels. Summaries of technical papers of Annual Meeting Architectural Institute of Japan, 699–700. (in Japanese)

Hisada, Y., Yamashita, T., Murakami, M., Kubo, T., Shindo, J., Aizawa, K., & Arata, T. (2012). Seismic response and damage of high-rise buildings in Tokyo, Japan, during the Great East Japan earthquake. In *Proceedings of the International Symposium on Engineering Lessons Learned from the Giant Earthquake*, 1110-1119.

Kishiki, S., Sato, R., Yamada, S. & Hasegawa, T. (2016). Evaluation method of cyclic deformation capacity for beam-end connections using various steel grades. J. Struct. Constr. Eng., AIJ, 81(723), 917-927. (in Japanese)

Seki, K., Matsumoto, S., Narihara, H., & Yasuda, S. (2013). Low cycle fatigue properties of welded beam-to-column connections using horizontal haunch-beam: Part 1 Outline of test. Summaries of technical papers of Annual Meeting Architectural Institute of Japan. pp.747–748. (in Japanese)

Suita, K. & Tanaka, T. (2000). Flexural strength of beam web to square tube column joints. Steel Construction Engineering. 7(26), 51–58. (in Japanese)

Suita, K., Hashida, I. & Sato, A. (2009). Cyclic loading test and crack growth characteristics: deformation capacity evaluation of welded beam to column connection subjected to repeated plastic strain Part1. Summaries of technical papers of Annual Meeting Architectural Institute of Japan,

1021-1022. (in Japanese)

Suita, K., Tanaka, T., Sato A., Manabe, Y., Tsukada, T. & Su, Z. (2011) Effect of ultimate flexural strength of beam end connection on deformation capacity: Deformation capacity of welded beam-to-column connection subjected to repeated plastic strain Part 1. J. Struct. Constr. Eng. 76(664), 1135–1142. (in Japanese)

Takatsuka, K., Suita, K., Tanaka, T. & Umeda, T. (2014). Effect of beam section size and connection detail on deformation capacity: Deformation capacity of welded beam-to-column connection subjected to repeated plastic strain Part 4. J. Struct. Constr. Eng. 79(696), 315–321. (in Japanese)

Takewaki, I., Murakami, S., Fujita, K., Yoshitomi, S., & Tsuji, M. (2011). The 2011 off the Pacific coast of Tohoku earthquake and response of high-rise buildings under long-period ground motions. *Soil Dynamics and Earthquake Engineering*, *31*(11), 1511-1528. (in Japanese)

Umeda, T., Takatsuka, K., Suita, K. & Tanaka, T. (2015). Deformation capacity of flange-welded web-bolted moment connection: Deformation capacity of welded beam-to-column connection subjected to repeated plastic strain Part 6. J. Struct. Constr. Eng. 80(781), 1971–1979. (in Japanese)

Uozumi, N., Tanaka, T., Suita, K. & Asakura, N. (2013). Deformation capacity evaluation of welded beam to column connection subjected to repeated plastic strain: Cyclic loading tests on composite beams with scallops Part 14. Architectural Institute of Japan Kinki Branch, 389–392. (in Japanese)

Uozumi, N., Tanaka, T., Suita, K., Asakura, N. & Takatsuka, K. (2014). Relationship between deformation capacity and strain amplitude on welded beam-to-column connection. Proceedings of constructional steel. No.22, 765–772. (in Japanese)

Yamada, S., Miki, N., Kishiki, S., Hasegawa, T. & Jiao, Y. (2016). Cyclic loading test of beam-to-column connection with low moment transferring efficiency in web. J. Struct. Constr. Eng. 81(720), 245-355. (in Japanese)

CHAPTER 4

NUMERICAL ANALYSIS ON

LOW-CYCLE FATIGUE PERFORMANCE EVAUATION OF

WELDED FLANGE-BOLTED WEB CONNECTION

4.1 Introduction

In recent years, low-cycle fatigue (LCF) behavior of beam-to-column connection during the massive earthquake, which have long-duration and long-period ground motion are causing great concern. The safety and cumulative damage of beam-to-column connections subjected to large number of cycles deformation is highlighted as a problem.

In Japan, many cyclic loading test have been carried out to clarify the fatigue curve of beam-to-column connection subjected to large number of cycles deformation. Much efforts have made the relationship between some variables and cyclic deformation somewhat clear (Suita et al; 2011, 2012a, 2012b, 2014, 2015a, 2015b; Hasegawa et al. 2014). In the previous study, it is reported that the LCF fatigue evaluation method was proposed based on the beam rotation amplitude, which can be evaluated with same fatigue curve considering the material's yield strength, beam section and span (Kishiki et al. 2016). And, LCF performance evaluation equation considering connection details was also proposed in **Chapter 3**. However, the number of samples considered in the experimental research is limited as shown in **Fig. 4.1** and the cyclic performance of beam-to-column connection depends on the materials' yield strength/ratio, geometry and loading history. The application range of the evaluation equation with beam section, span and steel grade not considered in the experiment was not confirmed. So, it is necessary to clarify the available range of evaluation proposed based on the experimental results.

In this chapter, numerical analysis on the welded flange-bolted web (WFBW) connection,

which is commonly used in the high-rise steel moment resisting frames in Japan, connection is carried out to clarify LCF performance evaluation range considering material's yield strength/ratio and geometry.
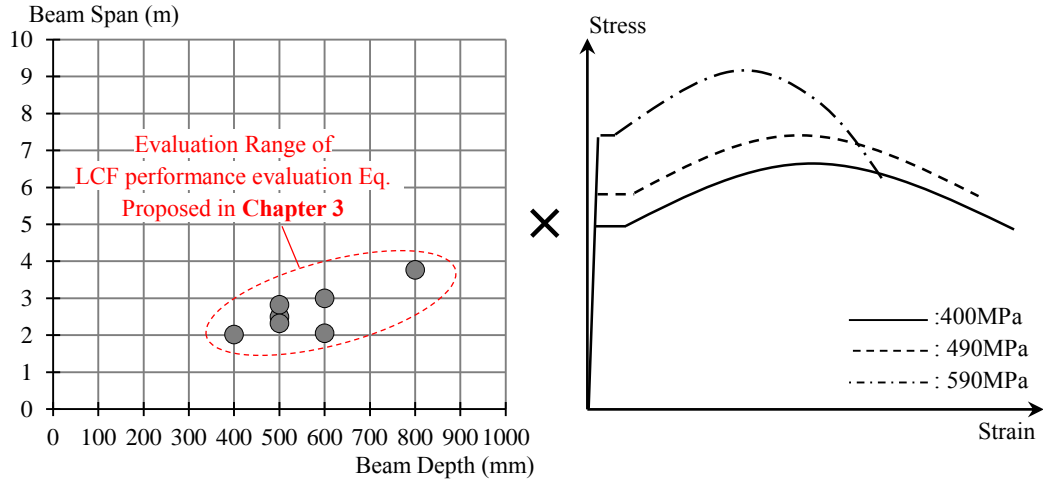

Fig. 4.1 Evaluation range of LCF performance evaluation Eq. proposed in **Chapter 3**

4.2 Relationship between Strain at the Beam-End Flange and LCF Performance

The relationship between number of cycles N_f versus and strain amplitude at the beam-end flange $\Delta\varepsilon_f$ in previous test (**Chapter 2**) is illustrated in **Fig. 4.2**. The $\Delta\varepsilon_f$ obtained in stable hysteresis loop (about 4cycle to 10cycle) during the cycles from the strain gauge glued on the beam-end flange defined as a critical section by a fracture section as shown in **Fig. 4.3**. As shown in **Fig. 4.2**, it was confirmed that there is a strong correlation between N_f versus $\Delta\varepsilon_f$. In this study, an analytical investigation is conducted to clarify the valid range of this correlation with various beam section and span. Here, the strain amplitude of longitudinal direction at the beam-end flange is calculated in analysis, and the tri-axial stress at the beam-end flange and stress concentration at the weld access hole are indirectly considered by using the N_f.
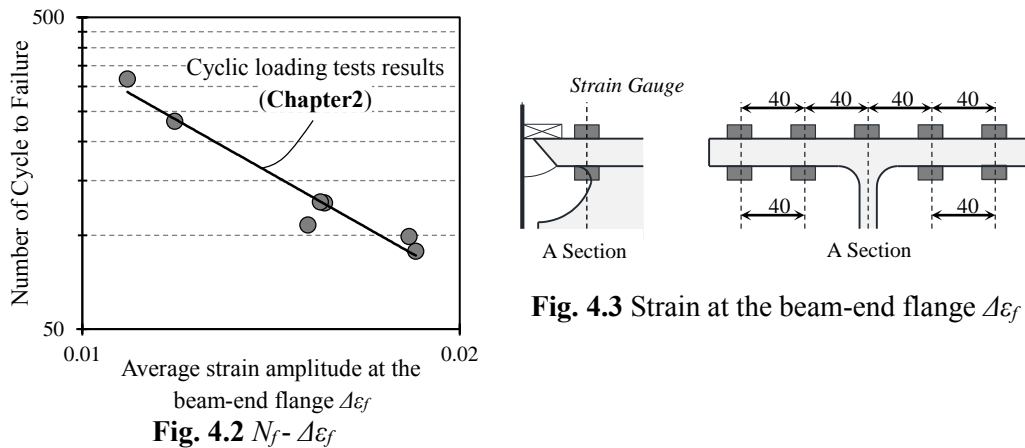

Fig. 4.2 N_f - $\Delta\varepsilon_f$

Fig. 4.3 Strain at the beam-end flange $\Delta\varepsilon_f$

4.3 In-Plane Analysis of Beam

4.3.1 General

In Japan, welded flange-bolted web (WFBW) beam-to-column connection, which beam flange are welded to the column and the beam web is bolted to a single shear plate, is extensively used in high-rise SMRFs. LCF performance of this connection type were experimentally investigated in Chapter 2. The test results indicated that LCF performance depends on the slip behavior under minor inelastic deformation, and moment transfer efficiency was decreased by slip behavior. The decrease the moment trasfer efficiency at the web connection cause the strain concentration at the beam-end flange, it leads to an early fracture. In this study, an analytical model considering slip behavior at the bolted web connection is proposed and verified based on the test results.

4.3.2 Analytical Methodology

The numerical analysis of cantilever beam is conducted based on the in-plane analysis method by numerical integration (Kato et al. 1966; Yamada et al. 1966 and Yamada et al. 1993). In the analysis, the assumption condition are as follows:

    I.   *There is no out-of-plane deformation and local buckling of the beam.*

    II.   *Deformation due to shear force is always considered to be elastic.*

Describe in-plane analysis of cantilever beam is shown in **Fig. 4.4**. The moment-curvature relation is obtained by applying Bernoulli-Euler's hypothesis on the internal force balance of the beam section (Stress-Strain Relationship). And moment-rotation relationship of beam is calculated by integrating moment-curvature relationship of each beam section along the beam span.
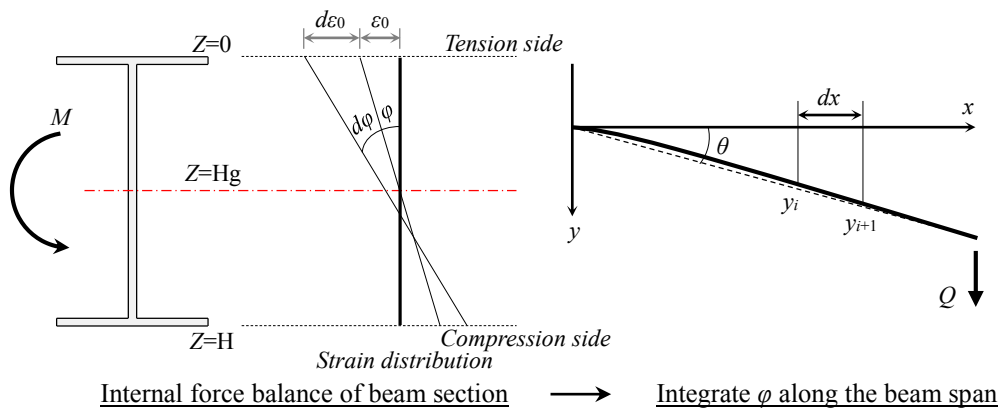

Fig. 4.4 In-plane analysis of cantilever beam

The moment-curvature relation can be calculation by the internal force balance in the beam section. As shown in **Fig. 4.4**, the axial force P and bending moment M can be written as:

$$P = \int_0^H f(\varepsilon) \cdot g(Z) dz = \int_0^H f(\varepsilon_0 + \phi \cdot Z) \cdot g(Z) dz \tag{4.1}$$

$$M = \int_0^H f(\varepsilon) \cdot g(Z) \cdot Z dz - P \cdot Hg \tag{4.2}$$

$$= \int_0^H f(\varepsilon_0 + \phi \cdot Z) \cdot g(Z) \cdot Z dz - P \cdot Hg$$

by given the section a small curvature increment d ϕ, Eqs.(4.1) and (4.2) can be written as:

$$P + dP = \int_0^H f(\varepsilon_0 + d\varepsilon_0 + (\phi + d\phi) \cdot Z) \cdot g(Z) dz \tag{4.4}$$

$$M + dM = \int_0^H f(\varepsilon_0 + d\varepsilon_0 + (\phi + d\phi) \cdot Z) \cdot g(Z) \cdot Z dz - P \cdot Hg \tag{4.5}$$

where, $d\varepsilon_0$ is the increment of tension edge strain. Here, the beams were subjected to pure bending, therefore, axial force, P, and increment axial force, dP, is zero. Eq. (4.4) and (4.5) were derived by using Taylor expansion. Terms after the 2nd term are considered negligible.

$$d\varepsilon_0 = \frac{\int_0^H f''(\varepsilon_0 + \phi \cdot Z) \cdot g(Z) \cdot Z dZ}{\int_0^H f''(\varepsilon_0 + \phi \cdot Z) \cdot g(Z) dZ} \cdot d\phi \tag{4.6}$$

$$dM = \int_0^H f''(\varepsilon_0 + \phi \cdot Z) \cdot (d\varepsilon_0 + d\phi \cdot Z) \cdot g(Z) \cdot Z dz \tag{4.7}$$

The moment-rotation relation of the beam derived by integrating the moment-curvature relation along the beam span.

$$y'' = \phi \tag{4.8}$$

$$\theta = y' = \phi_i \cdot x + C_1 \tag{4.9}$$

$$y = 0.5 \cdot \phi_i \cdot x^2 + C_1 \cdot x + C_2 \tag{4.10}$$

The Boundary condition of θ_i and y_i can be written as:

$$\theta_{i+1} = \theta_i + \phi_i \cdot \Delta x \qquad (4.11)$$

$$y_{i+1} = y_i + \theta \cdot \Delta x + 0.5 \cdot \phi_i \cdot \Delta x^2 + \frac{Q \cdot \Delta x}{G \cdot A_w} \qquad (4.12)$$

where, G is the shear stiffness, and A_w is the area of beam web section. So, the moment of i+1 step can be obtained by Eq. (4.13)

$$M_{i+1} = M_i - Q \cdot \Delta x \qquad (4.13)$$

4.3.3   Material Hysteresis Model
4.3.3.1 General

In order to evaluated deformation capacity of structural members and their joints, it is important to understand the hysteretic behavior of steel materials subjected to cyclic load. So far, many researches have been conducted to propose the hysteretic model of steel materials under cyclic loading such as earthquake motions (Ono et al. 1997; Lignos et al. 2010 and Karavasilis et al. 2012). Such hysteretic model proposed has been usefully applied to analytical approaches. In the previous studies (Kato et al. 1973; Oyamada et al. 1995 and Yamanouchi et al. 1997), it has been clearly demonstrated that the hysteresis characteristic under cyclic loading of steel material can be decomposed into the skeleton part, the Bauschinger part and the elastically unloading part, as well as skeleton curve that was made by connecting the skeleton part, is consistent with the monotonic loading curve. This is applied to the same concept as that of the structural members and their joints, and a concise bi-linear model has been proposed under arbitrary cyclic loading. In this study, analytical approaches were introduced with hysteresis model of steel materials. A concise hysteresis model of structural steel of 400MPa grades (SS400B and SN400B) was proposed considering the Bauschinger effect (Yamada et al. 2002). The cyclic deformation capacity of the beam-to-column connection was evaluated by using this hysteresis model (Yamada et al. 2014).

A concise hysteresis model of high performance 590MPa steel (SA440) for building construction is proposed for the analytical approaches on the cyclic deformation capacity of beam-to-column connection.

4.3.3.1 Cyclic Loading Test Program
Specimen

The test specimen are shown in **Fig. 4.5**. The test specimens is high performance 590MPa steel grade for building construction (SA440). All specimens were cut from a same block with a rolling direction. The length and diameter of the testing area are 17mm and 8mm, respectively. To concentrate stress into reduced section, fillet radios were optimized to 10mm.
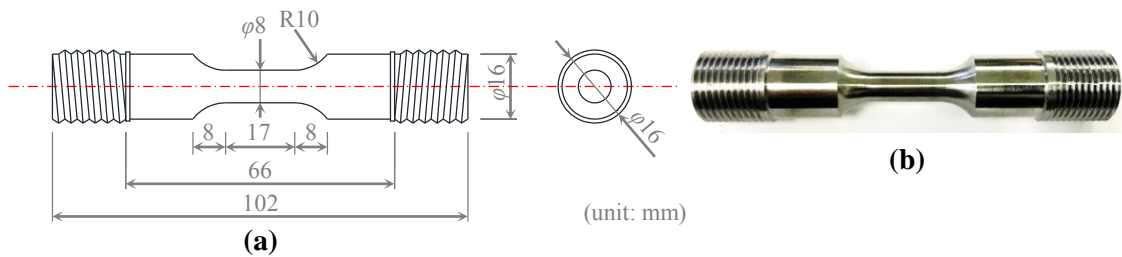

Fig. 4.5 (a) *Geometry the round test specimens of SA440 steel and* **(b)** *photo of specimen*

Tensile test was conducted on specimen of JIS Z3111 No. A2, Japanese Industrial Standards to examine the mechanical properties and monotonic loading curve. Tensile test results are summarized **Fig. 4.6** and **Table 4.1**.
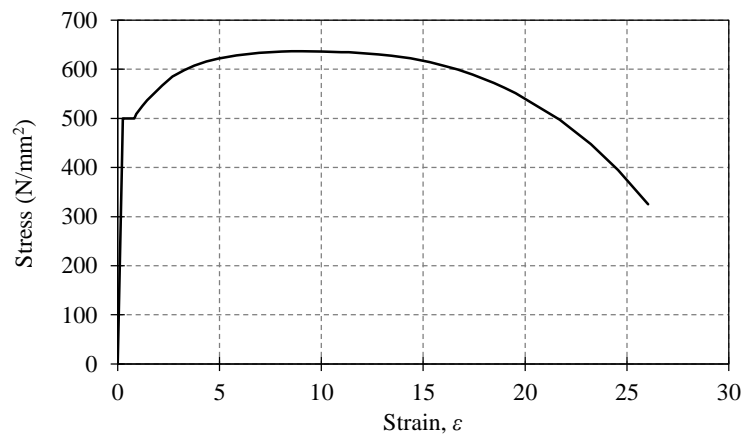

Fig. 4.6 Stress-Strain Curve

Table 4.1 Material Properties

Specimen	Parallel Section		Yield Stress	Tensile Stress	Yield Ratio	Elongation
	Length	Diameter				
	mm	mm	N/mm^2	N/mm^2	%	%
JIS Z311 No. A2	30	6.03	500	637	78	26

*Actual diameter

Test Setup and Loading Histories

Cyclic loading tests on the round specimens were conducted with a 500kN load cell as shown in **Fig. 4.7**. All the tests are considered to be quasi-static at a loading rate of 0.20mm/min (about 0.01%/sec strain amplitude). The imposed axial force to the specimens was measured by a load cell of adjustable crosshead. The strain of the parallel test length was measured with a strain gauge attached to both sides of the section as shown in **Fig. 4.7**. The strain obtained from strain gauge were used to control the loading histories. The loading history is summarized in **Table 4.2**. The loading history was set within the range where buckling deformation does not occur.
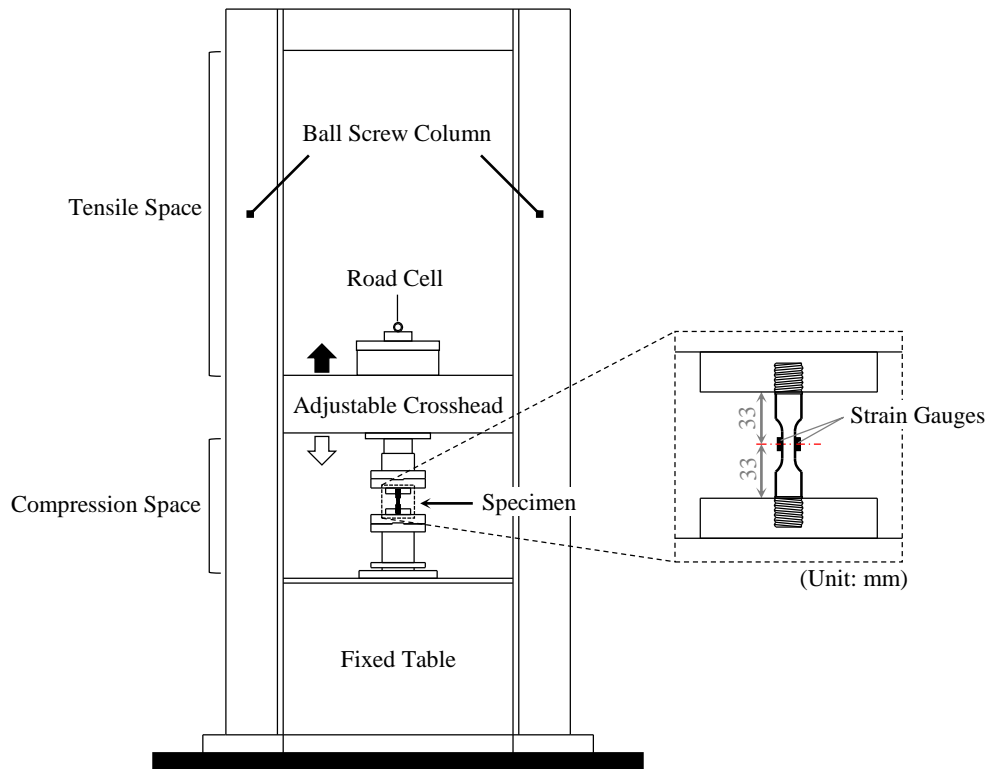

Fig. 4.7 Schematic diagram of the test setup with a location of strain gauges for measuring strain amplitude.

Table 4.2 Loading history

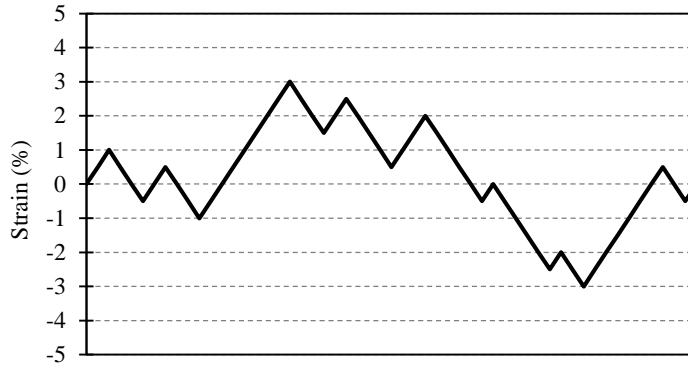| Specimen	Loading history (Strain amplitude)
SA440_0.5	±0.50% incremental strain loading amplitude
	±0.50% × 2 → ±1.00% × 2 → ±1.50% × 2……
SA440_1.0	±1.00% incremental strain loading amplitude
	±1.00% × 2 → ±2.00% × 2 → ±3.00% × 2……
SA440_P1	Random strain loading amplitude
	Program 1 (see **Fig. 4.8**)

Fig. 4.8 Random strain loading amplitude (Specimen SA440_P1).

4.3.3.2 Test Results

<u>True Stress, $_t\sigma$, and True Strain, $_t\varepsilon$, Relationship</u>

The hysteresis models are generally expressed in true stress, $_t\sigma$, - true strain, $_t\varepsilon$, relationship. The nominal stress, $_n\sigma$, and nominal strain, $_n\varepsilon$, measured in the test is derived by dividing axial force with original cross-sectional area and the amount that a material deforms per unit length, respectively. $_n\sigma$ and $_t\varepsilon$ are converted to $_t\sigma$ and $_t\varepsilon$ considering the applied load divided by the actual cross-sectional area of the specimen at that load and the natural log of the quotient of current length over the original length by using Eq. (4.14) to (4.15).

$$_t\sigma = \left(1 + {}_n\varepsilon\right) \cdot {}_n\sigma \tag{4.14}$$

$$_t\varepsilon = \ln\left(1 + {}_n\varepsilon\right) \tag{4.15}$$

<u>Hysteresis Characteristics</u>

The hysteresis characteristic under cyclic loading of steel material can be decomposed into the skeleton part, the Bauschinger part and the elastically unloading part as shown in **Fig. 4.9**. The skeleton curve is formed by sequentially connecting the paths of the loads that exceed the maximum load attained in the preceding cycle. The Bauschinger parts are defined softened part due to the Bauschinger effect. In the **Fig. 4.9**, $\Sigma\Delta_t\varepsilon_s$ indicate increment of cumulative plastic strain in skeleton curve, and $\Delta_t\varepsilon_B$ is increment of plastic strain in Bauschinger part at each cycle.
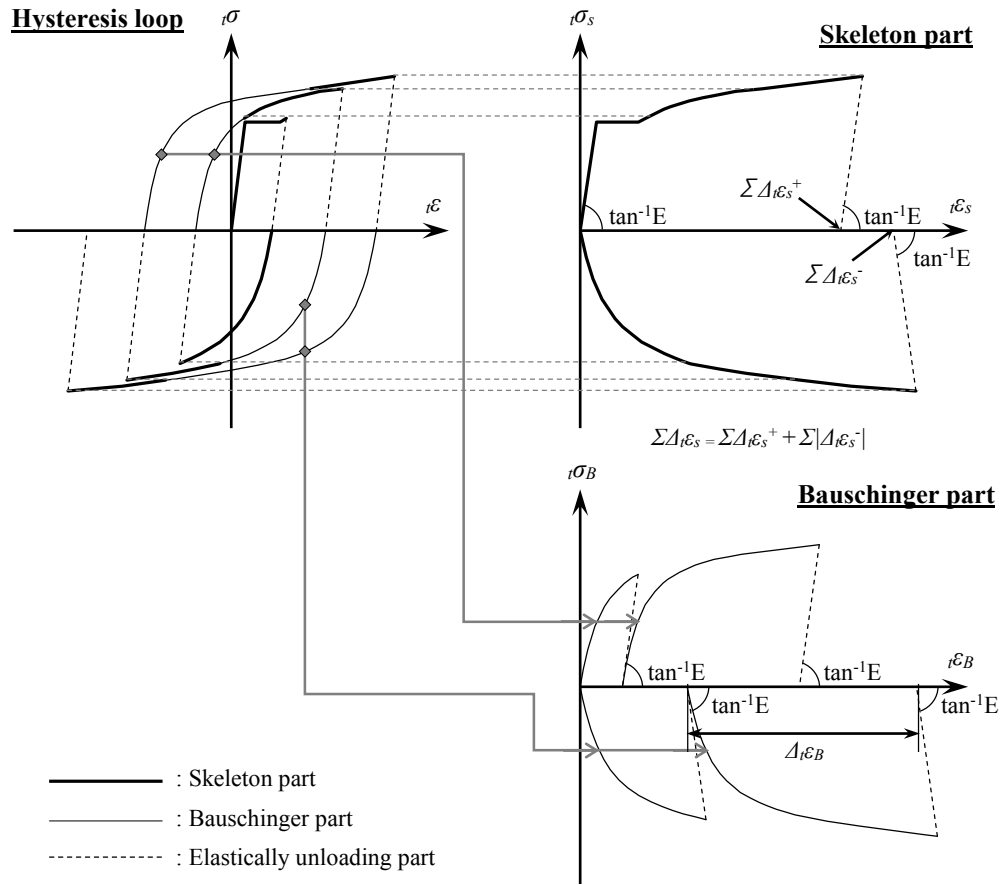
Hysteresis loop $_t\sigma$ $_t\sigma_S$ **Skeleton part**

$_t\varepsilon$

$\tan^{-1}E$ $\Sigma\Delta_t\varepsilon_S{}^+$ $\tan^{-1}E$ $_t\varepsilon_S$

$\tan^{-1}E$

$\Sigma\Delta_t\varepsilon_S{}^-$

$$\Sigma\Delta_t\varepsilon_S = \Sigma\Delta_t\varepsilon_S{}^+ + \Sigma|\Delta_t\varepsilon_S{}^-|$$

$_t\sigma_B$ **Bauschinger part**

$\tan^{-1}E$ $\tan^{-1}E$ $_t\varepsilon_B$

$\tan^{-1}E$ $\tan^{-1}E$

$\Delta_t\varepsilon_B$

—— : Skeleton part
—— : Bauschinger part
------- : Elastically unloading part

Fig. 4.9 Hysteresis characteristics.

Skeleton and Bauschinger Part

Skelton Part: The relationship between $_t\sigma$ and $_t\varepsilon$ obtained under monotonic loading is similar to the skeleton curve obtained from the skeleton part, and the compression side and the tension side exhibit symmetric relation (Akiyama et al. 1985). In this study, the skeleton curve in the hysteresis model is adopted as a monotonic loading curve obtained from tensile test.

Bauschinger Part: The shape of Bauschinger part is determined by cumulative strain history of steel material experienced until that step. In this study, the shape of Bauschinger part is modeled as a bilinear model with stress of entering-skeleton point, $_t\sigma_{Bs}$, elastic stiffness, E, strain increments in the Bauschinger parts in each cycle, $\Delta_t\varepsilon_B$, and stress of stiffness chang-ing point, $_t\sigma_E$. The stress of entering-skeleton point, $_t\sigma_{Bs}$, is set as the maximum stress from the previous cycle. In case of stiffness in unloading part, it is close to the elastic stiffness, E, and

E is used as stiffness in unloading part. strain increments in the Bauschinger parts in each cycle, $\Delta_t\varepsilon_B$, and stress of stiffness changing point, $_t\sigma_E$, are defined from test results.

The relationship between strain increments in the Bauschinger parts in each cycle, $\Delta_t\varepsilon_B$ and cumulative strain in skeleton curve, $\Sigma\Delta_t\varepsilon_s$, are shown in **Fig. 4.10** with previous test results (Yamada et al. 2002). As shown in **Fig. 4.10**, the two variables exhibit a linear relationship, and the simple linear regression Eq. is as follows.

$$\Delta_t\varepsilon_B = 0.72\sum\Delta_t\varepsilon_s \tag{4.16}$$

From above Eq., it is confirmed that constant in the relationship $\Delta_t\varepsilon_B$ and $\Sigma\Delta_t\varepsilon_s$ is different according to the steel grade, and SA steel is less $\Sigma\Delta_t\varepsilon_s$ under cyclic loading than SS&SN steel.
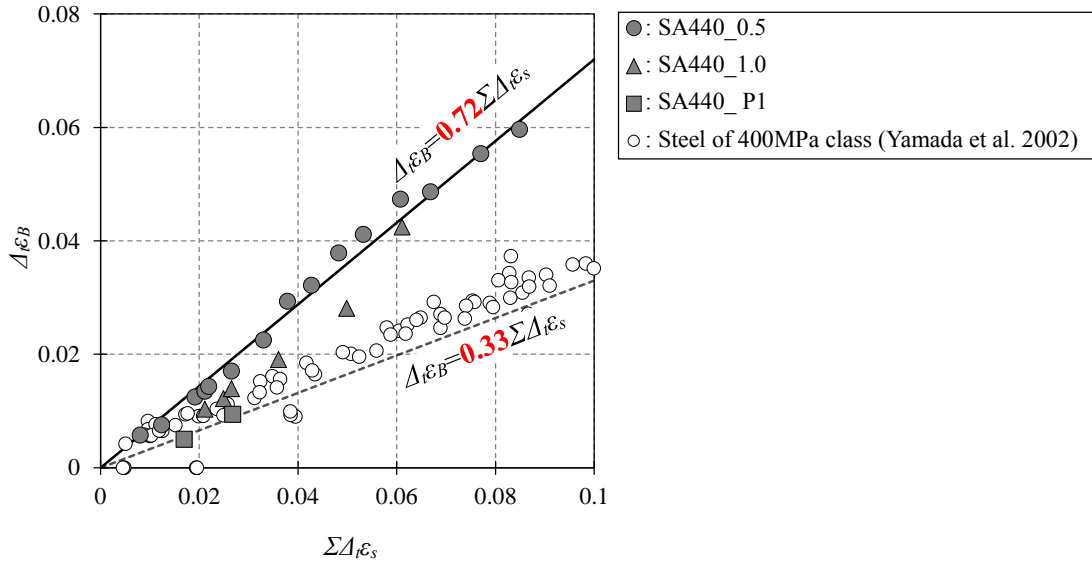

Fig. 4.10 Strain increments in the Bauschinger parts in each cycle, $\Delta_t\varepsilon_B$, versus cumulative strain in skeleton curve, $\Sigma\Delta_t\varepsilon_s$.

Coefficient of stiffness changing point, α_B, is defined the ratio of stress of stiffness changing point, $_t\sigma_E$, to stress of entering-skeleton point, $_t\sigma_{Bs}$ ($= _t\sigma_E/_t\sigma_{Bs}$). α_b is obtained by matching the starting point and $_t\sigma_{Bs}$ of test results with the bi-linear model, and identical absorbed energy point in the Bauschinger part as shown in **Fig. 4.11**. α_b in each Bauschinger part shown in **Fig. 4.12** with strain increments in the Bauschinger parts in each cycle, $\Delta_t\varepsilon_B$. These relationships are simplified as linear line can be obtained by Eq. (4.4)
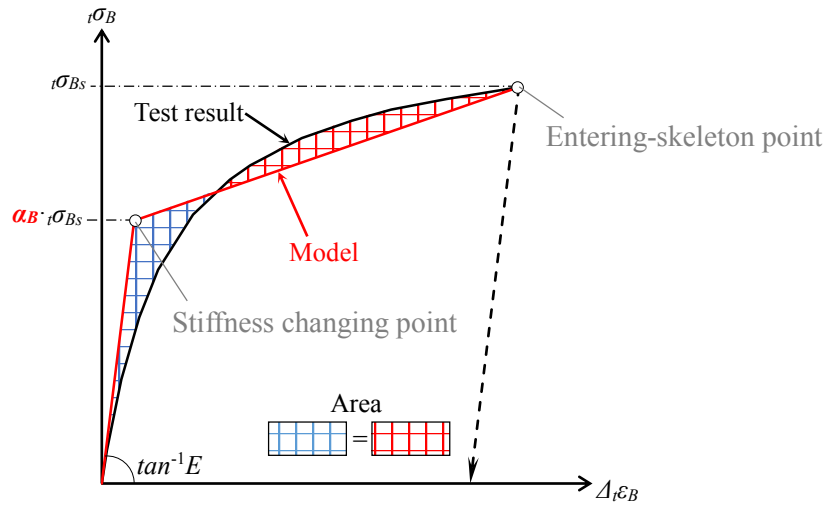
$$\alpha_B = 0.67 \tag{4.17}$$

Fig. 4.11 Bi-linear modeling of Bauschinger part.

Regarding these relationships, almost the same results as the previous experimental results of SS&SN steel grade, were obtained. Here, $\Delta_t\varepsilon_B$ in the LCF evaluation range is distributed from about 0.01 to 0.02, but it is assumed that the influence of these α_B on the strain amplitude at the beam-end flange (**Appendix E**)
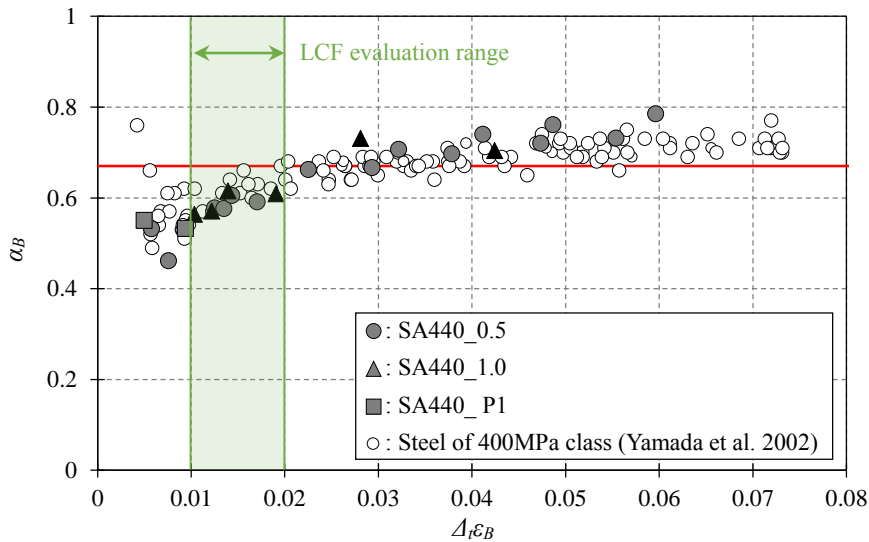

Fig. 4.12 α_B - $\Delta_t\varepsilon_B$

Multi-linear Hysteresis Model

As mentioned above, the hysteresis characteristic under cyclic loading of steel material is made up of the skeleton curves, Bauschinger parts and unloading part. In this study, hysteresis model considering Bauschinger effects was proposed as follow. Skeleton curves are
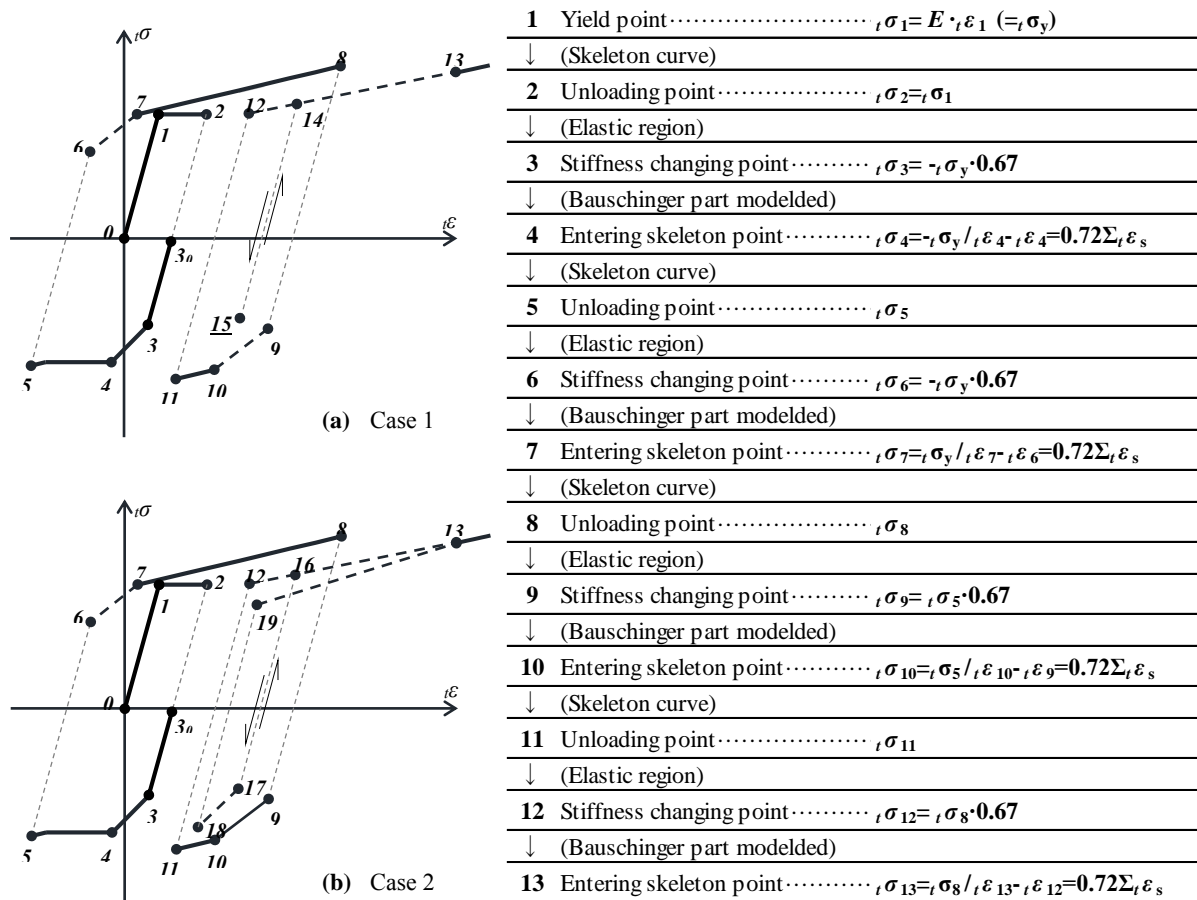
1	Yield point $\cdots\cdots\cdots\cdots\cdots\cdots\cdots$ $_t\sigma_1 = E \cdot {}_t\varepsilon_1$ $(=_t\sigma_y)$
$\downarrow$	(Skeleton curve)
2	Unloading point $\cdots\cdots\cdots\cdots\cdots$ $_t\sigma_2 = {}_t\sigma_1$
$\downarrow$	(Elastic region)
3	Stiffness changing point $\cdots\cdots\cdots$ $_t\sigma_3 = -{}_t\sigma_y \cdot 0.67$
$\downarrow$	(Bauschinger part modelded)
4	Entering skeleton point $\cdots\cdots\cdots\cdots$ $_t\sigma_4 = -{}_t\sigma_y / {}_t\varepsilon_4 - {}_t\varepsilon_4 = 0.72\Sigma_t\varepsilon_s$
$\downarrow$	(Skeleton curve)
5	Unloading point $\cdots\cdots\cdots\cdots\cdots$ $_t\sigma_5$
$\downarrow$	(Elastic region)
6	Stiffness changing point $\cdots\cdots\cdots$ $_t\sigma_6 = -{}_t\sigma_y \cdot 0.67$
$\downarrow$	(Bauschinger part modelded)
7	Entering skeleton point $\cdots\cdots\cdots\cdots$ $_t\sigma_7 = {}_t\sigma_y / {}_t\varepsilon_7 - {}_t\varepsilon_6 = 0.72\Sigma_t\varepsilon_s$
$\downarrow$	(Skeleton curve)
8	Unloading point $\cdots\cdots\cdots\cdots\cdots$ $_t\sigma_8$
$\downarrow$	(Elastic region)
9	Stiffness changing point $\cdots\cdots\cdots$ $_t\sigma_9 = {}_t\sigma_5 \cdot 0.67$
$\downarrow$	(Bauschinger part modelded)
10	Entering skeleton point $\cdots\cdots\cdots\cdots$ $_t\sigma_{10} = {}_t\sigma_5 / {}_t\varepsilon_{10} - {}_t\varepsilon_9 = 0.72\Sigma_t\varepsilon_s$
$\downarrow$	(Skeleton curve)
11	Unloading point $\cdots\cdots\cdots\cdots\cdots$ $_t\sigma_{11}$
$\downarrow$	(Elastic region)
12	Stiffness changing point $\cdots\cdots\cdots$ $_t\sigma_{12} = {}_t\sigma_8 \cdot 0.67$
$\downarrow$	(Bauschinger part modelded)
13	Entering skeleton point $\cdots\cdots\cdots\cdots$ $_t\sigma_{13} = {}_t\sigma_8 / {}_t\varepsilon_{13} - {}_t\varepsilon_{12} = 0.72\Sigma_t\varepsilon_s$

Fig. 4.13 Multi-linear hysteresis model considering Bauschinger effects

chosen as the tensile test results (True stress, $_t\sigma$ - True strain, $_t\varepsilon$ curve converted by Eq. (4.2) and (4.3)), and Bauschinger parts were simplified by equations (4.3) and (4.4). An example of the proposed hysteresis model is shown in **Fig. 4.13**. The following is a brief description of the multi-linear hysteresis model considering Bauschinger effect with the example shown in **Fig. 4.13**.

- The compressive side of the first cycle is taken as the skeleton curve due to the compressive stress experienced first of the steel material (loops 3_0-5), although the Bausinger effect is considered (loop 3-4).

- The entering skeleton point and the unloading point in the skeleton curve are reset every cycle (loops 0-2, 3_0-5, 7-8, 10-11 and 13-).

- Entering skeleton point is obtained by Eq. (3.4), and $\Delta_t\varepsilon_B$ in Eq. (3.4) is the increment of true strain experienced from the stiffness changing point to the next entering skeleton point (loops 9-10, 6-7 and 12-13)

- $\Sigma_t\varepsilon_s$ is the true strain in skeleton pat experienced it's entering skeleton point.

- $\alpha_B \cdot {}_t\sigma_{Bs}$ in **Fig. 4.11** is stiffness changing point, which is determined from the peak load of

the skeleton curve, $_t\sigma_{Bs}$, experienced at previous cycle (points 3,6,9 and 12).

- When the unloading starts in the elastically unloading region, the hysteresis loop returns to the previous loop until peak load experienced, and it grows back along the same loop.

Coparison of Hysteretic Model and Test Results

The Hysteresis behavior for high performance 590MPa steel for building construction was modeled. The comparison of hysteresis model and test results show in **Fig. 4.14** with skeleton part experienced. The black line and led dotted line represent test results and analysis results, respectively. The hysteresis model subjected to the same strain histories of the test. As shown in **Fig. 4.14**, the proposed hysteresis model indicates a good correspondence with the test results.
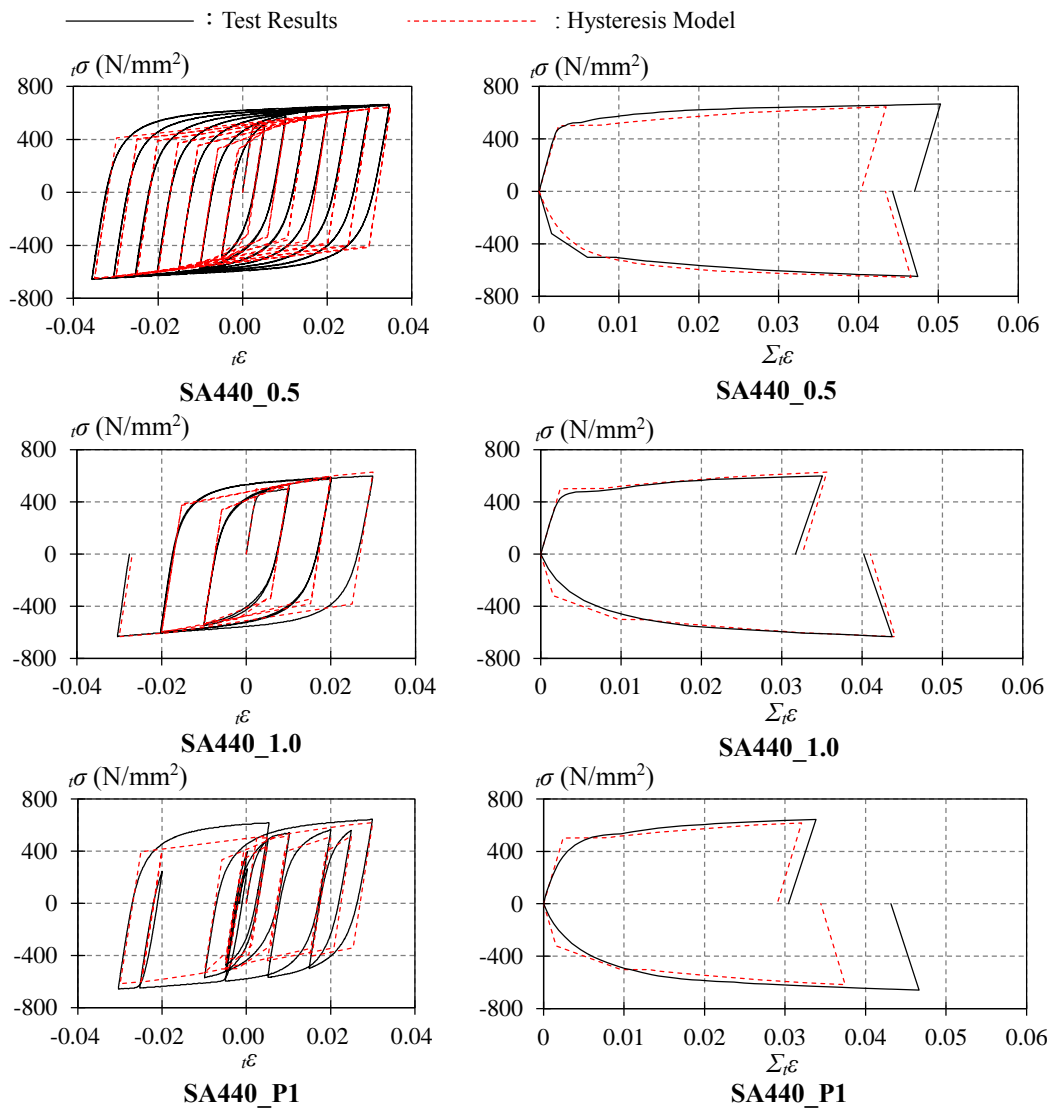
Fig. 4.14 Comparison of hysteresis model and test results with skeleton curve experienced.

4.3.4 Modeling of the WFBW Connection

In the previous studies (Suzuki et al. 1999; Yamada et al. 2014), the decrease moment transfer efficiency due to the out-of-plane deformation of column flange and loss of web section by weld access hole were modeled by setting the ineffective in transferring the bending stress at the beam web. In this study, WFBW connection is modeled considering slip behavior with the same concept above as shown in **Fig. 4.15**.

The length of the ineffective area in the web connection h_r is calculated by Eq. (4.18).

$$h_r = \sqrt{1-m}\left(H - 2t_f - 2W_r\right) \tag{4.18}$$

where H is beam depth, t_f is thickness of flange, W_r is the length from the start of the web to the washer of the first bolt, and m is normalized strength of slip-critical strength at the beam web connection (**APPENDIX C**) which is defined in Eq. (4.19).

$$_{jw}M_{y,ana.} = m \cdot {}_{Bw}M_s \tag{4.19}$$

where $_{jw}M_{y,ana.}$ is yield strength of web connection and $_{Bw}M_s$ is slip-critical strength of bolted web connection (**APPENDIX A**). In the analytical model, the bolted connection is assumed non-relative deformation. Therefore, the integrated region set the area within the bolt range including the washer. The plate thickness of this region was set to the sum of the shear plate and web plate.

Bolts Configuration **FR**   Bolts Configuration **F3**
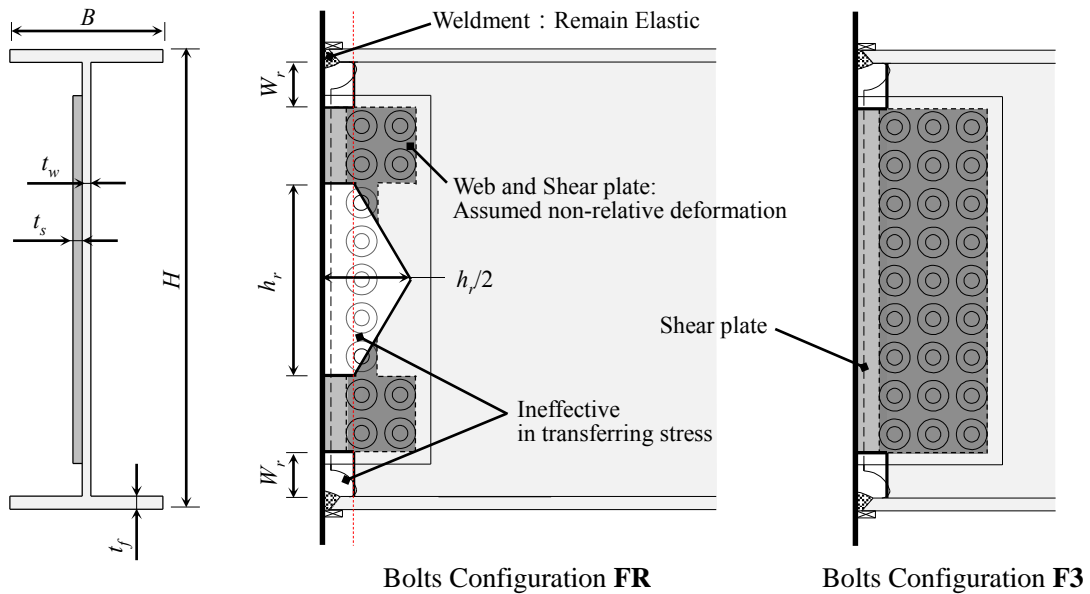
Fig. 4.15 Modeling of WFBW connection

4.3.5 Mesh Generation

The meshes size (**Fig. 4.16**) was evenly set at 10mm intervals along the beam span, while along the beam depth, meshes size were set differently depending on the in-plane moment. In case of beam flange and weld access hole, section along beam depth are split into 5 and 7 meshes, respectively. The rest of the web section is split into meshes within the 20mm.
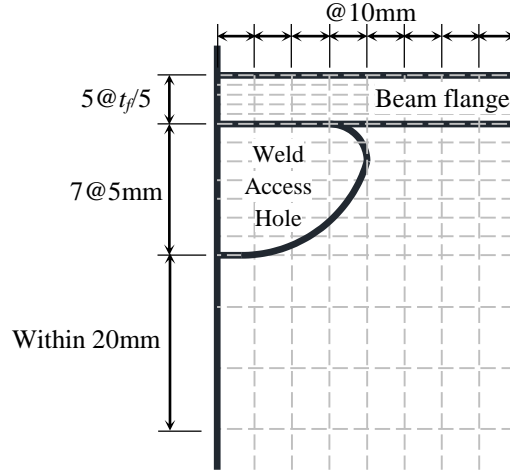

Fig. 4.16 Mesh generation at the beam-end

4.3.6 Verification of WFBW Model

4.3.6.1 Database

To verify the proposed model, experimental database on the WFBW connection is constructed for the calibration of the analytical method (**Table 4.3**). The database consists of specimens with five different bolts configuration as shown in **Fig. 4.17** (**Chapter 2**; Kishiki et al. 2016), and three types of steel grade: 400, 490 and 590MPa.

4.3.6.2 Modeling of WFBW Connection in Database

Fig. 4.17 shows the model of WFBW connection of **Chapter 2** based on the Eq. (4.5). In case of WFBW connection of Kishiki et al. (2016), model of beam-end connection is the same as the FR bolt configuration of **Chapter 2**, and only the h_r is different due to different steel grade. As defined above, the thickness of the bolted connection is set to the sum of the shear plate and web. These area is defined inner area of bolt washer, which can be considered effective friction region. Also, the areas from the loss of web section by weld access hole to the bolts washer placed upper and bottom side are set the ineffective in transferring stress area. In case of bolt configuration F3 and F4, the all section in the bolted web connection is set to be effective area in transferring stress because the slip-critical strength is sufficiently high.
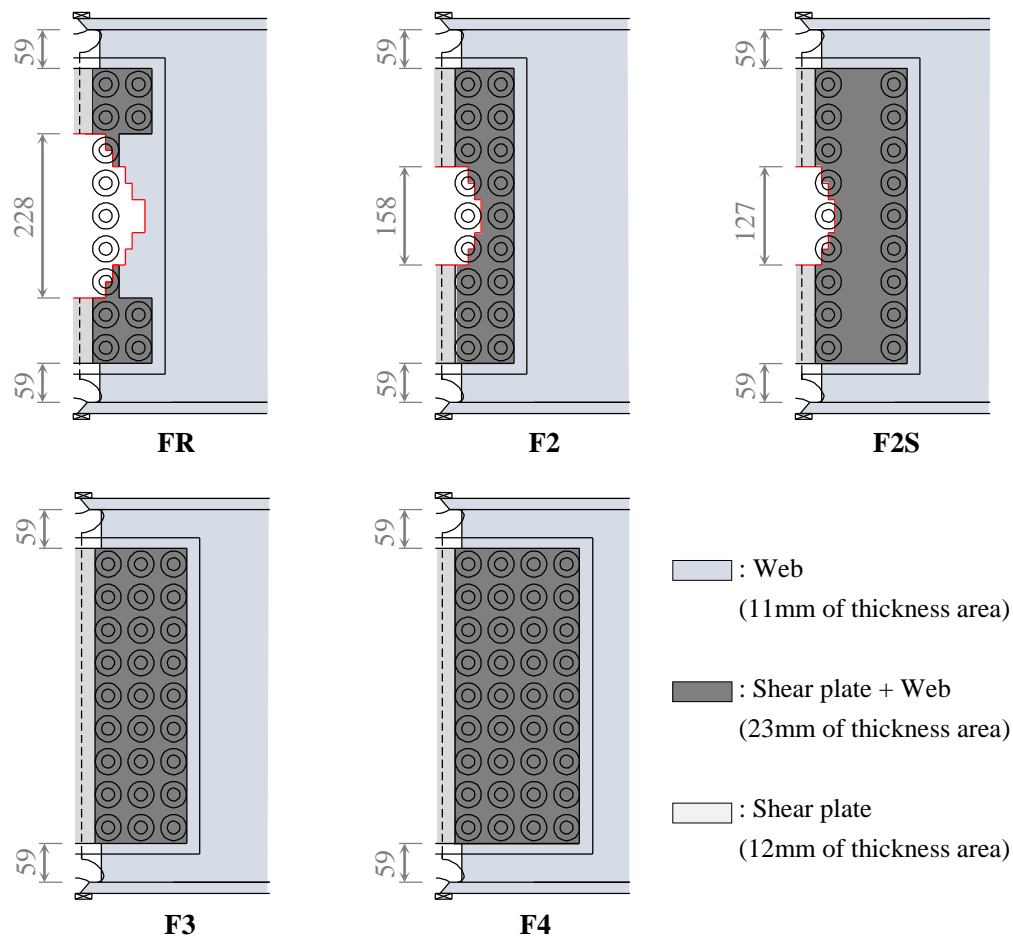
Fig. 4.17 Modelling of WFBW connection of **Chapter 2**

Table 4.3 Database of WFBW connection (**Chapter 2**; Kishiki et al. 2016)

Reference	Bolts Configuration	Beam Section (Steel grade / Span)	Yield Stress		Strength		Moment Ratio
			$_f\sigma_y$	$_w\sigma_y$	$_{js}M_y$	$_{Bw}M_s$	m
			N/mm²	N/mm²	kN·m	kN·m	
Chapter 2	FR	RH-600×200×11×17	347	391	157	116	0.74
	F2	(SN490B / 2050mm)				137	0.87
	F2S					144	0.92
	F3					214	1.00
	F4					298	1.00
Kishiki et al. (2016)	FR	RH-600×200×11×17 (SN400B / 3000mm)	298	319	117	99	0.85
		RH-600×200×11×17 (SN490B / 3000mm)	347	408	150	99	0.65
		RH-600×200×12×19 (SA440B / 3000mm)	510	539	216	134	0.62

4.3.6.3 Comparison of the Experimental and Analytical Results

The in-plane analysis of WFBW connection in the database was conducted to verify and calibrate the proposed model based on the WFBW connection. **Fig. 4.18** show comparison of experimental and analytical results on the experimental and analytical results of moment – beam rotation amplitude and the strain history at the beam-end flange of A section in **Fig. 4.19**. The strain history obtained from the test was used average value of inner and outer surfaces of the flange to neglect the effect of the bending. The strain amplitude at beam-end flange with moment and beam rotation relationship. In case of WFBW connection with 400MPa and 490MPa steel grade, hysteresis model proposed by Yamada et al. (2014) was used. As shown in **Fig. 4.18**, analysis results show good crrespondence with the test results both of moment-ratation relationship and strain amplitude on the critical section.

4.3.6.4 Comparison of the Experimental and Analytical Results on the Strain Amplitude at the Beam-End Flange

Fig. 4.20 shows comparison of experimental and analytical results on the strain amplitude at the beam-end flange. Experimental strain amplitude was obtained from the 4th to 10th cycles on the beam-end flange section fracture. As shown in **Fig. 4.20** the strain amplitude at the beam-end flange shows a good correspondence between test and analysis results.
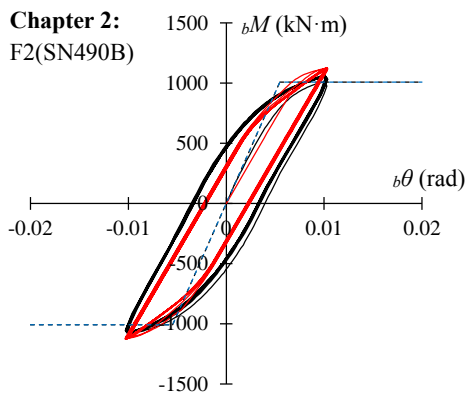
4.3.6.5 Stress Concentration and Tri-Axial Restraint near the Beam-End Flange

Fig. 4.21 shows way of thinking about the stress concentration and tri-axial restraint near the beam-end flange in the in-plane analysis. As shown in **Fig.4.21**, in the vicinity of the beam-end flange, it is considered that the plastic deformation is decreased as compared with the material test due to stress concentration and tri-axial restraint effect. In the LCF performance tests, strong correlation was confirmed between the average strain amplitude in the axial direction on the beam-end flange and the number of cycles to failure. In this research, the applicable range of the LCF performance evaluation Eq. is investigated based on the in-plane analysis focusing on the strain amplitude on the beam-end flange. In the in-plane analysis, the stress concentration and tri-axial restraint near the beam-end flange are not considered. However, by using the in-plane analysis, the average strain amplitude of axis direction on the beam-end flange can be calculated, and it shows good correspondence with test results.
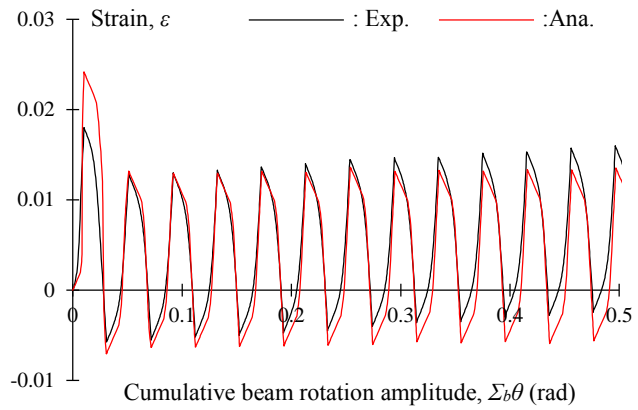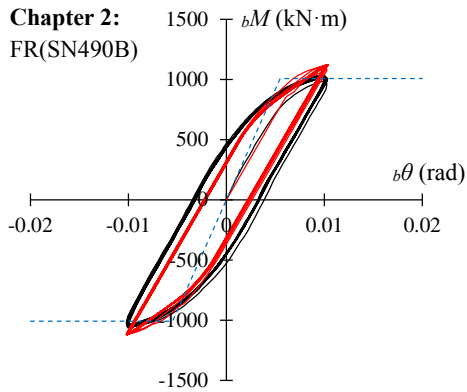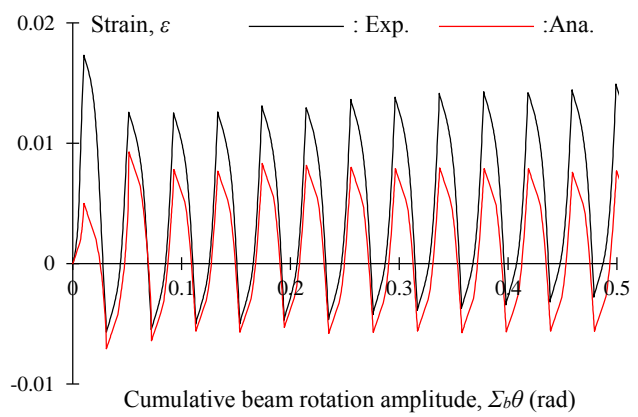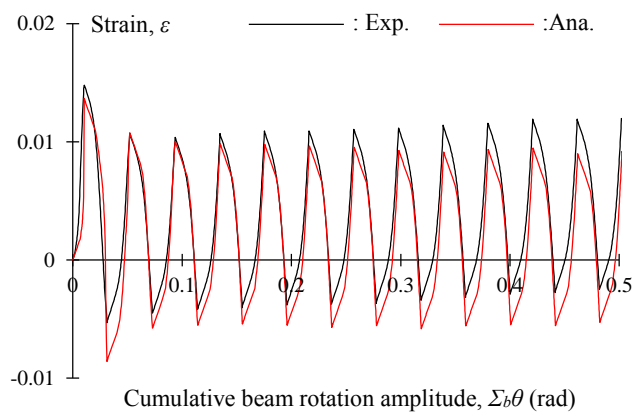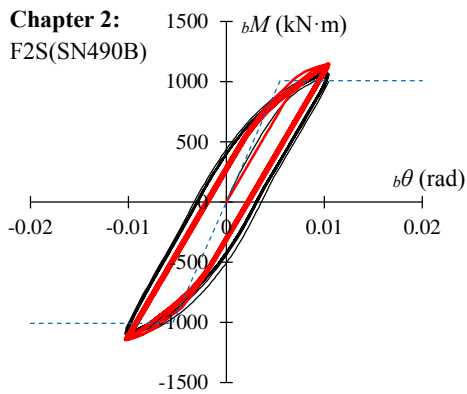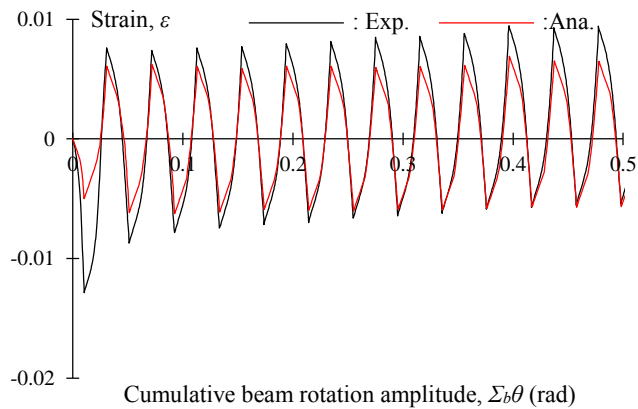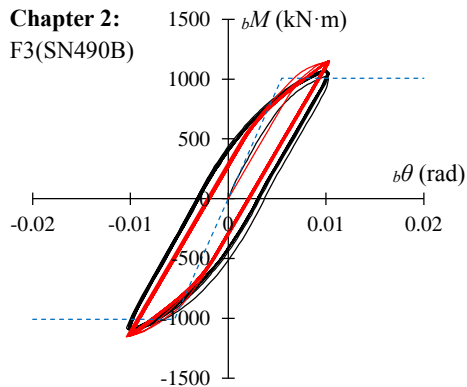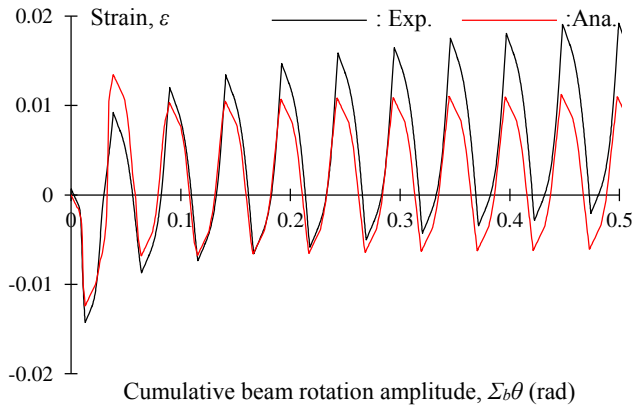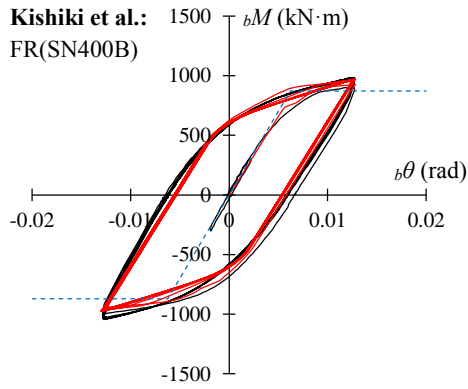
Chapter 2: F4(SN490B)
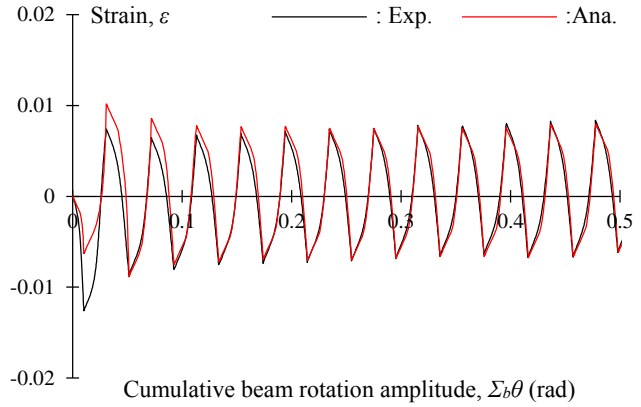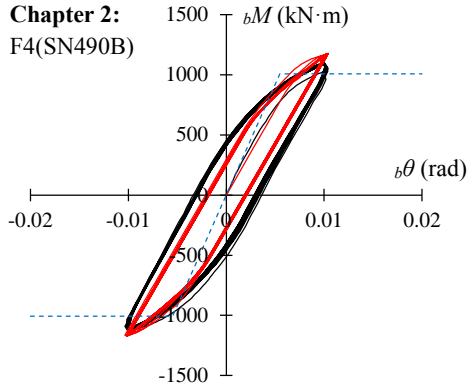
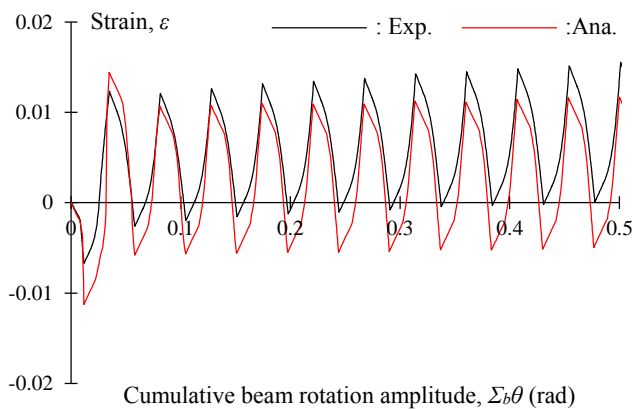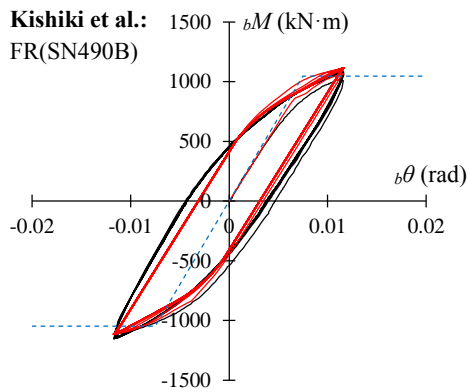Kishiki et al.: FR(SN400B)
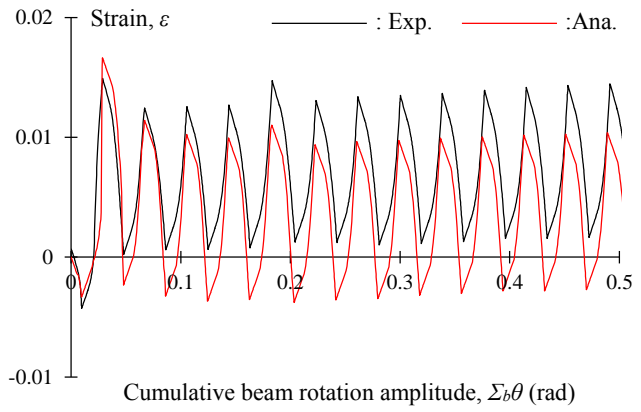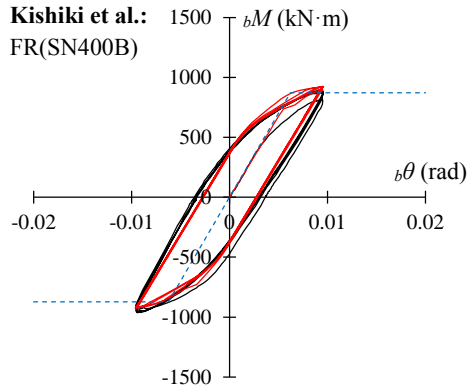
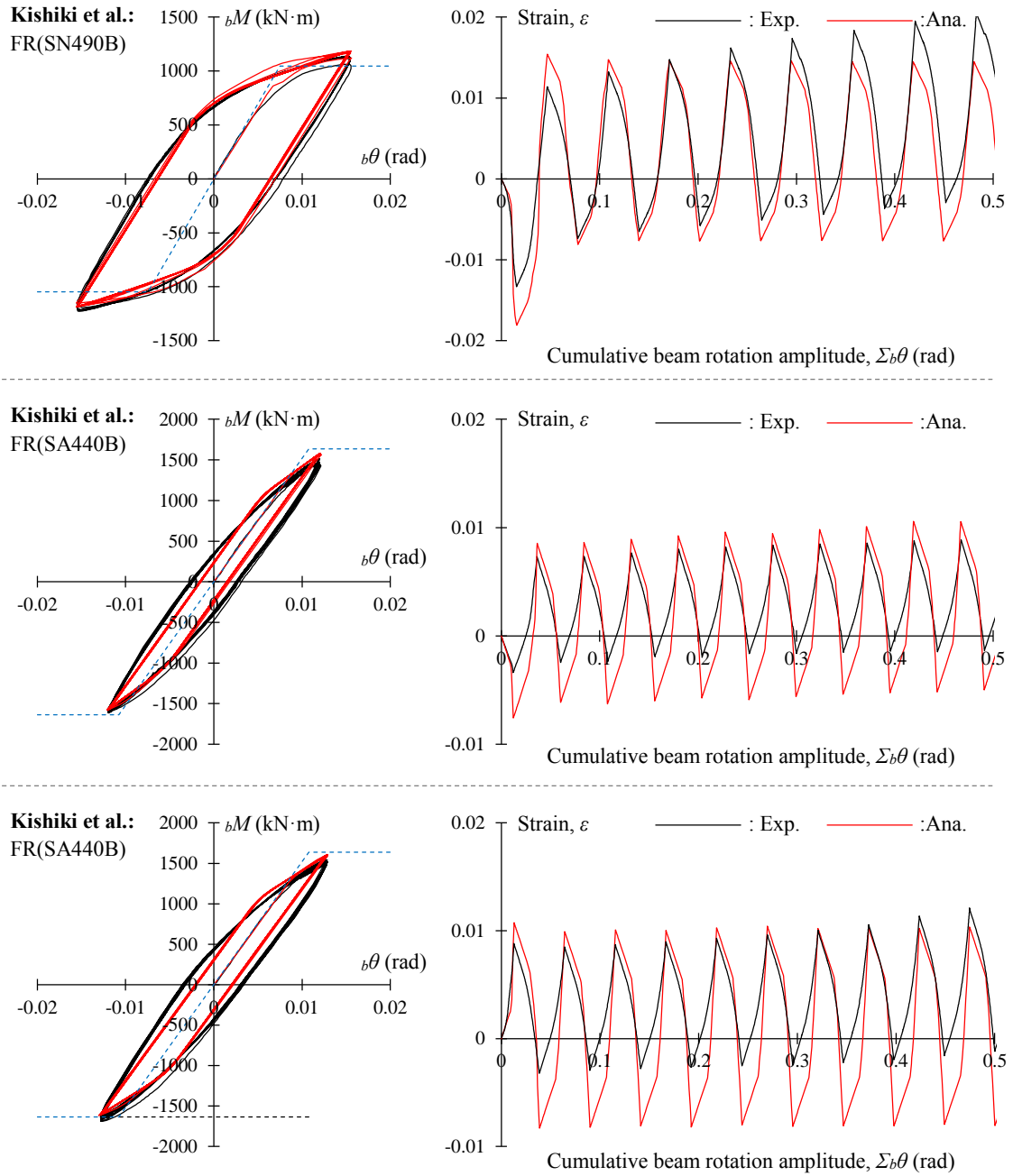Kishiki et al.: FR(SN400B)

Kishiki et al.: FR(SN490B)

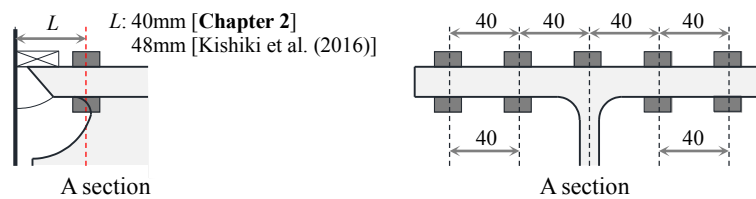**Fig. 4.18** Comparison of the test and analysis results

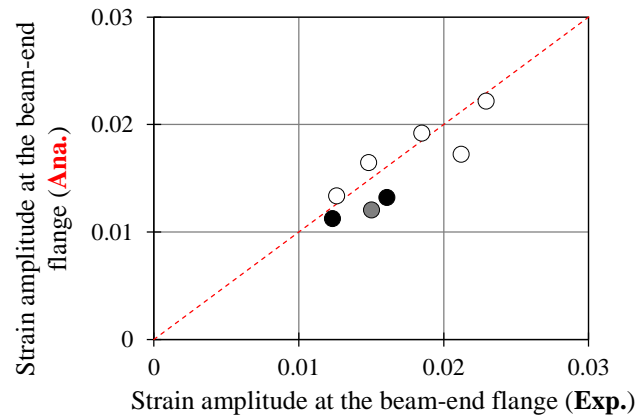**Fig. 4.19** Strain gauge location of beam-end flange

Fig. 4.20 Comparison of experimental and analytical results on the strain amplitude at the beam-end flange.
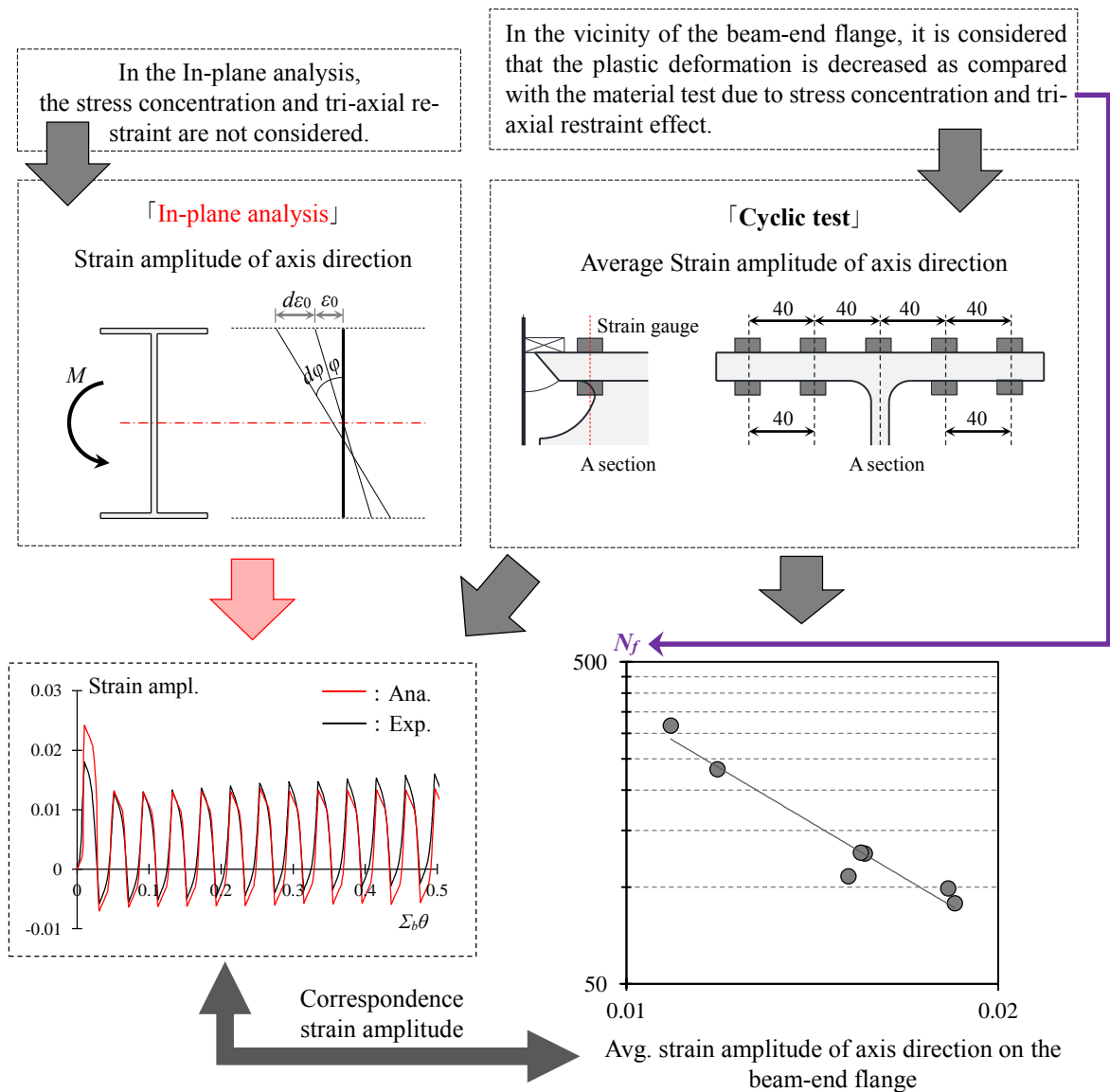

Fig. 4.21 Stress concentration and tri-axial restraint near the beam-end flange

4.4 Available Range of LCF Performance Evaluation

4.4.1　General

The cyclic deformation capacity of beam-to-column connection depends on the material's yield strength / ratio, shear span ratio, beam-end geometry and loading history. In the Chapter 3, LCF performance equation was proposed based on the experimental investigation. However, the experimental data are limited and since it is difficult to conduct much tests considering all of these parameters, an analytical investigation should be introduced together. In the experimental investigation (Kishiki et al. 2016), it is reported that LCF performance of WFBW connections were evaluated in the same fatigue curve regardless of three different steel grade and shear span ratio, but the shear span ratio and rotation amplitude considered in experiment is 3.5 to 5.0, and 0.0170 to 0.0568rad, respectively. So, it is necessary to clarify the scope of the LCF performance evaluation. The effects of shear span ratio, steel grade, and load history on LCF performance were analyzed quantitatively.

4.4.2　Analysis List

The analysis list is summarized in **Table 4.4** In order to clarify LCF evaluation range of WFBW connection, analysis list consists of different steel grade, beam section and span with FR and F3 bolt configuration. The strengths required for modeling beam-end connection are summarized in **Table 4.4** The material properties are summarized in **Table. 4.5** and stress-strain curve are shown in **Fig. 4.22**.

Table 4.4 Analysis list

Bolt Configuration	Beam Section	Span L	Steel Grade	Strength				m	θ_p
				$_bM_y$ kN·m	$_{bf}M_y$ kN·m	$_{js}M_y$ kN·m	$_{Bw}M_s$ kN·m		rad
FR & F3	H-600×200×11×17	3000	SN400B	739	574	176	FR: 94 F3: 176	FR: 0.53 F3: 1.00	0.0061
	H-400×200×8×13	2000	SN490B	398	338	49	FR: 22 F3: 49	FR: 0.45 F3: 1.00	0.0072
	H-600×200×11×17	1800 3000 4500 6000		861	669	225	FR: 110 F3: 200	FR: 0.49 F3: 0.89	0.0071
	H-900×300×16×28	4500		3082	2463	837	FR: 326 F3: 650	FR: 0.39 F3: 0.78	0.0072
	H-600×200×11×17	3000	SA440B	1265	983	294	FR: 161 F3: 297	FR: 0.54 F3: 1.00	0.0105
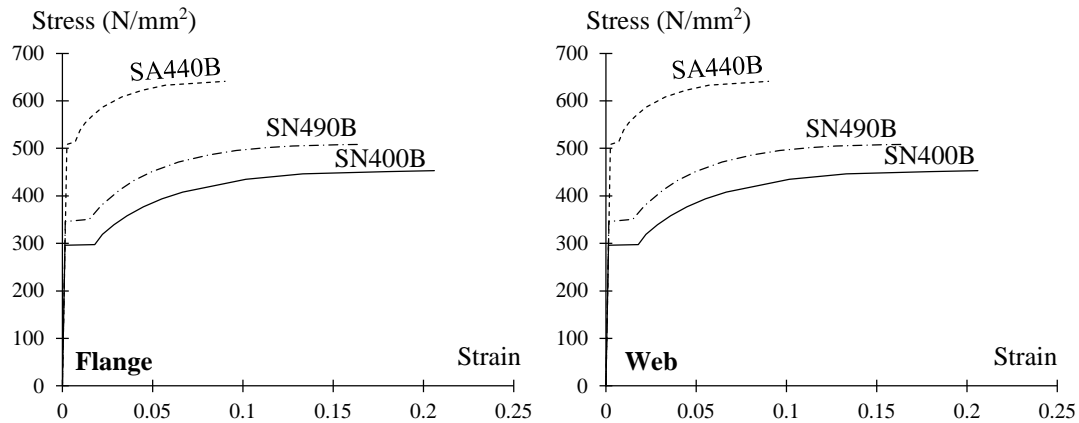
Fig. 4.22 Stress – Strain Curves

Table 4.5 Material properties

Steel grade	Part	Yield Stress N/mm^2	Tensile Stress N/mm^2	Yield Ratio %	Elongation %
SN400B	Flange	298	453	66	28
	Web	319	468	68	28
SN490B	Flange	347	508	68	27
	Web	408	554	74	26
SA440B	Flange	510	641	80	21
	Web	539	658	82	17

4.4.3 Critical Section at the Beam-End Flange

The LCF performance determined by ductile fracture are related to the plastic strain of the beam-end flange. In case of the 35R+10R detail in weld access hole configuration, the strain concentration was occurred at the weld access hole, so the critical section is defined at the flange section at the weld access hole as shown in **Fig. 4.23**. In the in-plane analysis, LCF performance is examined by focusing on the strain at the critical section.

Fig. 4.23 Critical section at the beam-end flange

4.4.4   Available Range of LCF Performance Evaluation with Different Steel Grade
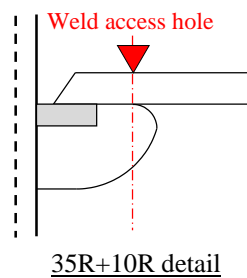
Fig. 4.24 shows the strain amplitude at the beam-end flange $\Delta\varepsilon_f$ with different steel grade which are SN400B, SN490B and SA440B, based on the ductile factor and beam rotation amplitude. The beam section and span is same as H600 and 3000mm. As shown in the **Fig. 4.24**, FR and F3 specimens of SN400B and SN490B indicate roughly the same $\Delta\varepsilon_f$ regardless of loading amplitude. On the other hand, $\Delta\varepsilon_f$ of specimens with SA440B steel grade increases sharply as the loading amplitude increases. However, in relation to beam rotation amplitude, it was confirmed that all steel grade exhibited roughly equal $\Delta\varepsilon_f$ up to about 0.02rad in plastic range. In this range, the cyclic performance can be evaluated equally regardless of the steel grade by using the beam rotation amplitude as evaluation index.
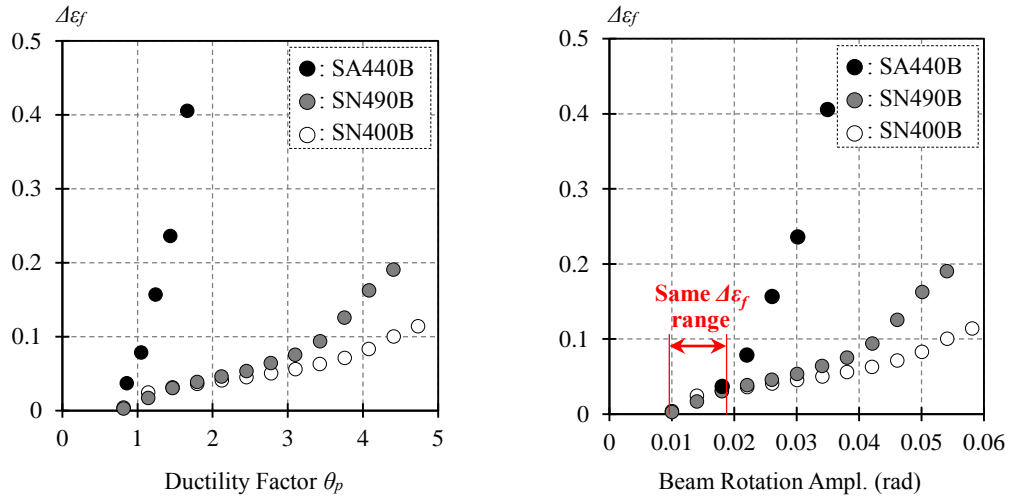
(a) FR Bolt Configuration of H600 Beam Section
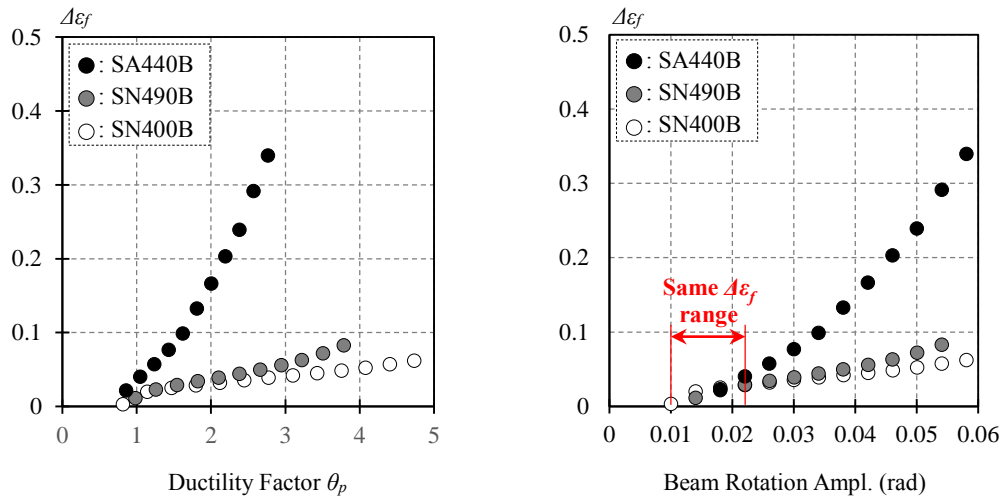
(b) F3 Bolt Configuration of H600 Beam Section

Fig. 4.24 Available range of LCF evaluation with different steel grade

4.1.1 Available Range of LCF Performance Evaluation with Different Beam Section

Fig. 4.25 shows $\Delta\varepsilon_f$ with different beam section, which are H900, H600 and H400. The beam span set 4500mm, 3000mm and 2000mm, respectively, to make same shear span ratio. The SN490B steel grade is selected in all specimens plotted in **Fig. 4.25**. The specimens of H900 and H400 indicate approximately the same $\Delta\varepsilon_f$. The specimen of H600, $\Delta\varepsilon_f$ exhibited roughly equal up to about 2-3θ_p and 0.035rad of beam rotation amplitude in plastic range. However, as the loading amplitude increases, the $\Delta\varepsilon_f$ is different according to the beam section. It can be seen that as the loading amplitude increases, the expansion of the plastic range can be varied by the combination of beam flange and web and the width‐thickness ratio, even if the shear span ratio is the same.

(a) FR Bolt Configuration

(b) F3 Bolt Configuration
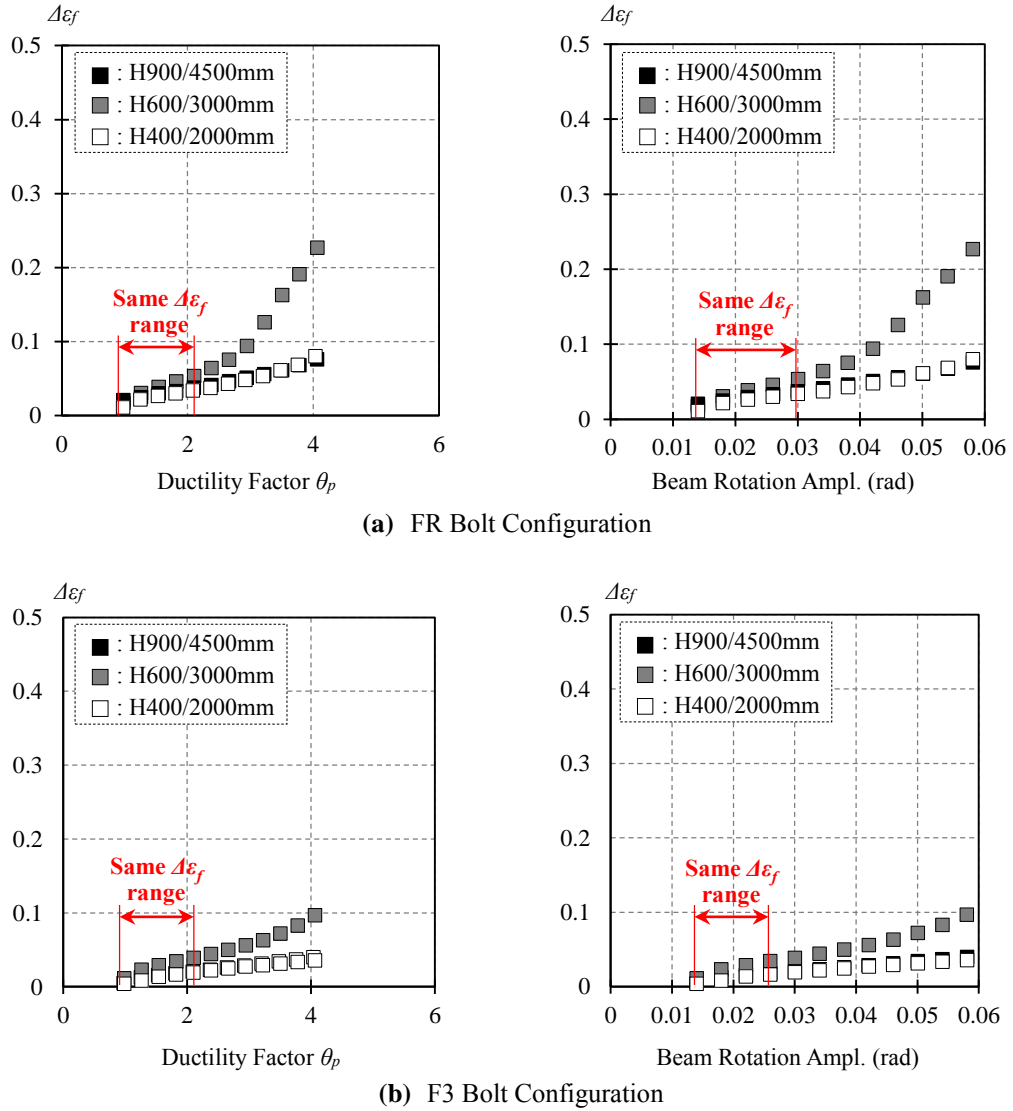
Fig. 4.25 Available range of LCF evaluation with different steel grade

4.1.2 Available Range of LCF Performance Evaluation with Different Beam Span

Fig. 4.26 shows $\Delta\varepsilon_f$ with different beam span, which are 1800mm, 3000mm, 4500mm and 6000mm of H600 beam section. Shear span ratio is set as 3.0, 5.0, 7.5 and 10.0, respectively. Steel grade is same as SN490B. As shown in **Fig. 4.26**, the $\Delta\varepsilon_f$ can be equally evaluated regardless of beam span if the ductility factor is used as evaluation index. On the other hand, in the relationship between $\Delta\varepsilon_f$ and beam rotation amplitude, as the loading amplitude increases, the $\Delta\varepsilon_f$ depending on the beam span. This means that the details of the weld access hole is not change even if the beam span becomes longer, and the shorter the beam span, the larger $\Delta\varepsilon_f$ with the same loading amplitude. The available range of LCF evaluation with different beam san is approximately 0.02rad of beam rotation amplitude.

(a) FR Bolt Configuration of H600 Beam Section
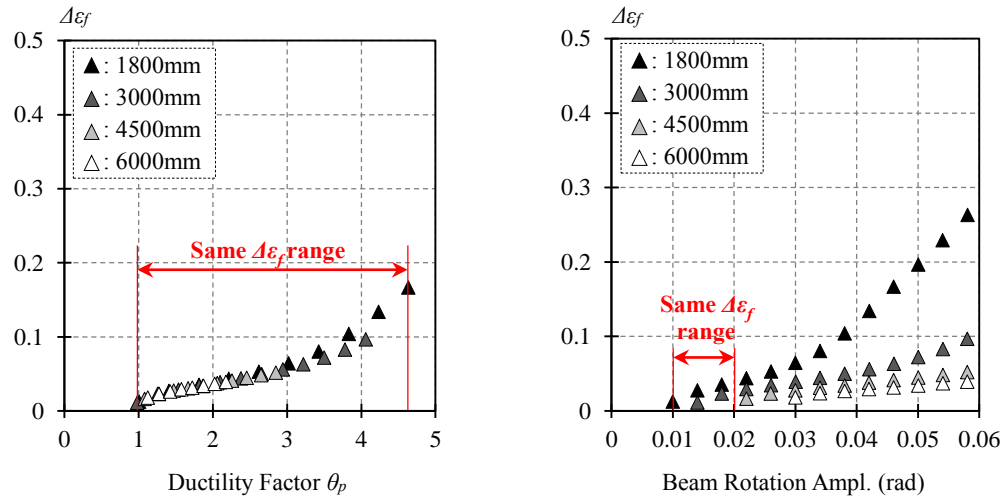
(b) F3 Bolt Configuration of H600 Beam Section

Fig. 4.26 Available range of LCF evaluation with different steel grade

4.5 Summary and Conclusion

This chapter introduces an analytical approach to evaluate the LCF performance of WFBW connections in high-rise SMRFs. The LCF performance determined by ductile fracture are related to the plastic strain of the critical section, which is weld access hole. The strain of critical section was calculated based on the in-plane analysis. In the analytical approach, a hysteresis model considering Bauschinger effect was proposed to consider the material characteristics under cyclic loading. Based on the hysteresis model of steel materials, numerical analysis was performed for the WFBW connection commonly used in Japanese high-rise SMRFs. The WFBW connection, analysis model considering slip behavior was introduced and verification based on the experimental results. In the analysis, available range of LCF performance evaluation with different steel grade, beam section and beam span were quantitatively investigated, and the scope of evaluation was clarified.

The following conclusion are made:

Available range of LCF performance evaluation with different steel grade: The subjected loading amplitude increases, strain amplitude varies depending on the steel material because the steel characteristics (yield strength / ratio and strain hardening) are taken. And the lower the joint efficiency, the larger the tendency is in the relationship between ductility and plastic strain amplitude. However, in the relationship between beam rotation amplitude and strain amplitude, the strain amplitude indicates almost same regardless of the steel grade up to about 0.02rad of beam rotation amplitude in the inelastic range. The LCF performance of beam-to-column connection is categorized in the range of about 0.02rad in plastic. As the results, LCF performance of beam-to-column connection can be evaluated comprehensively with different steel grade by using the beam rotation amplitude as the evaluation index.

Available range of LCF performance evaluation with different beam section: As the loading amplitude increases, the expansion of the plastic range can be varied by the combination of beam flange and web and the wid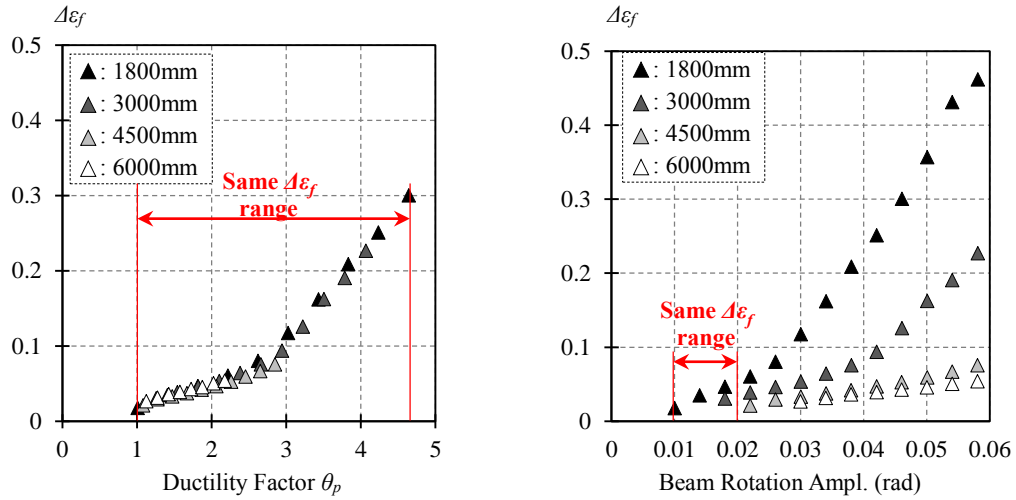th‐thickness ratio、even if the shear span ratio is the same.　However, LCF performance of WFBW connection can be roughly evaluated up to about 0.035rad of beam rotation amplitude in plastic range with different beam section.

Available range of LCF performance evaluation with different beam span: The $\Delta\varepsilon_f$ can be equally evaluated regardless of beam span if the ductility factor is used as evaluation index. On the other hand, in the relationship between $\Delta\varepsilon_f$ and beam rotation amplitude, as the loading amplitude increases, the $\Delta\varepsilon_f$ depending on the beam span. This means that the details of the weld access hole is not change even if the beam span becomes longer, and the shorter the beam span, the larger $\Delta\varepsilon_f$ with the same loading amplitude. The available range of LCF evaluation with different beam san is approximately 0.02rad of beam rotation amplitude.

References

Akiyama, H. (1985). "Earthquake-resistant limit-state design for buildings," Tokyo: University of Tokyo Press.

Building Research Institute: National research and development. (2014). Study on Seismic Performance for Super-High-Rise Steel Buildings against Long-Period Earthquake Ground Motions, No.160. (in Japanese).

Karavasilis, T. L., Kerawala, S., & Hale, E. (2012). Hysteretic model for steel energy dissipation devices and evaluation of a minimal-damage seismic design approach for steel buildings. *Journal of Constructional Steel Research*, *70*, 358-367.

Kishiki, S., Sato, R., Yamada, S. & Hasegawa, T. (2016). Evaluation method of cyclic deformation capacity for beam-end connections using various steel grades. J. Struct. Const. Eng., AIJ, 81(723), 917-927. (in Japanese)

Lignos, D. G., & Krawinkler, H. (2010). Deterioration modeling of steel components in support of collapse prediction of steel moment frames under earthquake loading. *Journal of Structural Engineering*, *137*(11), 1291-1302.

Ono, T., Kaminogo, T., Yoshida, F., Iwata, M. & Hayashi, K. (1997). Astudy on material properties and hysteretic behavior of metallic material. J. Struct. Const. Eng., AIJ, 498. 137-143. (in Japanese)

Oyamada, Y. & Aoki, H. (1995). Expression of Bauschinger effected part in cyclic stress-strain relationship at steels. Summaries of technical papers of Annual Meeting Architectural Institute of Japan. C-1, Structures III, Timber structures steel structures steel reinforced concrete structures. 191-192. (in Japanese)

Suita, K., Tanaka, T., Manabe, Y. & Takatsuka, K. (2012b). Effect of variable amplitude loading protocol on deformation capacity: Deformation capacity of welded beam-to-column connection subjected to repeated plastic strain Part 3. J. Struct. Const. Eng., AIJ, 77(682), 1951-1958. (in Japanese)

Suita, K., Tanaka, T., Sato, A., Manabe, Y., Tsukada, T. & Su, Z. (2011). Effect of ultimate flexural strength of beam end connection on deformation capacity: Deformation capacity of welded beam-to-column connection subjected to repeated plastic strain Part 1. J. Struct. Const. Eng., AIJ, 76(664), 1135-1142. (in Japanese)

Suzuki, T., Ishii, T., Moria, K. & Takanashi, K. (1999). Experimental study on fracture behavior of welded beam-to-column joint with defects. Steel Construction Engineering, 6(23), 149-164. (in Japanese)

Takatsuka, K., Manabe, Y., Suita, K., Tanaka, T., Tsukada, T. & Su, Z. (2012a). Effect of weld access hole on deformation capacity: Deformation capacity of welded beam-to-column connection subjected to repeated plastic strain Part 2. J. Struct. Const. Eng., AIJ, 77(673), 453-459. (in Japanese)

Takatsuka, K., Suita, K., Tanaka, T. & Umeda, T. (2014). Effect of beam section size and connection detail on deformation capacity: Deformation capacity of welded beam-to-column connection subjected to repeated plastic strain Part 4. J. Struct. Const. Eng., AIJ, 77(696), 315-321. (in Japanese)

Tanaka, T., Suita, K., Asakura, N., Tsukada, T., Uozumi, N. & Takatsuka, K. (2015a). Influence of floor slab on deformation capacity: Deformation capacity of welded beam-to-column connection subjected to repeated plastic strain Part 5. J. Struct. Const. Eng., AIJ, 80(707), 127-136. (in Japanese)

Umeda, T., Takatsuka, K., Suita, K. & Tanaka, T. (2015b). Deformation capacity of flange-welded web-bolted moment connection: Deformation capacity of welded beam-to-column connection subjected to repeated plastic strain Part 6. J. Struct. Const. Eng., AIJ, 80(718), 1971-1979. (in Japanese)

Yamada, S., Imaeda, T. & Okada, K. (2002). Simple hysteresis model of structural steel considering the Baushinger effect. J. Struct. Constr. Eng., AIJ, 559. 225-232. (in Japanese)

Yamada, S., Jiao, Y., Narigara, H., Yasuda, S. & Hasegawa, T. (2014). Plastic deformation capacity of steel beam-to-column connection under long-duration earthquake. International Journal of High-Rise Buildings, 3(3), 231-241.

Yamanouchi, H., Imanaka, N. & Fukuta, T. (1997). Stress-strain curves of 590N steel and aluminum alloy under cyclic and reverses loading. J. Struct. Constr. Eng., AIJ, 501. 117-123. (in Japanese)

CHAPTER 5

CONCLUSIONS AND FUTURE WORK

5.1 Conclusions

This dissertation detailed an experimental and analytical investigation of low-cycle fatigue (LCF) performance evaluation of beam-to-column connection in high-rise steel moment resisting frames. The following conclusion are made:

In the **Chapter 2**, cyclic loading test on the welded flange-bolted web (WFBW) connection was carried out to investigate effect of slip behavior on the LCF performance. The considered main parameter is the bolts configuration at the bolted web connection. All specimens indicated the similar failure mode, which is ductile fracture via the growth of cracks at the weld access hole or weld toe of the beam flange. The LCF performance carried according to the bolt configuration. The slip behavior at the bolted web connection was different according to the bolts configuration under minor inelastic deformation, the specimens that possess a larger slip-critical strength than yield bending strength of the shear plate exhibit an increase in the number of cycles to failure. The strength of the web connection for the WFBW connections determined the minimum value between the slip-critical strength and the yield bending strength of the shear plate. If the strength of bolted web connection of the WBFW connection is equal to yield strength of the welded web connection, the LCF capacity is the same.

In the **Chapter 3**, a methodology for LCF performance assessment of beam-to-column connections, which are welded and WFBW connection is presented based on the database of cyclic loading test results. The moment transfer efficiency was evaluated according to the connection details by defining a coefficient, J_b, that considered the slip behavior of the bolts, out-of-plane deformation of the column flange and loss of the web section strength due to the weld access hole.

It was confirmed that when the specimen coefficient, J_b, are almost the same, the fatigue curves are identical regardless of the mechanism of moment transfer. A coefficient, J_b, is reflected in the fatigue curve based on the relationship between the number of cycles to failure and the constant beam rotation amplitude obtained from cyclic loading tests. The proposed approach is applicable to evaluating the comprehensive fatigue performance of beam-to-column connections, considering the moment transfer efficiency of the web connection details and the steel grade.

In the **Chapter 4**, introduces an analytical approach to evaluate the LCF performance of WFBW connections in high-rise steel moment resisting frames. In the analysis, the effects of material's characteristic and geometry on the LCF performance of WFBW connection was quantitatively investigated, and the scope of evaluation was clarified. As an analysis on the beam section H400, H600 and H900, it was confirmed that if joint efficiency of the beam-end connection is calculated to be the same value, the LCF performance can be evaluated in the relationship between beam-rotation amplitude and strain amplitude regardless of the different beam section. While it was indicated that the ductility is a more appropriate evaluation index for LCF evaluation of beam-to-column connection with different shear span ratio. The subjected loading amplitude increases, strain amplitude varies depending on the steel material because the steel characteristics (yield strength / ratio and strain hardening) are taken. And the lower the joint efficiency, the larger the tendency is in the relationship between ductility and plastic strain amplitude. However, in the relationship between beam rotation amplitude and strain amplitude, the strain amplitude indicates almost same regardless of the steel grade up to about 0.02rad of beam rotation amplitude in plastic range. The LCF performance of beam-to-column connection is categorized in the range of about 0.02rad in plastic. As the results, LCF performance of beam-to-column connection can be evaluated comprehensively with different steel grade by using the beam rotation amplitude as the evaluation index.

5.2 Future work

This dissertation has been focused on the LCF performance evaluation of steel beam-to-column connection commonly used in high-rise steel moment resisting frames. Although the proposed approach is applicable to evaluate comprehensive fatigue performance of steel beam-to-column connection considering many parameters that effect cyclic performance additional parameters remain. The research directions and the parameters to be considered as the future work are summarized below.

➢Future Works 1: *Low-Cycle Fatigue Performance of Beam-to-Column Connection determined by Local Buckling and Ductile Fracture*

The failure mode of beam-to-column connection can be categorized into local buckling with ductile fracture and ductile fracture. The proposed approach in this dissertation is based on the evaluation of the LCF performance of the beam-to-column connection with stable history based on the number of cycles to failure determined by ductile fracture. The occurrence of local buckling at the beam flange and web under cyclic loading causes a decrease in the strength and stiffness. In order to clarify the relationship between the effect of local buckling and the cyclic deformation, the beam section dimensions, span, material's characteristic. etc. should be considered.

➢ Future Works 2: *Effect of Floor Slab on the Low-Cycle Fatigue Performance of Steel Beam-End Connection*

In general, it is known that the plastic deformation capacity of the beam-to-column connection determined by fracture at the beam-end flange is decreased by the increase of the tensile strain generated in the lower flange due to the ascent of the plastic neutral axis of the beam with the slab. In previous studies on the beam-to-column connection with floor slab under many inelastic cyclic deformations, the LCF performance of the beam-to-column connection with floor slab is degraded as compared with the steel beam. Since the beam depth is large and the thickness of the slab is constant, it is considered that the deterioration of the deformation capacity by the slab is not large, However, the slab should also be considered as a parameter in the LCF performance evaluation.

➤ Future Works 3: *Low-Cycle Fatigue Evaluation of Beam-to-Column Connection with Horizontal Haunchi*

A WFBW connection is commonly used in high-rise steel MRFs. In the case of the WFBW connection, the moment transfer efficiency at the bolted web connection could be decreased under cyclic loading due to slip at the bolt, so that it is often designed to be reinforced by horizontal Haunchi. A WFBW connection with horizontal Haunchi is difficult to evaluate cyclic deformation, because the moment distribution in the vicinity of the beam-end connection depends on the geometry of horizontal Haunchi. In order to evaluate the LCF performance of connection in the high-rise steel MFRs, the extensive investigation should be done considering the geometry of horizontal Haunchi, and the design recommendation should be presented.

APPENDICES

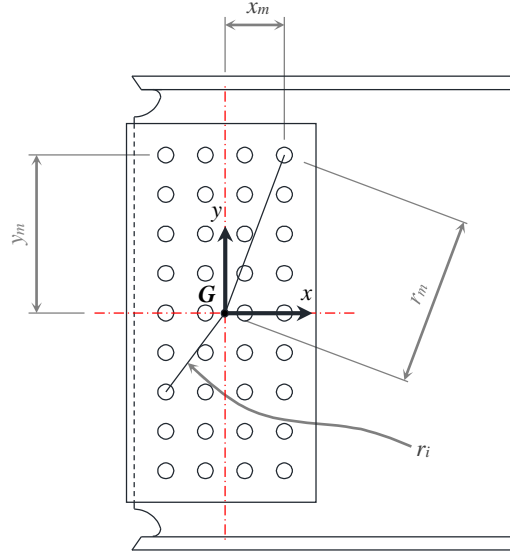## APPENDIX A. The slip-critical strength

Fig. A.1 local sharing in a bolted web connection by friction

The slip-critical strength, $_{Bw}M_s$, is determined as follows:

$$_{Bw}M_s = \frac{\sum r_i^2}{r_m} \sqrt{q_{by}^2 - \left(\frac{Q \cdot y_m}{n \cdot r_m}\right)^2} - \frac{Q \cdot x_m}{n \cdot r_m} \qquad (A.1)$$

where r_i is the distance between the center of the bolt group and the center of the i_{th} bolt hole; r_m is the distance between the center of the bolt group G and the most distant bolt hole; y_m is the distance between the center of the bolt group G and the most distant bolt hole along the y-axis; x_m is the distance between the center of the bolt group G and the most distant bolt hole along the x-axis; n is the number of bolts; q_{by} is the strength (slip resistance) of a slip plane (see **Fig. A.1**.); and Q is shear force defined by Eq. (A.2).

$$Q = {}_jM_y / L_b \qquad (A.2)$$

where L_b is the beam span, and $_jM_y$ is the effective bending moment for the beam connection considering the loss of a web section due to a weld access hole. $_jM_y$ is given by Eq. (A.3).

$$_{j}M_{y} = Z_{e} \cdot {}_{f}\sigma_{y} \qquad \text{(A.3)}$$

where Z_e is the effective section modulus for the beam connection considering the loss of a web section due to a weld access hole and $_{f}\sigma_{y}$ is yield stress of the beam flange.

APPENDIX B. Additional investigation on the relationship strain amplitude and beam rotation amplitude with cyclic deformation. (Kishiki et al. 2016)

In previous study (Kishiki et al. 2016), the effects of steel grade on the LCF performance of beam-to-column connection were evaluated through cyclic loading tests. The conclusions of these experimental investigations are summarized as follows.

The strains at the beam-end flanges were examined to understand the correlation with beam rotation amplitude, $\Delta_b\theta_{const.}$. The strains obtained during the cycles from the strain gauge glued on the beam end flange were used, as shown in **Fig. B1(b)**. The yield strain, εy, was defined as $\varepsilon_y=\sigma_y/E$, where σ_y is the yield stress obtained from a tensile test, and E is Young's modulus (**Fig. B1(a)**). In this study, it is assumed that the effect of material properties, such as strain hardening, is insignificant because of the relatively minor inelastic deformation; thus, the total axial strain on the beam flange was analyzed by decomposing it into elastic and plastic components, as shown in **Fig. B1(a)**. First, the cyclic loading test results for all the specimens are illustrated in **Fig. B1(c)**. The test results are plotted as the number of cycles to failure, N_f, versus the beam plastic rotation amplitude, $\Delta_b\theta_{pl}$. The strain amplitude plotted in **Fig. B1(d)** and **(f)** are the average values of the strain amplitude of 2 to 5 cycles showing a stable strain rate. The dotted lines represent the approximate curve for specimens SN40 (white/triangle), SN49 (gray/triangle) and SA59 (black/triangle). As shown in **Fig. B1(c)**, regardless of the steel grade, N_f decreased with increasing $\Delta_b\theta_{pl}$. In addition, $\Delta_b\theta_{pl}$ - N_f lines for specimens in each steel grade have similar slopes. In terms of the relationship between N_f and $\Delta_b\theta_{pl}$, the specimens of 400 N/mm² steel grade achieved the highest N_f; and the specimens of 590 N/mm² steel grade exhibited the worst behavior under identical $\Delta_b\theta_{pl}$. In addition, compared to the specimens of 400 N/mm² steel grade and 490 N/mm² steel grade, the reduction in N_f of specimens of 590 N/mm² steel grade is significantly larger. Understandably, LCF performance depends on the yield strength of the beam.

The relationship between the beam flange plastic strain amplitude, $\Delta\varepsilon_p$, and the beam plastic rotation amplitude, $\Delta_b\theta_{pl.}$, is shown in **Fig. B1(d)**. The specimen SA59 was not plotted

APPENDIX B. Additional investigation on the relationship strain amplitude and beam rotation amplitude with cyclic deformation

-Appendix B1 -

(a) Location of strain gauges on the beam flange

$\varepsilon_t = \varepsilon_p + 2\varepsilon_y$

$\times 2\ \varepsilon_y$

Cumulative bam angle, $\Sigma_b\theta$

(b) Definition strain amplitude

Strain, $\varepsilon = (\varepsilon_1 + \varepsilon_2)/2$

Yield strain, εy, was calculated from $\varepsilon_y = \sigma_y$, where, σ_y is yield strength obtained from tensile test and E is young's modulus.

(f) $\Delta_b\theta_{pl}$ versus N_f

(e) $\Delta_b\theta_{pl}$ versus $\Delta\varepsilon_p$

(c) $\Delta_b\theta$ versus $\Delta\varepsilon_t$

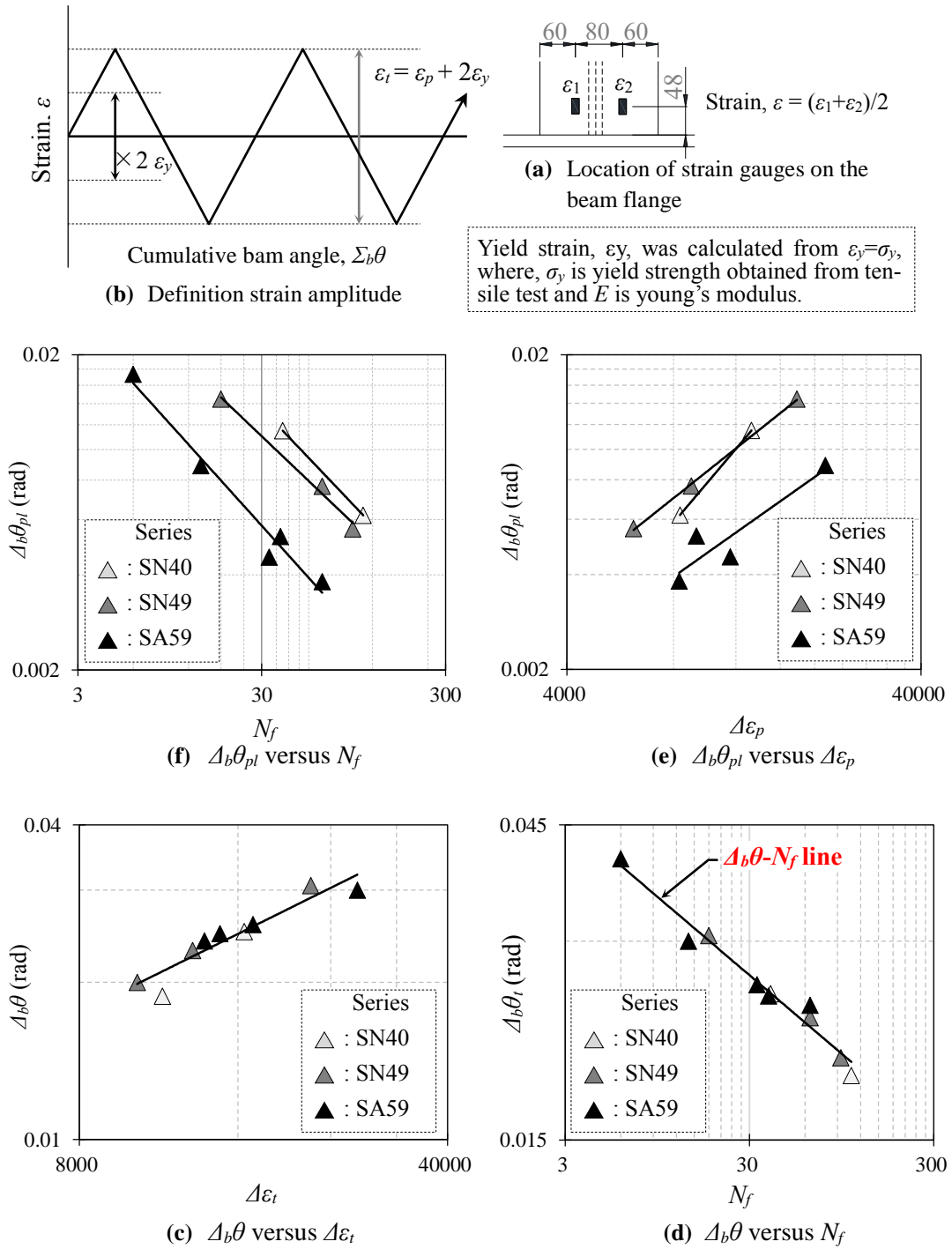**(d)** $\Delta_b\theta$ versus N_f

Fig. B1 Effect of steel grade on LCF performance of beam-to-column connection

because the beam flange strain measu rement failed during the test. The solid lines represent the $\Delta\varepsilon_p$-$\Delta_b\theta_{pl.}$ line for each steel grade. The approximate curve for specimens SN40 and SN49 correspond closely to each other because each yield stress was almost the same, with values of 298 N/mm² and 347 N/mm², respectively, and specimen SA59 indicates an overall increase

APPENDIX B. Additional investigation on the relationship strain amplitude and beam rotation amplitude with cyclic deformation

-Appendix B2 -

in $\Delta\varepsilon_p$ under the same $\Delta_b\theta_{pl.}$, corresponding to a yield strength of 510 N/mm^2. These results nearly correspond to the $\Delta_b\theta_{pl.}$ versus N_f relationship shown in **Fig. B1(c)**. In addition, irrespective of the steel grade, the $\Delta\varepsilon_p$-$\Delta_b\theta_{pl.}$ line for each steel grade represents nearly the same slope. In other words, yield strain, ε_y, depends on the steel grade; however, the increments in plastic strain amplitude, $\Delta\varepsilon_p$, correspond to the beam plastic rotation amplitude $\Delta_b\theta_{pl.}$, regardless of the steel grade. Thus, the total strain amplitude, $\Delta\varepsilon_t$, with beam rotation amplitude, $\Delta_b\theta_t$, that includes yield strain amplitude $\times 2\varepsilon_t$ and elastic beam rotation amplitude, $\Delta_b\theta_e$, is plotted in **Fig. B1(e)**. The solid line represents the $\Delta\varepsilon_t$-$\Delta_b\theta_t$ line for specimens SA40, SN49 and SA59. As shown in **Fig. B1(e)**, all specimens are in good agreement with the same $\Delta\varepsilon_t$-$\Delta_b\theta_t$ line. It is evident that the total rotation amplitude subjected to the beam corresponds to the total strain amplitude in the beam flange, irrespective of the yield strength of the steel used. Furthermore, the spread hinge region in the beam is generally affected by strain hardening (yield ratio); however, because the sections of interest in this test are the beam-to-column connection, which are of relatively low strength in comparison to the beam member, the hinge region becomes less susceptible to material properties, and most of the rotation in the hinge region can be concentrated at the beam end connection. Consequently, when $\Delta_b\theta_t$ is used for evaluating the LCF performance of beam-to-column connections, the strain hardening effect (yield ratio) of the material can be ignored.

The resulting LCF performance under various steel grades as plotted, $\Delta_b\theta_t$, corresponds to $\Delta\varepsilon_t$ versus N_f, as shown in **Fig. B1(f)**. The solid line represents the $\Delta_b\theta_t$-N_f line for all the specimens. As shown in **Fig. B1(f)**, the specimens tested under various steel grades are in good agreement with those of the $\Delta_b\theta_t$-N_f line. It is apparent that the LCF performance of a beam can be evaluated, regardless of steel grade, consistent with the plotted imposed beam rotation angle instead of the beam plastic rotation amplitude.

References
Kishiki, S., Sato, R., Yamada, S. & Hasegawa, T. (2016). Evaluation method of cyclic deformation capacity for beam-end connections using various steel grades. J. Struct. Constr. Eng., AIJ, 81(723), 917-927. (in Japanese)

APPENDIX C. Yield strength of beam web connection considering out-of-plane deformation of column flange (Suita et al. 2000)

The coefficient m, which considers the out-of-plane deformation and loss of web section due to the weld access hole, shall be determined as follows:

$$m = \frac{4}{kr^2}\sqrt{kr-4}\sqrt{kr^3 s^2 + 1} + \frac{4}{kr} - \frac{2}{kr^3} - 4s \qquad (C.1)$$

where r is the aspect ratio of the column flange, s is the ratio of the loss of the web section length due to the weld access hole, and k is the strength ratio of the web and column flange yield ranged. r, s and k are given by Eq. (C.2)- (C.4), respectively.

$$r = d_j / b_j \qquad (C.2)$$

where d_j and b_j are the height of the plastic region and width of the yield region of the column flange, respectively.

$$s = S_r / d_j \qquad (C.3)$$

where Sr is the length of the weld access hole.

$$k = \left(\frac{b_j}{_{cf}t}\right)^2 \frac{_{bw}t}{d_j} \cdot \frac{_{bw}F_y}{_{cf}F_y} \qquad (C.4)$$

where $_{cf}t$ and $_{bw}t$ are the thicknesses of the column flange and beam web; $_{cf}F_y$ and $_{bw}F_y$ are yield stress of the column flange and beam web, respectively.

Reference

Suita, K. & Tanaka, T. (2000). Flexural strength of beam web to square tube column joints. Steel Construction Engineering, 7(26), 51-58. (in Japanese)

APPENDIX D. Low-cycle fatigue performance evaluation of beam-to-column connection with 550MPa steel grade (Hirayama et al. 2000)

The LCF performance evaluation Eq. (D.1) of the beam-to-column connection proposed in **Chapter 3** was proposed based on the 400MPa, 490MPa and 590MPa. Additional investigation was coducted LCF performance evaluation of beam-to-column connection with 550MPa, which is commonly used in Japan.

$$N_{f,cal.} = 2.60 \times 10^{-3} J_b^{27.23} \cdot \Delta_b \theta_{const.}^{-(-6.06 J_b + 8.89)} \tag{D.1}$$

Hirayama et al. (2017) carried out cyclic loading test under constan loading amplitude on the WFBW connection with 550MPa. Unlike the WFBW connectioin, the beam web is welded to the coumn. The specimens list and test results with strength required for calculation of coefficient, J_b, are summarized in **Table D.1**. The specimens indicating brittle fracture were excluded from the evaluation range.

Table D. 1 Cyclic loading tests results and coefficient, J_b

Reference	Connection Type	Section & Steel grade & Span	Beam Rotation Amplitude rad	Number of Cycles to failure
Hirayama et al. (2017)	Flange: Field welding Web: Welded	Column: □-500×40(590MPa) Beam: H-700×300×16×25(550MPa) Beam Span: 3500mm Weld Access Hole: 35R+10R	0.0223	79

$_bM_y$: 2651kN/m / $_{bf}M_y$:2183kN/m / $_{jw}M_y$:404kN/m / Coefficient, J_b is 0.98
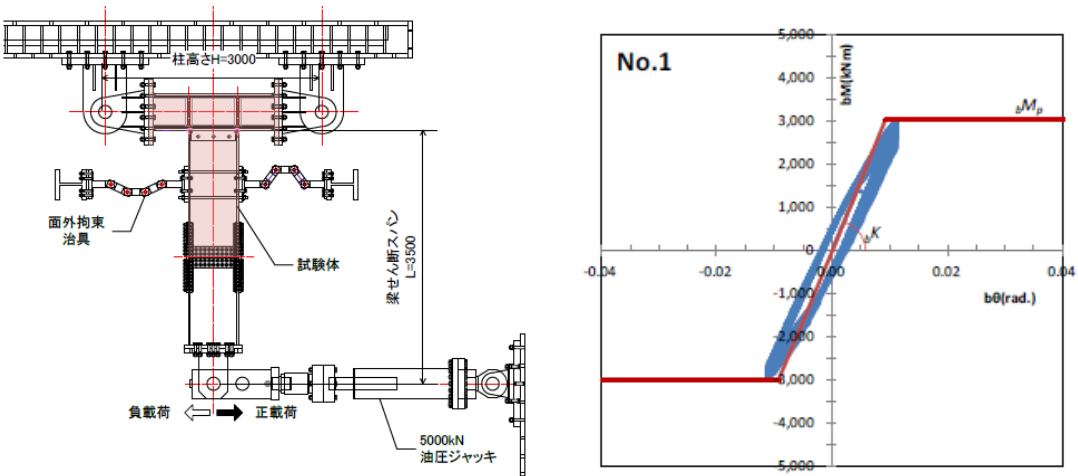

Fig. D.1 Reprinted test setup and Moment-Rotation relationship reprinted from (Hirayama et al. 2017)

A comparison between number of cycles to failure $N_{f,cal.}$ calculated by using Eq. (D.1) and cyclic loading tests results $N_{f,exp.}$ is shown in **Fig. D.2**. As shown in **Fig. D.2**, LCF performance of beam-to-column connection with 550MPa is also shown good correspondence.
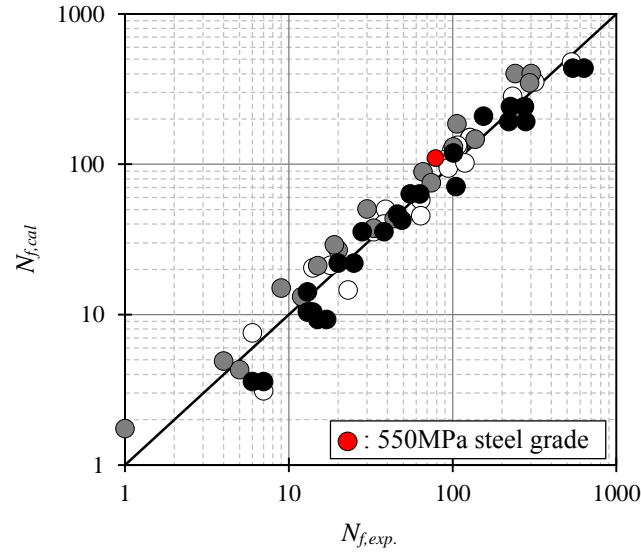

Fig. D.2 $N_{f,cal.}$ versus $N_{f,exp.}$ with 550MPa steel grade

Reference

Hirayama, H., Ito, H. & Hanya, K. (2017). Low cycle fatigue performance on welded end connection of wide flange beam built up with 550N/mm2 strength steel. Summaries of technical papers of Annual Meeting Architectural Institute of Japan, 793–794. (in Japanese)

APPENDIX E. **Effect of coefficient of stiffness changing point in bi-linear model considering Bauschinger effect on the strain amplitude of beam-end flange.**

The range of strain increments in the Bauschinger parts, $\Delta_t \varepsilon_B$, is investigated based on the test results as shown in **Fig. E.1**. The strain amplitude is obtained from the strain gauge glued on the critical section as shown in **Fig. E.1(a)**. **Fig. E.1(b)** and **(c)** indicate the strain amplitude on the critical section of the specimens, which is the subjected smaller and bigger beam rotation amplitude in the LCF range. The $\Delta_t \varepsilon_B$ in the LCF range is about 0.01 and 0.02. Here, in the constant loading amplitude, the maximum strange is reached at the first few cycles, the subsequent loading history is the Bausinger part and is stabilized as shown in **Fig. E.1(a)**. **Fig. E.1(b)**, so, the strain amplitudes are defined as $\Delta_t \varepsilon_B$.
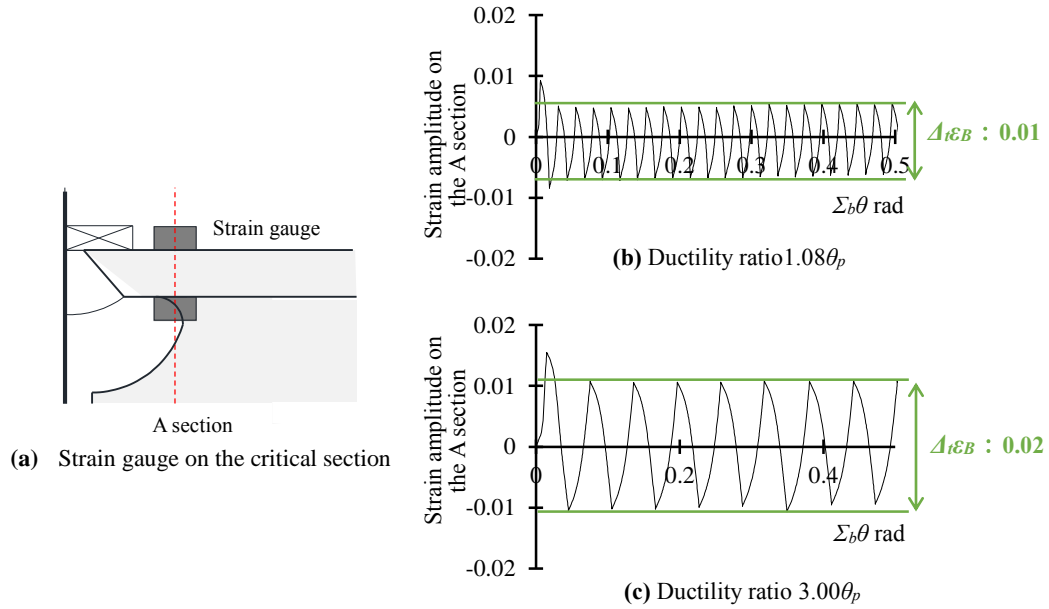

Fig. E.1 Range of strain increments in the Bauschinger parts of test result.

Fig. E.2 shows the relationship between α_B and $\Delta_t \varepsilon_B$. The d line in Fig. E.2 is the α_B of 0.67 defined in this Chapter 4 and the green area is approximately the α_B of 0.50 to 0.67 defined based on the specimens tested subjected constant beam rotation amplitude at the low plastic deformation. In-plane analysis of beam (H- 600×200×11×17_SN490B_L_b:3000mm) is conducted with the α_B of 0.50 to 0.67. **Fig. E.3** shows the relationship between the average strain amplitude on the critical section obtained from test and strain amplitude calculated from in-plane analysis on the same beam-end flange section. As shown in **Fig. E.3**, it was confirmed that the strain amplitude on the beam-end flange are approximately equal regardless
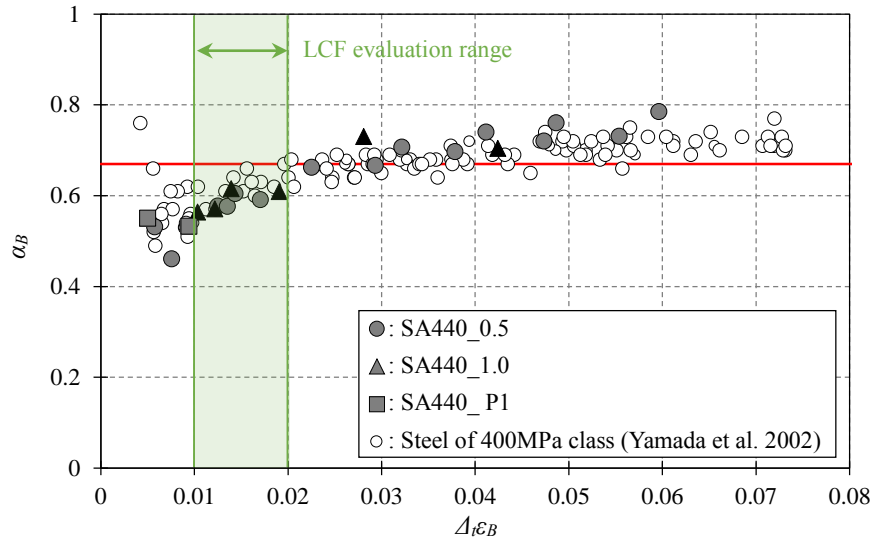
Fig. E.2 α_B - $\Delta_t\varepsilon_B$

of α_B. α_B is coefficient determined by the hysteresis curve of the Bausinger part in the Moment-Rotation relationship as shown in **Fig. E.4**, and even if it is defined from stable region, the influence on the strain amplitude in negligible.
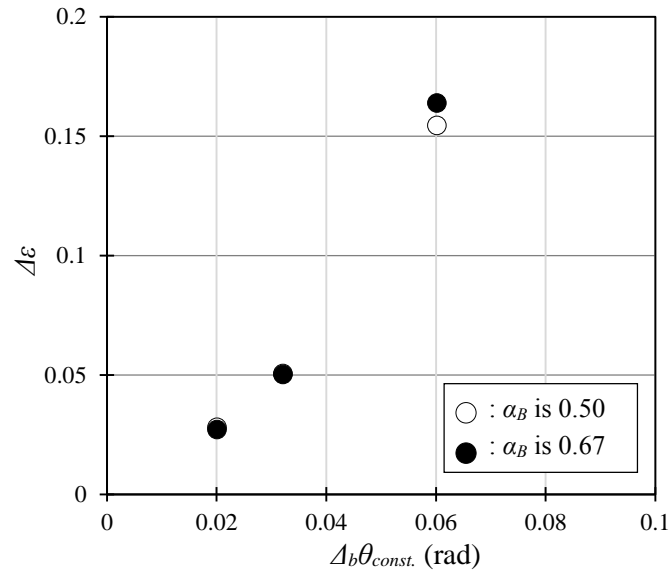

Fig. E.3 $\Delta_b\theta_{const.}$ - $\Delta\varepsilon$

APPENDIX E. Effect of coefficient of stiffness changing point in bi-linear model considering Bauschinger effect on 灸 *strain amplitude of beam-end flange*

-Appendix E2 -

(a) α_B : **0.50**   **(b)** α_B : **0.67**

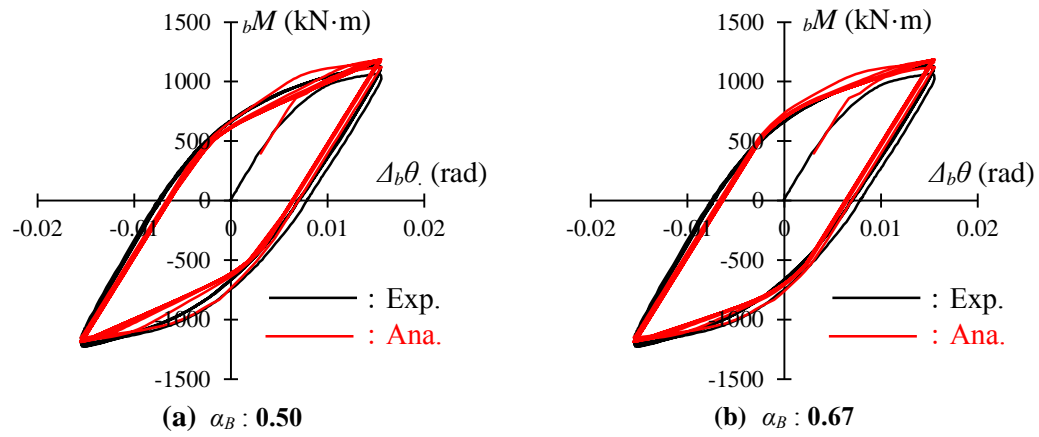**Fig. E.4**   Comparison of the experimental and analytical results on Moment – Rotation relationship